

**ELECTROMAGNETIC FIELDS IN RELATION
TO EDDY CURRENT GAUGING**

**A THESIS SUBMITTED FOR THE DEGREE OF
DOCTOR OF PHILOSOPHY
OF THE
UNIVERSITY OF SALFORD
(DEPARTMENT OF ELECTRONIC AND ELECTRICAL ENGINEERING)**

by JOSEPH DAVID HEYS, BSc., MPhil., C.Eng., MIEE.

May 1984



CONTENTSPage No.

CHAPTER 1 - INTRODUCTION

1.1 Preliminary Remarks 1

CHAPTER 2 - HISTORICAL REVIEW

2.1 Review of Eddy Current Gauging 4

CHAPTER 3 - THEORETICAL ANALYSIS

3.1 Introduction 20

3.2 Mathematical Model 21

3.2.1 Long Solenoid, Cylindrical Case 28

3.2.2 Short Solenoid, Cylindrical
Case 29

3.3 Evaluation of Mathematical Model 34

3.3.1 Long Solenoid, Cylindrical Case 34

3.3.2 Short Solenoid, Cylindrical
Case 363.4 Physical Limitations for Mathematical
Model 42

3.5 Surface Impedance Determination; Theory 54

3.6 Magnetic Field Strength Determination;
Theory 58

CHAPTER 4 - MEASUREMENT OF MODEL PARAMETERS

4.1 Introduction 61

4.2 Experimental Apparatus 63

4.3 Measurements 68

4.3.1 Measurements of Probe Coil
Voltage 684.3.2 Measurement of Magnetic Field
Strength 70

4.3.3	Measurement of Conductivity	75
4.3.4	Measurement of Surface Impedance, Non-Ferrous	76
4.3.5	Measurement of Surface Impedance, Phase Measurement	78
4.4	Mathematical Model Verification	84
4.5	Measurement of Surface Impedance, Mild Steel	88
4.6	Mathematical Model Verification	101
4.7	Distance Measurement	103
4.8	Conclusions	107
CHAPTER 5 -	IMPLEMENTATION OF A MICROPROCESSOR AIDED MEASURING SYSTEM	
5.1	Introduction	109
5.2	Basic System	114
5.3	System Hardware	116
5.4	System Software	118
5.5	Software Operation	128
5.6	Results	133
CHAPTER 6 -	CONCLUSIONS AND RECOMMENDATIONS FOR FURTHER WORK	
6.1	Conclusions	135
6.2	Recommendations for Further Work	136
CHAPTER 7 -	BIBLIOGRAPHY	139
APPENDICES		
1.	Symbol Definitions and Units	149
2.	Basic Magnetic Field Relationships and Coordinate Systems	151

3.	Bessel Functions	154
4a.	Basic Computer Program for Rigorous Mathematical Model	156
4b.	Basic Computer Program for Simplified Mathematical Model	164
5.	Composition of Brass and Aluminium Bars	166
6.	Determination of Magnetic Field Strength for a Single Wire Loop	167
7.	Assembled Program for Eddy Current Gauging	169

FIGURES AND TABLES

<u>FIGURES</u>	<u>Page No.</u>
3.1 Sectional view of the coil and metal sample arrangement	19
3.2 Coordinate system for the inducing coil	22
3.3 Phasor diagram for the rigorous mathematical model, cylindrical case, for an infinitely long coil, at various heights above the metallic surface	35
3.4 Assumed variation of the current density for a coil of finite length	37
3.5a Phasor diagram for the rigorous mathematical model, cylindrical case, for a short coil at various heights above the metallic surface	39
3.5b Phasor diagram for the rigorous mathematical model, cylindrical case, for a long coil at various heights above the metallic surface	40
3.6a Phasor diagram for the simplified mathematical model, for a short coil, at various heights above the metallic surface	49
3.6b Phasor diagram for the simplified mathematical model, for an infinitely long coil, at various heights above the metallic surface	51
3.7 Sectional view of the metal bar and coil arrangement	53
3.8 Line integral direction for probe coil	53
3.9 Phasor diagram showing the relationship between the emf's induced in the probe coils	56
3.10 Phasor diagram showing the elimination of the effect of probe coil height	56
4.1 Coil holder, support and base with 25.4 mm (1.00 in) diameter mild steel bar	64

	<u>Page No.</u>
4.2 Sectional view of probe coil and large outer coil	65
4.3 Circuit diagram showing the relationship between the probe coil and the external drive for the inducing coil	67
4.4 Concentrated coil for magnetic field strength determination	69
4.5 Graph to show magnetic field strength measurements using probe coils with close spacing, compared with theoretical values	73
4.6 Graph of surface impedance against frequency, measured for an aluminium bar of diameter 25.4 mm (1.00 in)	77
4.7a/b Circuit diagrams for probe coil amplifiers	79
4.8 Graph to show phase variation (error) with frequency for voltage proportional to surface impedance for a 25.4 mm (1.00 in) diameter aluminium bar	80
4.9 Graph to show variation of probe coil voltage with axial displacement	82
4.10 Graph to show variation of probe coil voltage with axial displacement after modification of outer coil	83
4.11 Circuit diagram for constant current source for coil segments	85
4.12 Graph of surface impedance against frequency, measured for a 25.4 mm (1.00 in) diameter mild steel bar	87
4.13 Graph of surface impedance against frequency measured for a 25.4 mm (1.00 in) diameter mild steel bar, for various magnetic states	89

	<u>Page No.</u>
4.14 Magnetic saturation and water cooling system	91
4.15 Cascaded R-C filters	95
4.16 Variation of the voltage proportional to surface impedance, for a mild steel bar, compared with the voltage producing the 50 Hz magnetic field	96
4.17a/b Variation of voltage proportional to surface impedance for a) non-metallic bar and b) aluminium bar, when subject to the 50 Hz magnetic field	97
4.18 Variation of voltage proportional to surface impedance for a mild steel specimen subject to a 50 Hz magnetic field	99
4.19 Representation of the phase angle of the voltage proportional to surface impedance for the mild steel specimen in its demagnetised state	99
4.20a/b Measurement of the phase angle of the voltage proportional to the surface impedance for a mild steel bar at maximum magnetisation	100
4.21 Phasor diagram for the eddy current gauging system	102
4.22 Graph of measured coil height against frequency for a 25.4 mm (1.00 in) mild steel bar	104
4.23 Graph of measured coil height against frequency for a 25.4 mm (1.00 in) diameter non-ferrous (aluminium) bar	105
5.1 Diagram showing the measurement period for the 10 kHz probe coil waveform	113
5.2 Block diagram for the microprocessor aided measuring system	115
5.3 Waveforms for the microprocessor aided measuring system hardware	117

5.4	Eddy current gauging system timing relative to the 10 kHz waveform	119
5.5	Flow chart for the microprocessor aided measurement system	122

TABLES

	<u>Page No.</u>
4.1 Mean radii of probe coils used for the magnetic field strength measurement	71
5.1 Memory map of RAM	129
5.2 Typical measurement for the microprocessor based eddy current gauging system	131

ACKNOWLEDGEMENTS

The author wishes to express his gratitude to Professor H Sutcliffe who supervised this research, for his guidance and encouragement throughout the course of its progress. The author is also indebted to Preston Polytechnic for providing equipment and financial backing for the project. Thanks are also due to my colleagues, both at the University of Salford and at Preston Polytechnic and especially Mr W Cobb and Mr A P Lowe, for their many suggestions during the research project, and to Mrs S Wasson for her patience and skillful typing of this thesis. Finally, I thank my wife Patricia for her never-failing sympathy and encouragement during the course of the project.

ABSTRACT

The work presented in this thesis describes some theoretical and experimental aspects of the relationships between electromagnetic fields and a non-contact type of eddy current gauge, which utilises a cylindrical solenoid and coaxially positioned metallic bar, either ferrous or non-ferrous.

A rigorous mathematical analysis of the eddy current gauging system is presented, together with an evaluation of the solutions produced. This rigorous mathematical treatment is simplified, and the mathematical model thus produced is verified experimentally.

The simplified mathematical model is used as a basis for a practical eddy current gauge operating at a frequency of 10 kHz, using ferrous or non-ferrous metal. A novel technique is then described in which the simplified mathematical model is used as part of a practical microprocessor-aided eddy current gauging system, which allows appropriate compensation to be introduced into the system for ferrous metallic conductors with magnetic flaws present. This system uses a type of magnetic saturation technique.

CHAPTER 1 INTRODUCTION

1.1 Preliminary Remarks

The research reported in this thesis is mainly concerned with the problems associated with non-contact eddy current gauging; in particular, of metallic cylindrical bars, of the ferrous and non-ferrous type.

In the metal forming industries there is a requirement for the non-contact type of eddy current gauge as opposed to the contact type of gauge. A contact distance gauge relies for its operation on two polished diamond points, spring loaded against the metal surfaces, and a measuring system to determine the separation of these points. This type of mechanical distance gauge suffers from a number of disadvantages and defects, the major ones being the tendency of the gauge to produce mechanical damage to the metallic surface and the fact that only the distance between the diamond points is measured.

Electrical eddy current gauges at present have only a limited use when used for gauging with ferrous materials, however a number of successful eddy current gauges have been produced for use with sheet metals of the non-ferrous type. Some of these gauges work at frequencies where the metal sheet appears to be thin, ie where the skin depth is small, and the sheet conductivity is known. Others use a transmission type of system, in which the effects of the conductivity of the metal may be eliminated, but where the sheet thickness may be accurately determined. These type of gauges, however, have tended to be limited to non-ferrous sheet material,

whereas the metal forming industries also produce a considerable quantity of ferrous type material.

The apparent absence of an eddy current gauge for this situation was the stimulation for the work presented in this thesis. The eddy current gauge considered was of the cylindrical type, which may be used on ferrous or non-ferrous solid bars of the order of 25 mm in diameter. The range of frequencies considered was large, typically kHz to MHz, but for practical implementation of this type of system, a particular frequency of operation was selected in order to satisfy theoretical and practical restraints which are outlined in Chapter 5.

The results of preliminary work, both theoretical and practical, indicated that an eddy current gauge of the type described above was feasible. When testing non-ferrous materials, such information as the test object's diameter, conductivity, and surface impedance was measurable. However with ferrous materials the problem was rather more intractable because of the variability of the permeability of the material and also the possibility that the sample may have become locally magnetised. It was also considered that other types of defect for example, rust, oil, heat spot and needle gun, may be a problem, however lack of time did not permit any detailed investigation to be carried out.

In order to overcome problems associated with the ferrous type of material, acceptable saturation techniques were introduced in order to make the permeability of the ferrous material more like that of

the non-ferrous type. This method also has the advantage of overcoming the problem of localised magnetic fields in the ferrous material.

A practical microprocessor-aided eddy current measuring system was produced, which in principle was capable of dealing with both ferrous and non-ferrous types of material, however to make the eddy current measuring system somewhat less complex, the practical system was limited to the ferrous type of material. Please refer to Chapter 5.

The application of the theoretical and experimental work reported in this thesis and its suitability for use in an industrial environment is discussed in detail in Chapter 5, together with the possibility of extension of the methods employed to cover non-ferrous materials and other types and sizes of metal bars.

2.1 Review of Eddy Current Gauging

The story of eddy currents began in 1824 when Gambey discovered that if a copper plate was placed close to a suspended oscillating magnet, the motion of the magnet was rapidly damped. In 1825, Arago, contemporary of Fresnel, showed that when a magnetic needle was suspended above a spinning metallic disc, the needle was deflected in the direction of the rotation of the disc. The existence of eddy currents in a copper disc, moving in a strong magnetic field was actually discovered by J.B.L. Foucault, who also showed that there was a heating effect resulting from the flow of these currents. In 1831 Michael Faraday discovered electromagnetic induction, and as a result producing an explanation for effects observed by Gambey and Arago, which were in fact due to the induction of eddy currents.

The unification of this early work was attempted by the publication of James Clerk Maxwell¹ in 1873 of a *book* entitled simply, 'A Treatise on Electricity and Magnetism' and has had a major influence on very nearly every published work in Electrical Engineering, persisting up to the present day, and probably continuing into the future. The Treatise was presented with the intention of uniting the entire known body of electric and magnetic phenomena. The mathematical completeness of Maxwell's potential theory and the practical utility of his circuit theory have influenced all branches of Electrical Engineering since that date.

However, despite Maxwell's success in describing electric and magnetic phenomena, fundamentally that described by Maxwell's equations, the phenomenon known as 'eddy-currents', was never adequately dealt with, and is still a rather difficult and intractable subject.

The study of eddy currents in metals is basic to the understanding and application of eddy current gauging techniques, however a complete review of the subject, including its many and varied applications, is, as a result of its very generality, beyond the scope of this thesis. Consequently this literature review will be limited to work which is closely linked with eddy current gauging, although some work which is more general in its nature has been included when it is considered an important or fundamental contribution to the general topic.

The first published work on eddy currents in metallic conductors was produced by Maxwell² in 1872. This paper describes a method of moving image currents, which were used to calculate the resulting fields due to the eddy currents induced into a thin sheet of metal. The method employs a technique of step variation of the external current distribution. The problems posed by Maxwell in this paper were further investigated and extended to sinusoidal waveforms by Morecroft and Turner³ (1925), King⁴ (1933), Lyons⁵ (1933) and by Levy⁶ (1936). Levy formulated a method which could be used to determine the screening effect of thin metallic sheets of infinite extent, placed between concentric coils of similar size.

The problems associated with the energy loss, as a result of induced eddy currents in metal sheets, appear to have been investigated first by Marchant and Miller⁷ in 1926, where a good agreement between theory and practice was produced. Eddy current losses in cylindrical conductors were first considered in a theoretical study by McLachlan and Meyers⁸ in 1934. In this work the theory was restricted to thick tubes, however in a later paper⁹ (1935) this restriction was removed. In both cases the analysis was restricted to metal with a constant permeability, which would appear to exclude ferrous materials, unless saturation of the ferrous material may be achieved.

Theoretical problems associated with fields over conducting surfaces have been studied by Foster¹⁰ (1931), Price^{11,12} (1949, 1950) and Wait¹³ (1951). These papers generally consider the problems of fields in the presence of conducting half-space. The half-space generally used is a conducting earth, considered to be layered and/or bounded in most cases. The results quoted are in general applicable to geophysics and allied subjects, and thus will not be considered further.

The first major work on surface impedance and skin effect formulation appears to have been carried out by Reuter and Sondheimer¹⁴ (1948). This work was, however, limited to metal of semi-infinite extent, and also to non-ferrous metals. This last point however is not made clear by the authors. The paper considers variation of skin depth and surface impedance with both temperature and frequency. This work was further extended, but only on a theoretical basis by Dingle¹⁵ (1953) and Gordon and Sondheimer¹⁶ (1953).

Much of the early work on eddy current thickness gauging was carried out by Förster¹⁷ and presented in a series of papers up to 1954. He describes the use of single sided and bilateral gauges, and uses phase sensitive detection methods in order to measure thickness and to eliminate possible errors caused by 'lift off' and variations in electrical conductivity.

As a result of this early work by Förster one of the first commercial applications of eddy current testing was reported by Cannon¹⁸ (1953). He describes the operation of several types of eddy current instruments, which are capable of measuring conductivity, detecting of cracks in metallic samples, and a coating thickness meter which it was claimed would function with both ferrous and non-ferrous metals. The frequency of operation for the conductivity meter was given as 60 kHz but for the other instruments no detailed principles of operation were given. Brenner and Garcia-Rivera¹⁹ (1953) also reported a thickness gauge based on the principle of skin depth of the metal, and a bridge circuit used to produce a deflection proportional to thickness.

Yates and Queen²⁰ (1954) produced an instrument based on a bridge circuit, which it was claimed would measure the plating thickness of a non-conductive cladding layer on a non-ferrous material. However, it is not clear from the paper, how sensitive the thickness measurement is to variations in the conductivity of the sample.

The work started by Förster was further continued and extended by Hochschild²¹ (1954). This work is mainly concerned with the

detection of defects in non-ferrous metallic cylindrical bars of various diameters. In 1954 Hochschild²² also produced a much cited work on the theory of eddy current testing. In this work much of the theory which had been omitted from his previous work was included.

Coating thickness measurement was further extended in 1954 and 1956 by Waidelich^{23,24,25}, when he used pulsed eddy currents to measure thickness. Refinements to the instrumentation and measuring systems for this type of thickness gauge was also carried out by Renken and Meyers²⁶ (1959), who developed an eddy current testing system which used a double pulse type arrangement. This system was further extended in 1960 by Renken²⁷ who reported on a through transmission type of system, again using pulsed eddy currents.

Libby²⁸ (1956) outlined the basic principles of eddy current tests, using, in his case, two coils. He demonstrated the use of a cathode ray oscilloscope to display phase and amplitude information, and also how the effects of conductivity, sample surface defects and lift-off error may be eliminated.

In the late 1950's, the theoretical understanding of eddy currents had reached the stage where the problems associated with flaw detection in small diameter metal pipes and tubes could be attempted. Work in this field was carried out by McClurg²⁹ (1957), Allen and Oliver³⁰ (1957), Robinson and Perriam³¹ (1957-58), Graneau³² (1959) and Graneau and Swann³³ (1960). However, as flaw detection in metallic tubes is not specific to this project, the

detailed concepts will not be covered here.

A rather different method of using eddy currents was reported by Hochschild³⁴ in 1957. This system employed a type of phase sensitive detection. This type of detection, it was claimed, could detect flaws in metallic rods and bars. It was reported to be able to also measure 'hardness', conductivity, and the diameter of the bars. However only non-ferrous materials were considered, but selected test results were presented.

In 1959 Foerster³⁵ reported on an investigation made using eddy currents with metallic cylindrical objects, such as metal rods or tubing. The arrangement used was that of a fixed cylindrical coil surrounding the test object, with or without an air space between the coil and the test object. The problems associated with defects, cracks in the test objects, and an extensive range of test results were given.

The work presented by Foerster in early 1959 was also presented in late 1959 by McLurg³⁶, the two papers being almost identical.

The problems associated with eddy currents induced in a solid metallic body by a circular coil placed above, were discussed by Hammond³⁷ in 1962, but with particular reference to rotating machines. However this approach is of a somewhat general nature and his conclusions are equally applicable to other eddy current problems. Hammond's basic conclusions are that the eddy currents induced in a metallic 'slab' by a circular current loop are dependent upon three factors: i) the ratio of the distance of the

coil to the slab, to the coil radius, ii) the relative permeability of the slab, iii) the ratio of the coil radius to the skin depth. It was also concluded that the impedance of the slab has a phase angle of 45° assuming a constant relative permeability. In his method of analysis Hammond uses the method of magnetic images which he fully described³⁸.

Applications of circular coils to the art of eddy current thickness gauging was further advanced and extended in 1964 by Dodd³⁹. In his paper he described an instrument which was capable of measuring the thickness of a non-ferrous sample using a large circular driving coil, with smaller co-axial probe coils. The change in phase of the probe coil voltage gave a measure of the metal thickness. This approach was further refined and extended in 1968⁴⁰ when Dodd reported on a portable phase-sensitive eddy current instrument. This instrument, it was claimed, could measure thickness and also detect small flaws in the metal, at a depth of up to 2.54 mm (0.10 in) for a flaw diameter of 0.710 mm (0.0280 in).

In 1966 McMaster⁴¹ reported on a further variation of eddy current methods. This method involved a circular coil over a conducting surface, but used in conjunction with a Hall effect device, for detecting magnetic fields, located on the metallic surface. This type of arrangement, together with associated amplification and detection circuits, was claimed to be able to measure magnetic permeability, conductivity and coating thickness for both ferro-magnetic and non-ferro-magnetic conductors over a frequency range of 20 Hz to 100 kHz. As no detailed mathematical analysis of the theoretical basis of the method was presented, the author has

doubts as to the validity of the method for the ferro-magnetic materials at low frequency, ie below about 50 kHz. However the method appears to be valid for non-ferro-magnetic materials over the frequency range indicated.

In the mid to late 1960's, with the rapid growth in the semiconductor industries, computers of ever greater size were being produced. As a result, it became a possibility that the solution to some eddy current problems could be attempted on these new machines. The results produced by these machines would be numerical solutions to the analysis of eddy current problems being considered at the time.

It appears that the solution of the basic wave equation was first presented in 1967 by Moser⁴². This preliminary work was further extended and improved by Ryan⁴³ (1967) and Bannister^{44,45} (1968 and 1969).

In 1962 Russell, Schuster and Waidelich⁴⁶, produced an analysis for the impedance of a coil in the proximity of a ferrite core, with the assembly placed near to a sheet of metallic non-ferrous material. This type of analysis was further extended by Vine⁴⁷ (1964) who, included in his analysis, the case where the conducting sheet was of finite thickness and variable conductivity. Vine also used a digital computer to derive the numerical solutions to his analysis.

Cheng⁴⁸ (1965) also considered the same type of coil problem as Vine had, and further extended the solution by formulating the

analysis as a boundary value problem, and then solving the wave equations for the resulting magnetic vector potential. Chang also extended his method to the case of the stratified media.

By 1967 Dodd and Deeds⁴⁹ were presenting analytical solutions to eddy current problems based on a two layered conducting rod (non-ferrous), surrounded by a delta-function coil. The computer solution presented used the 'BASIC' computer language and the numerical solutions produced, no time factor given, are claimed to give the coil impedance for any distance above the conductor and for any, constant, conductivity of the conductor combination. The method is limited, however, to non-ferrous conductors.

This analytical work by Dodd and Deeds was extended to various other coil arrangements⁵⁰, and by 1969 a range of six or more differing coil arrangements has been analysed and solutions, with a claimed accuracy of 0.1% obtained. However, it was stated that the solutions were rather more inaccurate for lower frequencies, with no figures being quoted, and the conducting materials used in each case were non-ferrous.

The majority of eddy current problems thus far considered have been with the non-ferrous type of materials. The apparent lack of interest in ferrous materials is very easily explained. Non-ferrous materials have a linear B/H relationship, which is readily assimilated in any eddy current analysis. However the same may not be said of most ferrous materials.

One of the first attempts to quantify eddy currents in ferrous materials was reported by Lim and Hammond in 1970⁵¹. This paper

consisted of the production of a loss chart for the calculation of eddy currents in thick steel plates. The basis of the loss calculations are with reference to the saturation effects in the steel, while the B/H characteristic is represented by the Frohlich equation and the losses computed using a numerical finite-difference scheme. The accuracy claimed is 10% without taking into account the hysteresis loss. Hammond and Lim further refined their method in 1972⁵², and produced a numerical method for the determination of the electromagnetic field in saturated steel plates. The method used was that based upon the Dufort-Frankel analysis, for the solution of the non-linear diffusion equation that arises in the study of flux and current penetration into saturated steel plates.

In 1972 O'Kelly⁵³ extended the prediction of losses in steel plates, to include those of both eddy currents and hysteresis. His method used the complex permeability to relate B to H, but the method neglects any harmonic quantities. The method appears to be accurate to within about 5%, depending on the thickness of the steel plates. However only two frequencies were considered, namely 50 Hz and 70 Hz. Hence the extension of this method to higher frequencies must be considered rather doubtful.

Whilst progress on the theory of eddy currents and eddy current gauging was making steady gains, it is perhaps instructive, at this point, to consider the type and range of practical instruments which were available using the principles of eddy currents. In general, at this time (early 1970's) only non-ferrous materials (aluminium, brass etc) were being tested, by the use of eddy current techniques in a manufacturing environment.

In 1970 Regan and Potsco⁵⁴ reported on an instrument which it was claimed was capable of identifying defects in aluminium strips, which at this time, could be produced at a maximum rate of 670 m/s (2,200 ft/s). The information regarding the defects, together with a considerable quantity of noise, was recorded on a suitably positioned chart recorder. However, no detailed theory regarding the method was presented.

In 1971 Reynolds⁵⁵ presented a review of the range of differing types of contact and non-contact gauges, indicating the accuracy of measurement in each case. The paper, however, states that eddy current gauges are not generally used because they suffer from problems arising from the variation of the resistivity of the sample. This paper is basically a review of non-electrical types of strip thickness gauges. In 1972 Hutcheson⁵⁶ gave a wide ranging practical description of several types of eddy current instruments used for thickness gauging. Again, however, no detailed theory was presented. Birchenough and Marshall⁵⁷ gave a review of three differing principles of the electrical measurement of coating thickness. For example paint on a metal base. From the review it would appear that the eddy current method of coating thickness measurement gave the best accuracy and also the promise of the most improvement for the future.

The theory of eddy current testing was extended in 1972 by Jones and Pezdirtz⁵⁸ when they extended the work began by Waidelich²⁵ (1956), McMaster⁴¹ (1966) and Dodd et al⁵⁰ (1969). The analysis presented was a closed form expression for the magnetic field of a semi-infinite coil above a semi-infinite non-ferrous medium and

also considered was the case of a single loop of wire above a semi-infinite medium. The results of the analysis were then used to determine the conductivity of the semi-infinite conducting medium.

Also in 1972 Scheiber⁵⁹ made a fundamental contribution to eddy current theory by outlining a method of approach with a view to obtaining a solution of the transient eddy currents in thin metallic sheets. These sheets, however were of the non-magnetic type and few practical results were quoted.

Callarotti and Alfonzo⁶⁰ (1972) used an eddy current method to measure the conductivity of metallic cylinders, based on a sound eddy current analysis of the experimental situation. They also pointed out a number of errors made by previous authors.

Birtles^{61,62} (1972) presented two papers in which he produced a closed-form expression for the magnetic scalar potential field due to a single-layer cylindrical coil. The resulting expression was in a form which could be evaluated using a digital computer.

In 1974 Sutcliffe⁶³ presented a paper outlining the principles of distance gauging in relation to metallic surfaces, both magnetic and non-magnetic. This paper discusses some of the problems associated with the measurement of the surface impedance (Z_s) and its apparent 45° phase angle. In a second paper by Sutcliffe in 1977⁶⁴ the principles of eddy current gauging were extended and improved and the principle of the measurement of the surface impedance at a frequency of the order of MHz was outlined. Also discussed were

some of the problems associated with surface defects and contaminations.

This second paper by Sutcliffe forms the basis for much of the work associated with this thesis, but it was also extended into bi-lateral gauging by Ball⁶⁵ 1979 and by Ball and Staniforth⁶⁶ in 1981.

However the treatment was limited to non-ferrous materials.

Bi-lateral gauging is not considered in detail in this thesis, but this development does indicate an additional area to which eddy current gauging has been extended from the original paper by Sutcliffe in 1977⁶⁴.

Since the late 1970's a considerable number of general papers on eddy currents have been published. However none of these appear to have specifically dealt with the problems discussed in this thesis. For example in a series of papers^{67,68,69} Balchin and Davidson present a method of 3-dimensional eddy current calculations. Their method is obviously attractive, but by making reference to papers they quote⁷⁰, it is apparent that the method is limited to power frequencies. Surprisingly the frequency of operation is omitted and no comment is made on the frequency range for which their method is valid. It is thus reasonable to assume that the method will not be valid for frequencies much above 50 Hz.

It is now clear, and evident from the paper by Sutcliffe in 1977⁶⁴, that for relatively low frequency applications, of the order of a few kilohertz, the parameter denoted by the term surface impedance, and in particular the measurement of that quantity, is of considerable importance when discussing eddy current gauges. It is important that techniques for the accurate measurement of the

surface impedance be developed for eddy current gauging at the relatively low frequencies considered in the work reported on in this thesis. This type of measurement is very important to the application of eddy current gauges to the problems of gauging for on-line strip gauging in steel rolling mills. In particular it is important to know how the surface impedance varies with magnetisation of the steel surface. Measurements with this type of contamination is discussed in detail in Chapter 4.

It is considered that the principles outlined in this thesis have significantly improved and extended the theory of eddy current gauging. In particular the range of frequency of operation of the eddy current gauge has been extended down to frequencies of the order of a few kilohertz, see Chapter 3 for detailed analysis of the eddy current gauge at this frequency. Also the type of metallic conductor which may be used has been extended to include that of a cylindrical conductor either solid or tubular, and either ferrous or non-ferrous materials. However it should be noted that if a tubular material is used, the frequency of operation for the eddy current gauge must be such that the skin depth is small when compared with the thickness of the tube wall. A factor of ten is considered to be well into the safe region of operation.

It is demonstrated in Chapters 3 and 4 that the analysis of the distance gauging system, using cylindrical coordinates, may be approximated to by the use of cartesian coordinates, although the exact approach requires the use of cylindrical coordinates. However this type of analysis is somewhat complex and contains many difficulties and pitfalls for the unwary. The author, however,

considers that by the extensive use of modern sophisticated computing techniques and by continually comparing the results so obtained, with practical measurements, a good agreement between the theoretical mathematical model and the practical measurements has been achieved, see Chapters 4 and 5.

In particular, it is felt that the extension of the theory of eddy current gauging down to a frequency of a few kilohertz, with both magnetic and non-magnetic specimens, is a significant contribution to the theory of eddy current gauging. It must be noted, however, that there are still several broad problem areas remaining before the theory may be said to be complete.

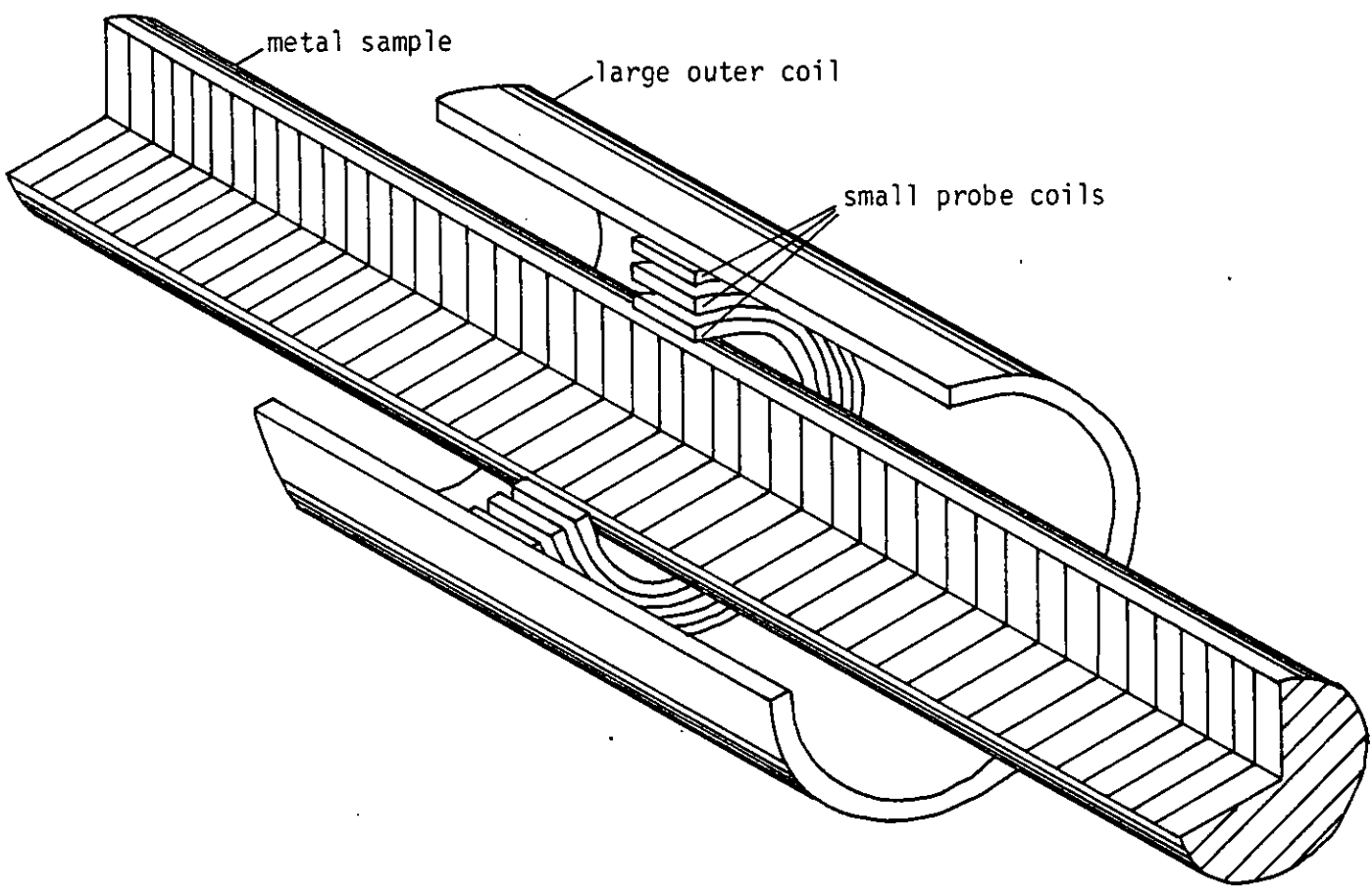


Figure 3.1 Sectional view of the coil and metal sample arrangement

CHAPTER 3 THEORETICAL ANALYSIS3.1 Introduction

This chapter deals with the detailed mathematical analysis of the eddy current gauging system. In the mathematical modelling which follows, the concept of surface impedance is an important factor, and it is this factor which differentiates between the behaviour of ferrous and non-ferrous bar material, the latter having significantly lower values of surface impedance. In the detailed analysis which follows, it is assumed that the bar material may be specified by constant values of permeability and conductivity; consequently the field equation for both ferrous and non-ferrous bars will be of the same form.

The quantitative results of this chapter and also the results of the experimental work presented in Chapter 4, relate basically to bars of 25.4 mm (1.00 in) diameter, since bars of this size are readily available in a variety of materials, such as mild steel, brass and aluminium.

In all eddy current gauging systems a broad principle, which is usually adopted, is to operate with frequencies sufficiently high to ensure that the skin-depth is small when compared with the required dimension. This assumption will be made in the case of the analysis which follows, thus permitting a slightly simplified treatment of the boundary conditions at the discontinuity between the metal and air.

The arrangement of coils and the metallic bar used during this research project is shown in section, in Figure 3.1. The analysis

is largely directed towards an understanding of the basic principles of the system's behaviour, as derived from Maxwell's original electromagnetic equations. The treatment is initially rigorous, however, for a number of practical reasons, which will be discussed later, it will be shown that appropriate approximations may be introduced to the system's mathematical model, accompanied by only minimal loss of precision, but thus enabling the eddy current gauging system to be readily implemented and understood from a practical view point.

3.2 Mathematical Model

In order to proceed with the theoretical analysis it is necessary to understand the physical constraints regarding the metallic bar.

The metal bar is excited by an external magnetic field, provided by a relatively long solenoid of approximately 50 mm (2.0 in) diameter, which was placed coaxially with the metallic bar as shown in Figure 3.1 and 3.2. The small probe coils, placed between the metallic bar and the large outer coil, shown in Figure 3.1, are for measurement purposes. The precise arrangement of these probe coils is discussed in detail in Chapter 4.

The basic arrangement of the metallic bar and the large outer coil is that of a cylinder. This immediately suggests that for any mathematical model to describe the system rigorously, a cylindrical coordinate system should be employed. Appendix 2 gives the basic magnetic field relationships for the coordinate system used.

For the type of system shown in Figure 3.2, the basic mathematical forms of Maxwell's equations in a source-free region are given in

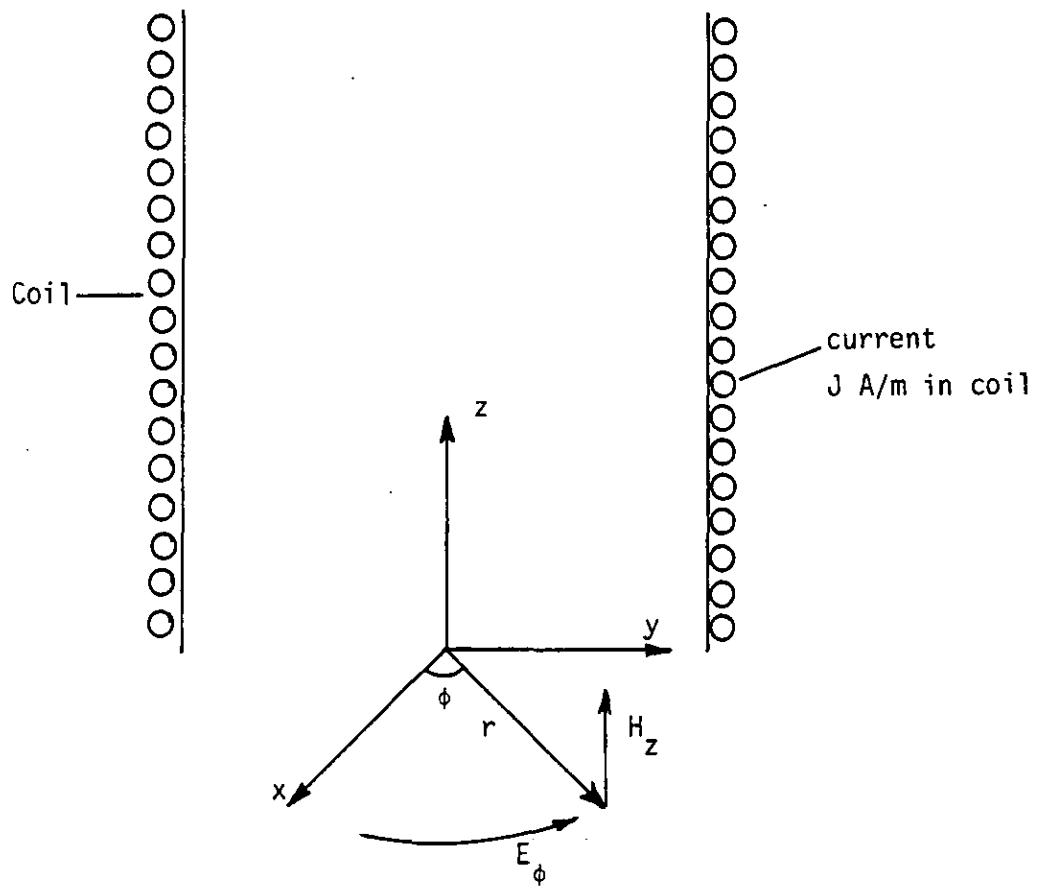


Figure 3.2 Coordinate System for the Inducing Coil

Appendix 2 and are repeated here for convenience.

$$\nabla \times \underline{E} = \frac{-\partial \underline{B}}{\partial t} \dots\dots\dots 3.1$$

and $\nabla \times \underline{H} = \underline{J} + \frac{\partial \underline{D}}{\partial t} \dots\dots\dots 3.2$

For sinusoidal waveforms then, employing phasors:

$$\nabla \times \underline{E} = -j\omega \underline{B} = -j\omega \mu \underline{H} \dots\dots\dots 3.3$$

and $\nabla \times \underline{H} = \underline{J} + j\omega \underline{D} = (\sigma + j\omega \epsilon) \underline{E} \dots\dots\dots 3.4$

For the system detailed in Figure 3.2, E_ϕ is the only non-zero component of the \underline{E} field, ie E_z and E_r are both zero. Hence using the system of cylindrical coordinates, see Appendix 2, and setting $E_z = E_r = 0$ gives:

$$\frac{\partial E_\phi}{\partial z} = j\omega \mu H_r \dots\dots\dots 3.5$$

and $\frac{\partial}{\partial r}(rE_\phi) = j\omega \mu r H_z \dots\dots\dots 3.6$

also $\frac{\partial H_r}{\partial z} - \frac{\partial H_z}{\partial r} = (\sigma + j\omega \epsilon) E_\phi \dots\dots\dots 3.7$

For the region outside the metal conductor, $\sigma \ll \omega \epsilon$. However for the region within the high conductivity metal, $\sigma \gg \omega \epsilon$.

Hence $(\sigma + j\omega \epsilon) = \sigma$

Equation 3.7 then becomes, within the metal

$$\frac{\partial H_r}{\partial z} - \frac{\partial H_z}{\partial r} = \sigma E_\phi \quad \dots\dots\dots 3.8$$

From equation 3.5

$$\frac{1}{j\omega\mu} \frac{\partial^2 E_\phi}{\partial z^2} - \frac{\partial H_r}{\partial z} = \sigma E_\phi \quad \dots\dots\dots 3.9$$

and from equation 3.6

$$\frac{\partial H_z}{\partial r} = \frac{-1}{j\omega\mu} \frac{\partial}{\partial r} \left[\frac{1}{r} \frac{\partial}{\partial r} (rE_\phi) \right] \quad \dots\dots\dots 3.10$$

$$\frac{\partial H_z}{\partial r} = \frac{-1}{j\omega\mu} \left[\frac{\partial^2 E_\phi}{\partial r^2} + \frac{\partial E_\phi}{\partial r} \frac{1}{r} - \frac{E_\phi}{r^2} \right] \quad \dots\dots\dots 3.11$$

Combining equation 3.9 and 3.11, and substituting in equation 3.8 gives:

$$\frac{1}{j\omega\mu} \left[\frac{\partial^2 E_\phi}{\partial r^2} + \frac{\partial E_\phi}{\partial r} \cdot \frac{1}{r} - \frac{E_\phi}{r^2} \right] + \frac{1}{j\omega\mu} \frac{\partial^2 E_\phi}{\partial z^2} = \sigma E_\phi \quad \dots\dots\dots 3.12$$

It is now necessary to introduce variation in the z direction by considering a single sinusoidal component of a general z variation. Appropriately the following relationship is introduced.

$$E_\phi = A \cos z/\ell \quad \dots\dots\dots 3.13$$

where A is a function of r only.

$$\therefore \frac{\partial E_{\phi}}{\partial z} = \frac{-A \sin z/\ell}{\ell}$$

$$\text{and } \frac{\partial^2 E_{\phi}}{\partial z^2} = \frac{-A \cos \frac{z}{\ell}}{\ell^2} = \frac{-E_{\phi}}{\ell^2} \dots\dots\dots 3.14$$

substituting for $\frac{\partial^2 E_{\phi}}{\partial z^2}$ in equation 3.12 yields

$$\frac{1}{j\omega\mu} \left[\frac{\partial^2 E_{\phi}}{\partial r^2} + \frac{\partial E_{\phi}}{\partial r} \cdot \frac{1}{r} - \frac{E_{\phi}}{r^2} \right] - \frac{E_{\phi}}{j\omega\mu\ell^2} = \sigma E_{\phi}$$

rearranging gives:

$$r^2 \frac{\partial^2 E_{\phi}}{\partial r^2} + r \frac{\partial E_{\phi}}{\partial r} - E_{\phi} \left[1 + \frac{r^2}{\ell^2} + j\omega\mu\sigma r^2 \right] = 0 \dots\dots\dots 3.15$$

$$\therefore \frac{\partial^2 E_{\phi}}{\partial r^2} + \frac{1}{r} \frac{\partial E_{\phi}}{\partial r} - E_{\phi} \left[\frac{1}{r^2} + \frac{1}{\ell^2} + j\omega\mu\sigma \right] = 0 \dots\dots\dots 3.16$$

Equation 3.16 is a modified Bessel equation and its solution contains modified Bessel functions of the first and second kinds. Appendix 3 shows the relationships for the various types of Bessel function.

Solving equation 3.16 yields

$$E_{\phi} = A_1 I_1 \left[\left(\frac{1}{\ell^2} + j\omega\mu\sigma \right)^{\frac{1}{2}} r \right] + B_1 K_1 \left[\left(\frac{1}{\ell^2} + j\omega\mu\sigma \right)^{\frac{1}{2}} r \right] \dots\dots\dots 3.17$$

where A_1 and B_1 are constants.

The first term of equation 3.17 represents the inward or incident part of the wave, and the second term represents the outward or reflected part of the wave.

It should be noted that in the case of the metal bar; the attenuation of the field within the metal is high. Thus, in practice, the reflected field, in the metal, does not exist.

It is now convenient, for the moment, to limit the analysis to the case of an infinitely long uniformly wound solenoid. In which case \underline{J} and hence \underline{H} will be uniform, and the quantity ℓ will be correspondingly large. The function $(1/\ell^2 + j\omega\mu\sigma)^{\frac{1}{2}}$ will tend to $(j\omega\mu\sigma)^{\frac{1}{2}}$.

Consider now the term which represents the incident part of the wave; the only part to exist, in practice, in the metal. Thus from equation 3.17

$$E_{\phi} = A_1 I_1 (r [j\omega\mu\sigma]^{\frac{1}{2}}) \dots\dots\dots 3.18$$

Combining equation 3.18 with equation 3.6 gives:

$$\frac{\partial [r A_1 I_1 \{r(j\omega\mu\sigma)^{\frac{1}{2}}\}]}{\partial r} = -j\omega\mu r H_z$$

$$\therefore H_z = \frac{A_1}{-j\omega\mu r} \left[I_1 \{r(j\omega\mu\sigma)^{\frac{1}{2}}\} + r \frac{\partial I_1}{\partial r} \{r(j\omega\mu\sigma)^{\frac{1}{2}}\} \right]$$

However, from McLachlan, reference 71 page 163

$$\frac{\partial I_1 [r(j\omega\mu\sigma)^{\frac{1}{2}}]}{\partial [r(j\omega\mu\sigma)^{\frac{1}{2}}]} = \frac{-I_1 [r(j\omega\mu\sigma)^{\frac{1}{2}}]}{r} + I_0 [r(j\omega\mu\sigma)^{\frac{1}{2}}]$$

and $\frac{\partial [r(j\omega\mu\sigma)^{\frac{1}{2}}]}{\partial r} = (j\omega\mu\sigma)^{\frac{1}{2}}$

$$\therefore H_z = \frac{A_1}{-j\omega\mu r} \left[I_1 \left\{ r(j\omega\mu\sigma)^{\frac{1}{2}} \right\} + (j\omega\mu\sigma)^{\frac{1}{2}} r \left\{ -\frac{I_1 \left\{ r(j\omega\mu\sigma)^{\frac{1}{2}} \right\}}{r(j\omega\mu\sigma)^{\frac{1}{2}}} + I_0 \left\{ r(j\omega\mu\sigma)^{\frac{1}{2}} \right\} \right\} \right]$$

$$H_z = \frac{A_1 (j\omega\mu\sigma)^{\frac{1}{2}}}{-j\omega\mu} \left[I_0 \left\{ r(j\omega\mu\sigma)^{\frac{1}{2}} \right\} \right] \dots\dots\dots 3.19$$

Substituting for A_1 from equation 3.18 gives

$$\frac{E_\phi}{H_z} = -\left(\frac{j\omega\mu}{\sigma}\right)^{\frac{1}{2}} \frac{I_1 [r(j\omega\mu\sigma)^{\frac{1}{2}}]}{I_0 [r(j\omega\mu\sigma)^{\frac{1}{2}}]} \dots\dots\dots 3.20$$

The impedance for the wave is given by Schelkunoff, reference 72, page 273 as $-E_\phi/H_z = Z_\omega$

$$Z_\omega = \left(\frac{j\omega\mu}{\sigma}\right)^{\frac{1}{2}} \frac{I_1 [r(j\omega\mu\sigma)^{\frac{1}{2}}]}{I_0 [r(j\omega\mu\sigma)^{\frac{1}{2}}]} \dots\dots\dots 3.21$$

Thus at the surface of the metal bar, the impedance is given by

$$\frac{E_s}{H_s} = \left(\frac{j\omega\mu}{\sigma}\right)^{\frac{1}{2}} \frac{I_1 [r_0(j\omega\mu\sigma)^{\frac{1}{2}}]}{I_0 [r_0(j\omega\mu\sigma)^{\frac{1}{2}}]} \dots\dots\dots 3.22$$

It should be noted that the term $r_0(j\omega\mu\sigma)^{\frac{1}{2}}$ will be large for the case considered in this thesis. Hence the term

$$\frac{I_1(r_0(j\omega\mu\sigma)^{\frac{1}{2}})}{I_0(r_0(j\omega\mu\sigma)^{\frac{1}{2}})} \longrightarrow 1$$

Thus equation 3.22 becomes

$$\frac{E_s}{H_s} = \left(\frac{j\omega\mu}{\sigma}\right)^{\frac{1}{2}} \dots\dots\dots 3.23$$

which is in accordance with the surface impedance for a plane wave or for a uniform plane H.

3.2.1 Long Solenoid, Cylindrical Case

At the surface of the metal bar, and from equation 3.23

$$Z_s = \frac{E_s}{H_s} = \left(\frac{j\omega\mu}{\sigma}\right)^{\frac{1}{2}}$$

The line integral of E at the metal surface and at a radius r is related to H by:

$$E_r \ 2\pi r - E_s \ 2\pi r_0 = j\omega\mu\sigma(\pi r^2 - \pi r_0^2) \ H \ \dots\dots\dots 3.24$$

$$\therefore 2\pi r E_r = 2\pi r_0 H \left[Z_s + j\omega\mu\sigma \left(\frac{r^2 - r_0^2}{2r_0}\right) \right]$$

$$\therefore E_r = \frac{r_0}{r} \left[Z_s + j\omega\mu \left(\frac{r^2 - r_0^2}{2r_0}\right) \right] \ H \ \dots\dots\dots 3.25$$

Evaluation of equation 3.25 will give the E field at the radius r. See section 3.3, page 34 for numerical evaluation of equation 3.25.

3.2.2 Short Solenoid, Cylindrical Case

Consider now the case of a short solenoid, and the region between this solenoid and the surface of the metal bar. For this air space the quantity $(1/\ell^2 + j\omega\mu\sigma)^{\frac{1}{2}}$ becomes $1/\ell$, where ℓ is related to the longitudinal sinusoidal variation in the field pattern, and the component to be considered is of the form $\cos(z/\ell)$. It should be noted that the longitudinal ⁱⁿ current density function for this type of short solenoid, may be resolved, by Fourier analysis into sinusoidal components, see section 3.3.2 page 36. This analysis considers one such component. However, by use of the principle of superposition, it is possible to extend the number of components used to any convenient number.

In the region above the metal there will be an incident and a reflected wave pattern or an inward and an outward field. This field pattern may be described in terms of the respective impedances as follows:

i) the incident field

$$\frac{E^-}{H^-} = Z^- \quad \dots\dots\dots 3.26$$

also

ii) the reflected field

$$\frac{E^+}{H^+} = -Z^+ \quad \dots\dots\dots 3.27$$

From equation 3.17 for the incident wave

$$E_{\phi} = E^{-} = A_1 I_1(r/\ell) \dots\dots\dots 3.28$$

Combining equation 3.28 with equation 3.6 gives

$$\frac{\partial [r A_1 I_1(r/\ell)]}{\partial r} = -j\omega\mu r H^{-} \dots\dots\dots 3.29$$

Using the relationship from McLachlan reference 71 page 163

$$\frac{\partial I_1(r/\ell)}{\partial r} = -\frac{I_1(r/\ell)}{r} + I_0(r/\ell) \dots\dots\dots 3.30$$

$$\therefore H^{-} = \frac{1}{j\omega\mu r} \left[r A_1 I_0(r/\ell) \right] \dots\dots\dots 3.31$$

The impedance of the wave is given by Schelkunoff reference 72, page 273 as $-E^{-}/H^{-}$

$$\text{Thus } \frac{E^{-}}{H^{-}} = \frac{j\omega\mu}{1/\ell} \frac{I_1(r/\ell)}{I_0(r/\ell)} \dots\dots\dots 3.32$$

$$Z^{-} = j\omega\mu\ell \frac{I_1(r/\ell)}{I_0(r/\ell)} \dots\dots\dots 3.33$$

Similarly for the reflected part of the wave and using the relationship from McLachlan reference 71 page 165

$$\frac{\partial K_1(r/\ell)}{\partial r} = -\frac{K_1(r/\ell)}{r} + K_0(r/\ell) \dots\dots\dots 3.34$$

then

$$Z^+ = \frac{E^+}{H^+} = j\omega\mu\ell \frac{K_1(r/\ell)}{K_0(r/\ell)} \dots\dots\dots 3.35$$

Consider now that the outer coil is a circulating current sheet of density \underline{J} per unit length. The \underline{E} field is continuous across the sheet, and from Schelkunoff, reference 72,

$$\frac{J}{E^-} = Y^+ + Y^- \dots\dots\dots 3.36$$

$$\therefore E^- = \frac{J}{Y^+ + Y^-} \dots\dots\dots 3.37$$

$$\text{Thus } H^- = \frac{E^-}{Z^-} = \frac{J}{1 + Z^-/Z^+} \dots\dots\dots 3.38$$

For the inward travelling wave, at the surface of the metal, the equations are:

$$E^-_{r_0} = A_1 I_1(r_0/\ell) \dots\dots\dots 3.39$$

$$\text{and } E^-_{r_c} = A_1 I_1(r_c/\ell) \dots\dots\dots 3.40$$

where r_c is the outer coil radius

$$\therefore E^-_{r_0} = E^-_{r_c} \frac{I_1(r_0/\ell)}{I_1(r_c/\ell)} \dots\dots\dots 3.41$$

Similarly for the \underline{H} field

$$H^-_{r_0} = H^-_{r_c} \frac{I_0(r_0/\ell)}{I_0(r_c/\ell)} \dots\dots\dots 3.42$$

Thus at any radius r , in the air space above the metal surface

$$E_r^- = E_{r_c}^- \frac{I_1(r/l)}{I_1(r_c/l)} \dots\dots\dots 3.43$$

and $H_r^- = H_{r_c}^- \frac{I_0(r/l)}{I_0(r_c/l)} \dots\dots\dots 3.44$

It is now necessary to consider the field after reflection at the surface of the metal bar. The \underline{E} and \underline{H} fields are continuous at the bar surface. Omitting suffixes to aid the presentation of the analysis gives:

$$E_s = E^- + E^+ \dots\dots\dots 3.45$$

and $H_s = H^- - H^+ \dots\dots\dots 3.46$

For the reflection of the \underline{E} field at the metal surface, it is convenient to introduce the reflection ratios

$$K_E = \frac{E^+}{E^-} \dots\dots\dots 3.47$$

and for the \underline{H} field

$$K_H = \frac{H^+}{H^-} \dots\dots\dots 3.48$$

and $Z_s = \frac{E_s}{H_s} = \frac{E^- + E^+}{E^-/Z^- - E^+/Z^+} \dots\dots\dots 3.49$

substitute for K_E in equation 3.49

$$Z_s = \frac{(1 + K_E)}{1/Z^- - K_E/Z^+} \dots\dots\dots 3.50$$

rearranging gives

$$K_E = \frac{Z^+ (Z_S - Z^-)}{Z^- (Z_S + Z^+)} \dots\dots\dots 3.51$$

Substitute for Z^+ and Z^- and from equation 3.48 above gives

$$K_H = \frac{H^+}{H^-} = \frac{(Z_S - Z^-)}{(Z_S + Z^+)} \dots\dots\dots 3.52$$

The reflected wave at the bar surface may now be found from these these two expressions.

For the reflected field, in the air space above the metal surface, the following relationships may be used, which are similar to the expressions of equations 3.43 and 3.44 for the incident field.

At a radius r , and re-introducing suffixes

$$E_r^+ = E_{r_0} + \frac{K_1(r/\ell)}{K_1(r_0/\ell)} \dots\dots\dots 3.53$$

and
$$H_r^+ = H_{r_0} + \frac{K_0(r/\ell)}{K_1(r_0/\ell)} \dots\dots\dots 3.54$$

Equations 3.43, 3.44, 3.53 and 3.54 represent expressions for the predicted field patterns produced by a solenoid surrounding a cylindrical metallic conductor.

Evaluation of the mathematical model produced in sections 3.2.1 and 3.2.2 is described in the next section.

3.3 Evaluation of Mathematical Model

The evaluation of the mathematical model for the cylindrical case is achieved in two stages. The first stage is for the case of a long solenoid as discussed in section 3.2.1 and the second stage is for the short solenoid of section 3.2.2.

3.3.1 Long Solenoid Cylindrical Case

It is instructive at this stage, to ascribe values associated with the mathematical model, however it will be left to a later section to comment on the practical justification and measurement of these parameters. Please see Chapter 4, where a detailed account may be found.

The following parameter values are regarded as appropriate at this stage:

Frequency: 10 kHz

Conductivity of the mild steel bar : 1×10^7 S/m

Relative permeability of steel: 200 (assumed)

Radius of mild steel bar: 12.7 mm (0.50 in)

It should be noted that whilst the value for relative permeability of the mild steel bar was assumed to be 200, the mathematical model is valid for all positive values of this parameter, whether these values may be measured or not. The measurement and/or prediction of accurate values for the relative permeability is not easy with this type of eddy current system, and thus a method has been developed to control the problem, details of which may be found in Chapter 4.

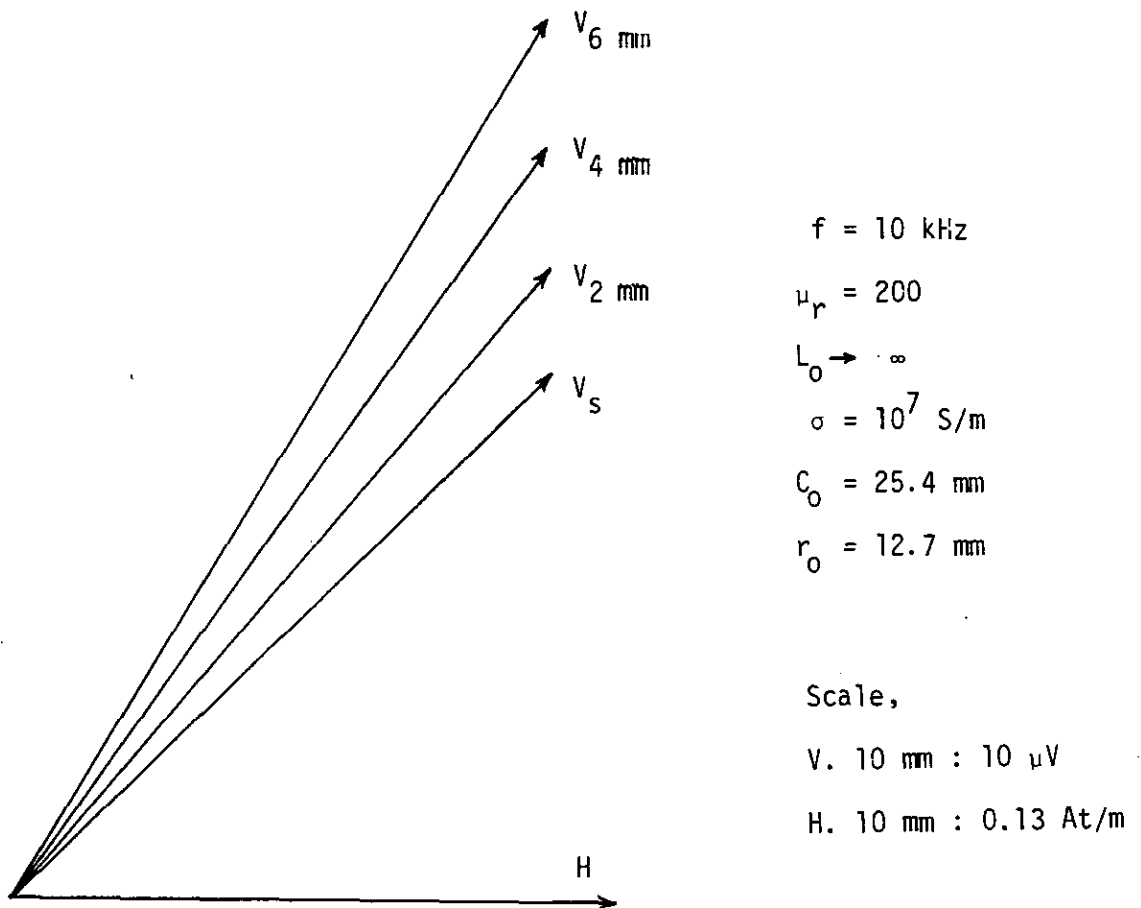


Figure 3.3 Phasor diagram for the rigorous mathematical model, cylindrical case, for an infinitely long coil, at various heights above the metallic surface

The evaluation of Z_s , the surface impedance, given by equation 3.22, page 27 and in particular $I_1(r(j\omega\mu\sigma)^{\frac{1}{2}})/I_0(r(j\omega\mu\sigma)^{\frac{1}{2}})$ may be evaluated using the computer program of reference 73 and modified to produce $I_0(x)$ and $I_1(x)$. Extensive checks on the accuracy of the program were achieved by using the tables of reference 74.

It is however clear that the ratio $I_1(r(j\omega\mu\sigma)^{\frac{1}{2}})/I_0(r(j\omega\mu\sigma)^{\frac{1}{2}})$ will be very close to unity at the frequency considered here, and thus the error introduced by assuming this ratio to be unity will be small.

For a very long coil, the longitudinal field will be almost constant, and thus using the parameter values given above, in association with equation 3.25 page 28, the following predicted values were produced. These values for convenience of representation, are shown in the phasor diagram of Figure 3.3. The values given by equation 3.25, page 28, are in the form of the \underline{E} field. In order that these values may be compared directly with the measurements made on the eddy current system, the following relationship between \underline{E} and V was made

$$V = 2\pi r E_r \dots\dots\dots 3.55$$

for the position of each probe coil.

3.3.2 Short Solenoid, Cylindrical Case

For the evaluation in section 3.3.1 above, it was assumed that the inducing coil was very long, and this resulted in a longitudinal field which was constant. This assumption of an infinitely long solenoid is clearly not valid for any practical coil, that is any

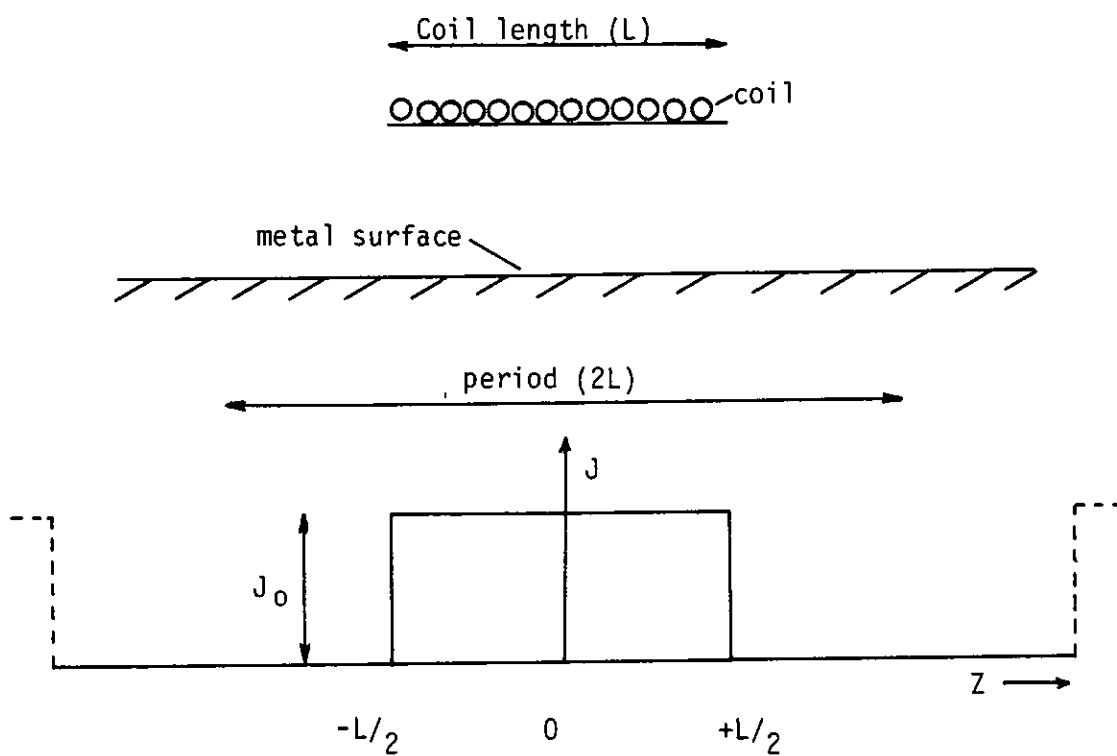


Figure 3.4 Assumed variation of the current density for a coil of finite length

axial coil which may be wound must have a finite length. Thus the longitudinal field will not now be constant.

For a longitudinal field which is not constant, it becomes necessary to assign some function to it. For convenience, this function will be of the form of a Fourier series, that is, it will have a number of differing frequency components. The most convenient form for the function is of the form shown in Figure 3.4. The mathematical form for this function, reference 75, is given by:

$$J_y = \frac{J_0}{2} + \frac{2J_0}{\pi} \left[\cos \frac{\pi z}{L} - \frac{\cos 3\pi z/L}{3} + \frac{\cos 5\pi z/L}{5} - \dots \right] \dots \dots \dots 3.56$$

$$J_y = f(z/L) \dots \dots \dots 3.57$$

It is important to note that the function given in equation 3.56 is a recurring function, whilst the longitudinal field for the solenoid will fall to zero outside the limits $-L/2$ to $+L/2$, as shown by Figure 3.4. The function, as a consequence will only be considered between these limits, as the \underline{E} field of the system will indeed be zero outside these limits. Evaluation of this function, when appropriate, will be limited to the 'dc' term plus the most significant harmonics. This will give acceptable accuracy whilst simplifying the computation.

It is now assumed that L for the longitudinal case will be typically 63.0mm (3.70 in) giving a value for the fundamental component of the longitudinal field variation of 20.0mm (1.20 in). The other parameters used in the mathematical model are as described in section 3.3.1, page 34. Thus evaluation of the model using equations 3.43, 3.44, 3.53 and 3.54 is achieved using the computer program given in Appendix 4(a).

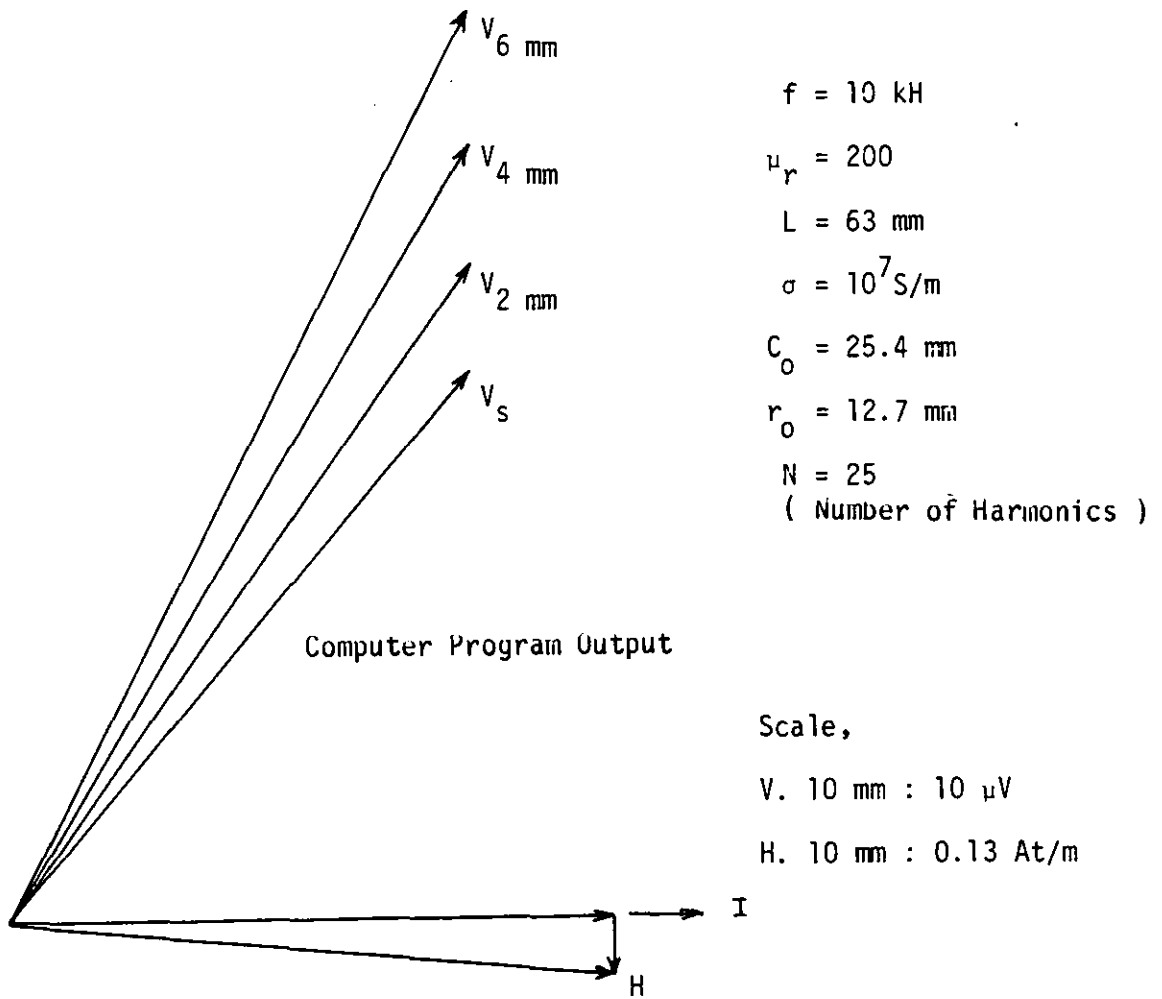


Figure 3.5a Phasor diagram for the rigorous mathematical model, cylindrical case, for a short coil at various heights above the metallic surface

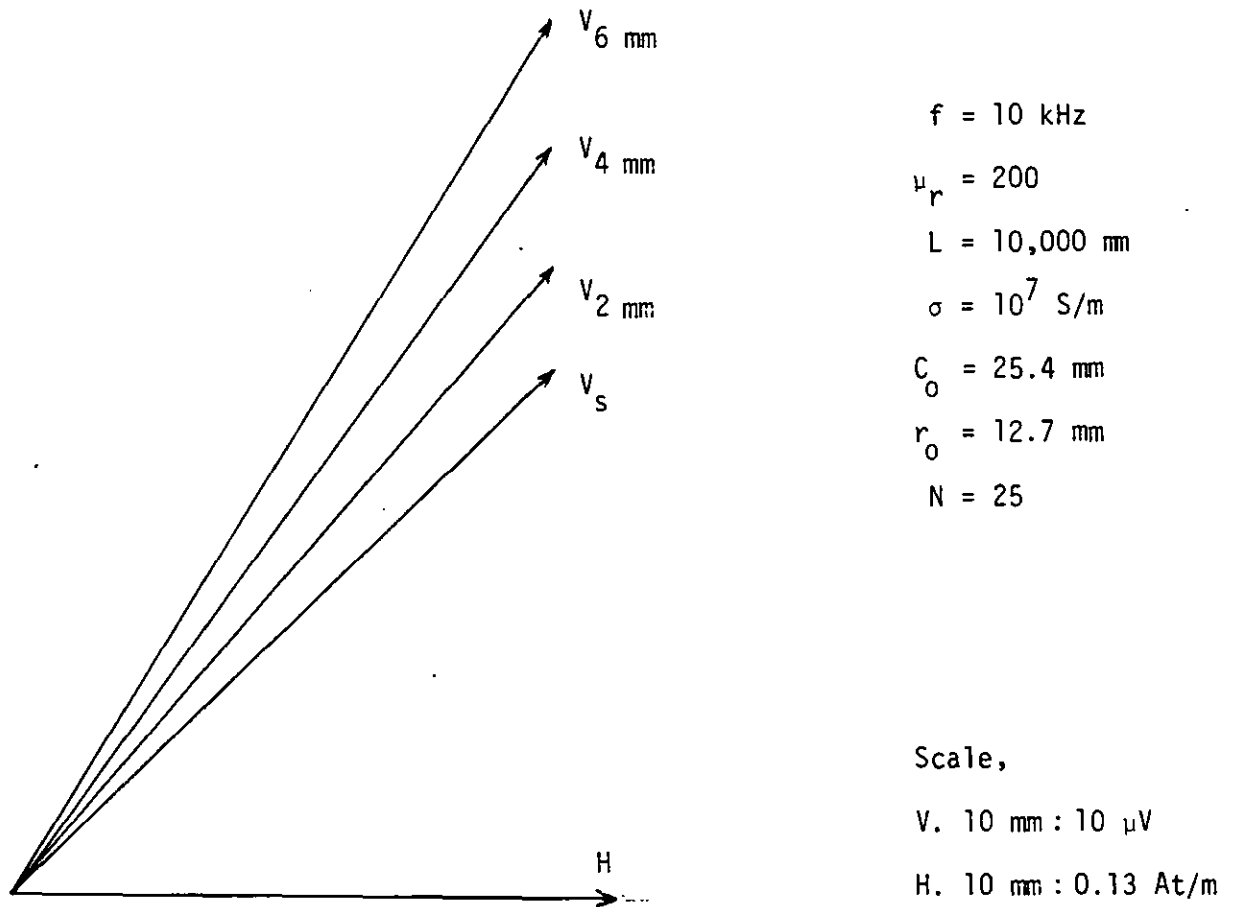


Figure 3.5b Phasor diagram for the rigorous mathematical model, cylindrical case, for a long coil at various heights above the metallic surface

The evaluation of the Bessel functions $I_0(r/\ell)$, $I_1(r/\ell)$, $K_0(r/\ell)$ and $K_1(r/\ell)$ is achieved using the polynomial approximations given by Abramowitz and Stegun reference 76. The results obtained from the program of Appendix 4(a), and using an inducing coil radius of 25.4 mm (1.00 in) are given for convenience in phasor diagram form in Figures 3.5a and 3.5b.

The mathematical model was evaluated for various coil lengths, in the cases presented in Figure 3.5a and 3.5b a typical coil length of 63.0mm and 10,000 mm was used. The representation presented in Figure 3.5b may be compared directly with the evaluation presented in Figure 3.3, page 35.

It may be seen from the evaluation shown by Figure 3.5b and Figure 3.3 that the agreement between the different models is very close, ie to within 1%, providing the inducing coil is longer than 60.0mm. This agreement indicates that the arguments used to produce both the simple and the rigorous mathematical model are valid, and may be used to some effect, providing care is taken with the length of the inducing coil. For inducing coils of less than about 50.0 mm in length, the mathematical model is not considered to be sufficiently accurate without further extensive refinement. These refinements are considered to be beyond the scope of this project, and thus inducing coils considered will be of 50.0 mm or greater.

The evaluation of section 3.3.1 page 34, and 3.3.2 page 36, compare well with the practical measurements made on the eddy current system, these measurements are recorded in Chapter 4. This good agreement between theory and practice indicates that the main assumptions regarding the

production of the mathematical model are indeed correct.

However, despite the fact that the mathematical model is 'good', the program used for its evaluation is complex and takes several minutes to achieve the required convergence. Thus, in the next section, certain changes are introduced into the mathematical model in order to make the model less complex and rather simpler to incorporate in a practical eddy current gauging system.

3.4 Physical Limitations for Mathematical Model

It is now clear that the mathematical model produced in section 3.2, page 21 is a rigorous model of the eddy current system. However this model does contain anomalies and it would seem that from the complexity of the mathematical model, and thus the length of the computer program required for the solution and evaluation of the equations, given in Appendix 4(a), this rigorous mathematical model will not be readily assimilated into an easy to operate practical eddy current gauge. It is however also clear that the principles outlined in section 3.2 page 21 must be retained for any practical eddy current gauge. Hence it is necessary to develop a method or methods of simplifying the mathematical model, without the need to sacrifice the precision and accuracy of the original analysis.

For this simplification it is necessary to proceed in careful steps, in order to produce a 'good' mathematical model which may be used as the basis of a practical eddy current gauge utilising electronic techniques which are currently available. With this end in view, it is necessary to make the following simplifications and changes which will enable the mathematical model to produce the predictive response necessary for a practical eddy current gauge.

In section 3.2, page, 21 the cylindrical coordinate system was used. This was, and indeed still is, considered to be the most appropriate system to use, as the system to be modelled is of cylindrical form. However it is useful, at this stage to consider a possible change of the coordinate system, if this results in a simplification of the mathematical model, and also if this change results in a mathematical model which adequately describes the eddy current system under consideration.

At a frequency of 10 kHz a mathematical model of the eddy current system using cartesian coordinates will be a good approximation of the system only if the thickness of the relevant region of the field is much less than the radius of curvature. Thus for solenoids close to the surface of the metal, and for small skin depth, a cartesian mathematical model provides an effective basis for the modelling of the system, as this will result in considerable simplification without appreciable loss of accuracy.

From Schelkenoff reference 72 and in conjunction with the relationships given in Appendix 2

$$\frac{\partial H_x}{\partial z} - \frac{\partial H_z}{\partial x} = (\sigma + j\omega\epsilon) = \sigma E_y \quad \dots\dots\dots 3.58$$

$$\frac{\partial E_y}{\partial z} = j\omega\mu H_x \quad \dots\dots\dots 3.59$$

$$\frac{\partial E_y}{\partial x} = -j\omega\mu H_z \quad \dots\dots\dots 3.60$$

$$H_x = \frac{1}{j\omega\mu} \frac{\partial E_y}{\partial z} \quad \dots\dots\dots 3.61$$

$$H_z = \frac{1}{j\omega\mu} \frac{\partial E_y}{\partial x} \dots\dots\dots 3.62$$

Substituting for H_x and H_z in equation 3.58 gives:

$$\frac{\partial^2 E_y}{\partial z^2} + \frac{\partial^2 E_y}{\partial x^2} = j\omega\mu\sigma E_y \dots\dots\dots 3.63$$

also $\frac{\partial^2 E_y}{\partial x^2} = \gamma_x^2 E_y$

and $\frac{\partial^2 E_y}{\partial z^2} = \gamma_z^2 E_y$

Hence $\gamma_x^2 + \gamma_z^2 = j\omega\mu\sigma \dots\dots\dots 3.64$

Now let $\gamma_z = \frac{\pm j}{\ell}$

$$\gamma_z = \frac{j2\pi}{\lambda_z} \dots\dots\dots 3.65$$

$\therefore \gamma_z^2 = j\omega\mu\sigma + \frac{1}{\ell^2} \dots\dots\dots 3.66$

The quantities E_y and H_x are continuous at the surface of the metallic conductor. E_y may now be expressed as follows:

$$E_y = E_0 e^{\gamma_x x} f(z/L) \dots\dots\dots 3.67$$

Differentiation gives

$$\frac{\partial E_y}{\partial x} = \gamma_x E_0 e^{\gamma_x x} f(z/L) \dots\dots\dots 3.68$$

$$\frac{\partial E_y}{\partial x} = \gamma_x E_y \dots\dots\dots 3.69$$

Substitution for $\frac{\partial E_y}{\partial x}$ in equation 3.60 yields

$$\frac{E_y}{H_z} = - \frac{j\omega\mu}{\gamma_x} \dots\dots\dots 3.70$$

In the air above the metal

$$\gamma_x^2 = \frac{1}{\ell^2} \dots\dots\dots 3.71$$

Thus $Z_1 = \frac{-j\omega\mu}{-1/\ell} = j\omega\mu\ell \dots\dots\dots 3.72$

For propagation in the x direction, then \underline{E} in E_y only, thus

$$\underline{E} = E_1 e^{-x/\ell} + E_2 e^{x/\ell} \dots\dots\dots 3.73$$

and $\underline{H} = (E_1 e^{+x/\ell} - E_2 e^{-x/\ell})/j\omega\mu_0 \ell \dots\dots\dots 3.74$

For the metal

$$Z_2 = \frac{1}{\left[\frac{\sigma}{j\omega\mu_0\mu_r} + \left(\frac{1}{j\omega\mu_0\mu_r\ell} \right)^2 \right]^{\frac{1}{2}}}$$

$$Z_2 = \left[\frac{j\omega\mu_0\mu_r}{\sigma} \right]^{\frac{1}{2}} \left[\frac{1}{\left(1 + \frac{1}{j} \left(\frac{d}{\ell} \right)^2 \right)} \right]^{\frac{1}{2}} \dots\dots\dots 3.75$$

where $d = \left(\frac{1}{\omega\mu_0\sigma} \right)^{\frac{1}{2}}$

The expression given in equations 3.72 and 3.75 is in a rather more convenient form, for case of evaluation, than equations 3.43, 3.44, page 32, 3.53 and 3.54, page 33 providing that the conductivity of the metal is accurately known or may be accurately measured. It is also assumed that the metal is either non-ferrous or is in a magnetically saturated state. Thus the above equations may be evaluated.

Consider the case now with no variation in the field in the z direction and the radius of the metal bar tends to infinity.

For this case

$$Z_2 = Z_s = [j\omega\mu/\sigma]^{1/2} \dots\dots\dots 3.76$$

and at a frequency of 10 kHz with $\sigma = 10^7$ S/m and $\mu_r = 1$ (saturated steel)

$$\text{then } Z_s = \sqrt{j} 8.885 \cdot 10^{-5} \Omega/\text{sq}$$

For the region above the metallic surface, reference Schelknoff 72 page 273, the outward looking impedance approaches infinity whilst the inward looking impedance approaches $Z_s +$ the height term.

Consider now the case where there is a field variation in the z direction. Assume initially a value for ℓ of 20.0 mm and for $f = 10$ kHz.

$$\begin{aligned} \text{Hence in air } Z_1 &= j\omega\mu_0\ell \\ &= j1.58 \cdot 10^{-3} \Omega \end{aligned}$$

and for the metal ($\mu_r = 1$)

$$Z_2 = \left[\frac{j\omega\mu_0\mu_r}{\sigma} \right]^{\frac{1}{2}} \left[\frac{1}{\left(1 + \frac{1}{j} \left(\frac{d}{\ell}\right)^2\right)} \right]^{\frac{1}{2}} \dots\dots\dots 3.77$$

$$Z_2 = \sqrt{j} 8.885 \cdot 10^{-5} \left[\frac{1}{1 - j3.164 \cdot 10^{-3}} \right]^{\frac{1}{2}}$$

$$Z_2 = \sqrt{j} 8.885 \cdot 10^{-5} \Omega/\text{sq as before.}$$

For the case of the longer coil, $\ell = 380 \text{ mm}$

$$Z_1 = j\omega\mu_0 \ell = j3.00 \cdot 10^{-3} \Omega$$

$$\text{also } Z_2 = \sqrt{j} 8.885 \cdot 10^{-5} \left[\frac{1}{1 - j8.764 \cdot 10^{-4}} \right]^{\frac{1}{2}}$$

$$= \sqrt{j} 8.885 \cdot 10^{-5} \Omega/\text{sq as before.}$$

It is now necessary to evaluate equations 3.72 and 3.75 assuming the longitudinal field has a harmonic content of the form given by equation 3.56, page 38. Thus the current in the outer coil may be assumed to have the form

$$\underline{J} = J_0 \left\{ \frac{1}{2} + \frac{2}{\pi} \left[\cos z/\ell - \frac{1}{3} 3z/\ell + \frac{1}{5} \cos 5z/\ell \dots\dots\dots \right] \right\} \dots\dots\dots 3.78$$

The quantity ℓ in equation 3.72 to 3.75 will be replaced by ℓ/n , where n is 1, 3, 5 ----- . Also, using the reflection at the surface, and the continuity equations at the metal surface;

$$E_s = E_i + E_r \quad \dots\dots\dots 3.79$$

$$H_s = H_i - H_r \quad \dots\dots\dots 3.80$$

where E_i and H_i are the incident fields and H_r and E_r are the reflected fields.

Thus $Z_2 = E_s/H_s$ and $Z_1 = E_i/H_i = E_r/H_r$

also by letting $\frac{E_r}{E_i} = k$ (reflection coefficient)

$$\text{then } Z_2 = \frac{Z_1 (1 + k)}{(1 - k)} \quad \dots\dots\dots 3.81$$

$$k = \frac{(Z_2 - Z_1)}{(Z_2 + Z_1)} \quad \dots\dots\dots 3.82$$

From above it may be seen that

$$Z_1 \gg Z_2$$

Hence $k \approx -1$

at the metal surface $\frac{H_r}{H_i} = +k$ as above.

Thus the equations may be evaluated taking into account the harmonic nature of the fields.

Equations 3.72 and 3.75 in association with the reflection at the metal surface have been evaluated, using the program listed in Appendix 4b for a value of L , the coil length, of 63.0 mm and at a

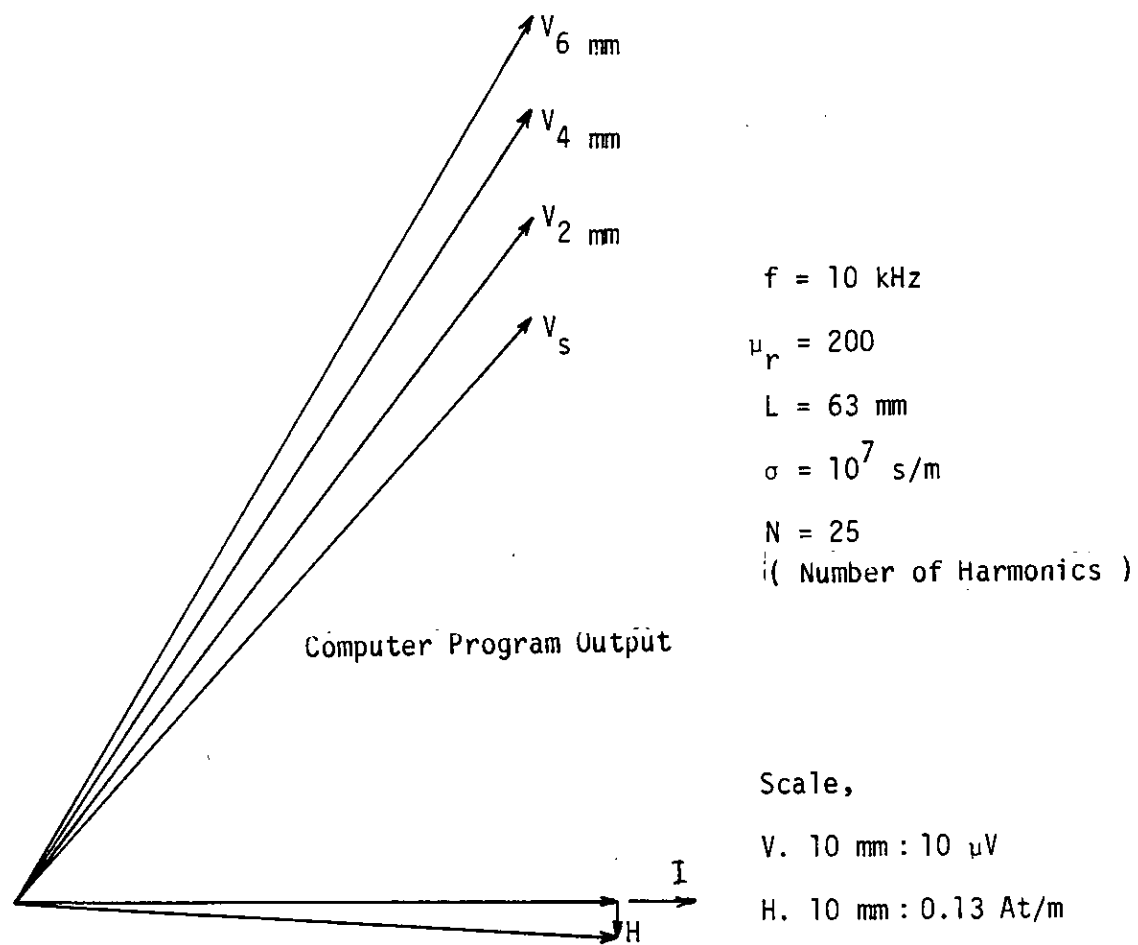


Figure 3.6a Phasor diagram for the simplified mathematical model, for a short coil, at various heights above the metallic surface

frequency of 10 kHz, for various heights above the metal surface. The results of this evaluation is presented in diagramatic form in Figure 3.6a.

The evaluation of the simplified mathematical presented in Figure 3.6a should be compared with the evaluation of the rigorous mathematical model of section 3.3, page 34, and with the practical measurements on the eddy current gauge system presented in Chapter 4. When comparisons are made, it may be seen that the agreement between the various models and measurements is in fact good.

However, it is thought that, and as stated in section 3.3.2, page 36, the inducing coil length should not be less than 62.0 mm and the lower limit of frequency of operation for this type of gauge should be 10 kHz. For very short coils, ie less than 62.0 mm and/or for frequencies of operation less than 10 kHz, both the mathematical modelling and measurements on the eddy current system become much more difficult.

For the case of an infinitely long coil above the metallic surface then the following analysis is appropriate.

Let $2\pi r$ be the length of the probe coil wire. Thus in the air space above the metal surface, assuming no variation in the z direction then

$$(E_1 - E_s)_{2\pi r} = \underline{H}j\omega\mu_0 h 2\pi r \quad \dots\dots\dots 3.83$$

where $h2\pi r$ is the area

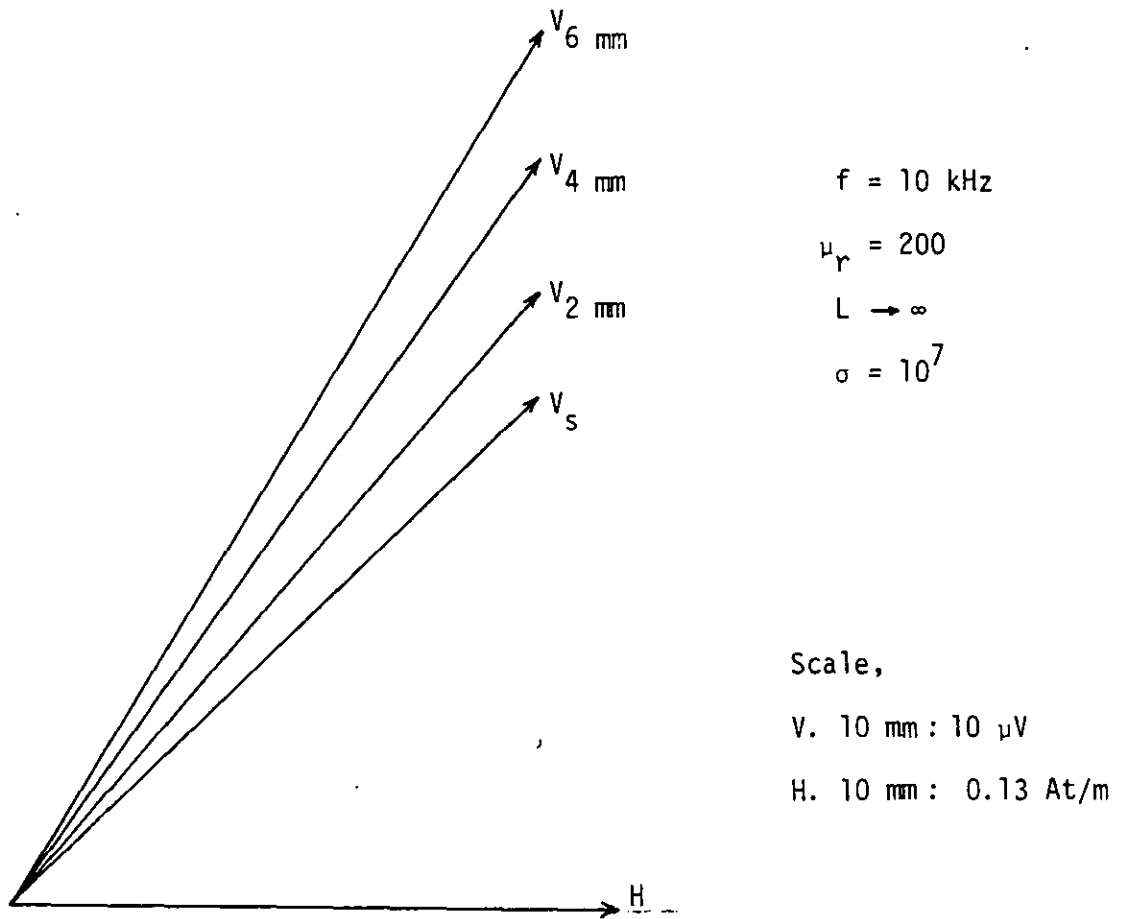


Figure 3.6b Phasor diagram for the simplified mathematical model, for an infinitely long coil, at various heights above the metallic surface

$$E_1 = E_s + H j \omega \mu_0 h \quad \dots\dots\dots 3.84$$

$$E_1 = H \left[\frac{E_s}{H} + j \omega \mu_0 h \right] \quad \dots\dots\dots 3.85$$

but from equation 3.23 $\frac{E_s}{H} = Z_s$

$$\therefore E_1 = H [Z_s + j \omega \mu_0 h] \quad \dots\dots\dots 3.86$$

$$E_1 = \frac{nI}{\ell} [Z_s + j \omega \mu_0 h] \quad \dots\dots\dots 3.87$$

$$\therefore V_1 = nI [Z_s + j \omega \mu_0 h] \quad \dots\dots\dots 3.88$$

Equation 3.88 is very similar in form to equation 3.25 page 28 for the cylindrical case. Evaluation of equation 3.88 gives the phasor diagram of Figure 3.6b.

The evaluation shown in Figure 3.6b is very similar to the evaluations produced in Figure 3.5b page 40, and Figure 3.3 page 35, thus no further comment is considered necessary.

The predictions of the simplified mathematical used in this section are considered quite acceptable for most practical purposes, and thus the simplifications introduced to produce this mathematical model are considered to have been vindicated.

However, during the course of research into the principles of eddy current gauging, the quantity Z_s , the surface impedance, must be measured, as part of the research programme, to ensure that in the final gauge, Z_s has a phase angle of 45° . But once this 45° phase

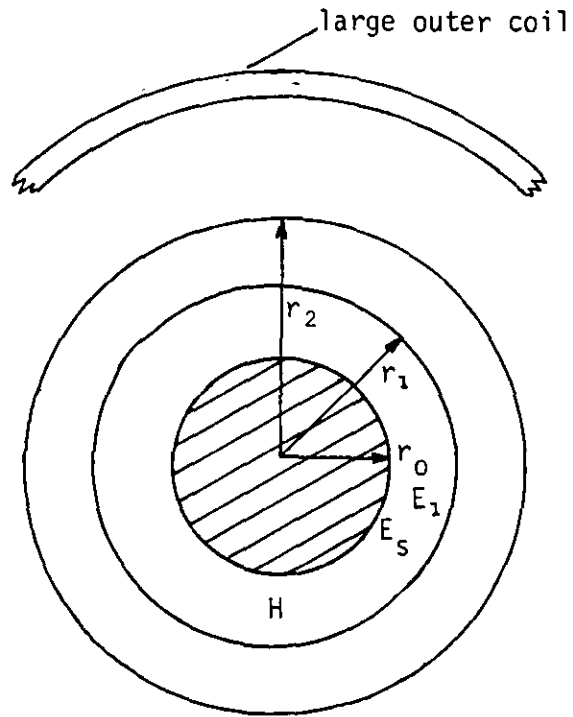


Figure 3.7 Sectional view of the metal bar and coil arrangement

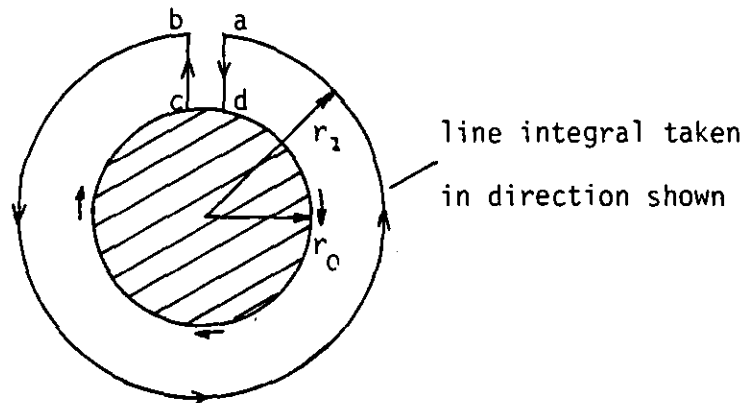


Figure 3.8 Line integral direction for probe coil

angle has been assumed, Z_s may vary without degrading the gauge calibration.

In practical terms, this implies that any measurement of Z_s must be made at the boundary between the air and the surface of the metal. It is clear that this type of measurement may not be physically possible, but also, it may in fact, not be desirable to do so. Thus a method of eliminating the effect of the distance from the metallic surface to the point at which the surface impedance may be measured must be developed. The basic principles involved with the proposed method of surface impedance measurement are outlined in section 3.5.

3.5 Surface Impedance Determination; Theory

From the preceding sections it has become clear that for progress to be made in the analysis of the type of eddy current gauge considered in this thesis, a method, or the principles of a method for the measurement of the surface impedance of the metallic conductor is required. It is also clear that it is unrealistic to expect this measurement of surface impedance to be carried out at the interface between the metal and the air. All probe coils will need to be insulated and obviously will then not be at the surface of the metal. It is thus necessary to extend the theory, so far considered, to include the addition of probe coils, for measurement purposes, in the space between the large outer coil and the metallic bar.

Consider the situation as shown in Figure 3.7. The field configuration is a rather complex one, in that the \underline{H} field may not be assumed to be constant over the whole region, the presence of the metal bar ensures that. However for practical purposes, the \underline{E} field in the region

above the bar in the vicinity of the probe coils is assumed to be constant. This is confirmed by measurements given in Chapter 4. Thus if the concept of emf induced in the coil by the change of linked flux is considered, by using the line integral of the \underline{E} field around the loop abcd as shown in Figure 3.8 then:

$$E_1 2\pi r_1 - E_s 2\pi r_0 = j\omega\mu_0 (\pi r_1^2 - \pi r_0^2) \underline{H} \quad \dots\dots\dots 3.89$$

However from equation 3.23 $Z_s = +\frac{E_s}{\underline{H}}$

$$\therefore E_1 2\pi r_1 = 2\pi r_0 \underline{H} \left[Z_s + j\omega\mu_0 \frac{(r_1^2 - r_0^2)}{2r_0} \right] \quad \dots\dots\dots 3.90$$

For a coil of n turns the induced emf is given by:

$$V_1 = 2\pi r_1 n E_1$$

$$\text{Thus } V_1 = 2\pi r_0 n \underline{H} \left[Z_s + j\omega\mu_0 \frac{(r_1^2 - r_0^2)}{2r_0} \right] \quad \dots\dots\dots 3.91$$

$$\text{let } h_1 = r_1 - r_0$$

Substituting for h_1 in equation 3.91 gives:

$$V_1 = 2\pi r_0 n \underline{H} \left[Z_s + j\omega\mu_0 \left(h_1 + \frac{h_1^2}{2r_0} \right) \right] \quad \dots\dots\dots 3.92$$

Equation 3.92 would give an almost direct approach to a method for the measurement of the surface impedance, if the term $j\omega\mu_0 (h_1 + \frac{h_1^2}{2r_0})$ were absent. A method will now be described in which an addition to the circuit configuration will enable this desirable elimination to be achieved.

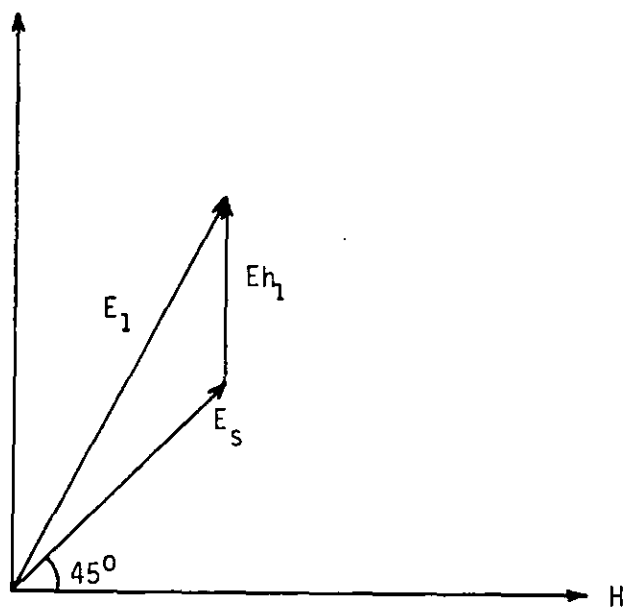


Figure 3.9 Phasor diagram showing the relationships between the emf's induced in the probe coil

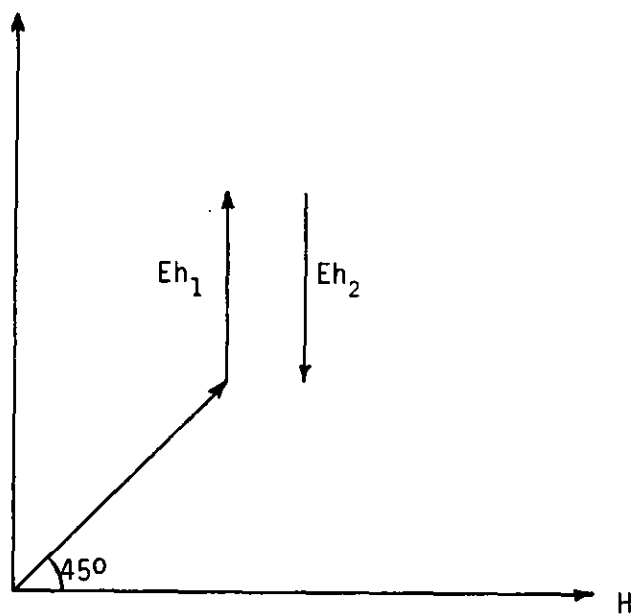


Figure 3.10 Phasor diagram showing the elimination of the effect of probe coil height

The phasor diagram for the situation given in mathematical form by equation 3.92 is shown in Figure 3.9. The elimination of the vertical component, as suggested previously, is shown in Figure 3.10. The method employed to achieve this elimination is given below.

Consider now the case of two probe coils, physically mounted one above the other, having n_1 and n_2 and radii r_1 and r_2 respectively. Let the voltages induced in each coil, by the current I , flowing in the large outer solenoid, which is external to, and surrounding the two small probe coils, be V_1 and V_2 . V_1 and V_2 are determined by letting n in equation 3.92 be n_1 and n_2 respectively. Thus subtracting V_1 and V_2 gives:

$$V_1 - V_2 = 2\pi r_0 H \left\{ (n_1 - n_2) Z_S + j\omega\mu_0 \left[(h_1 n_1 - h_2 n_2) + \frac{(n_1 h_1^2 - n_2 h_2^2)}{2r_0} \right] \right\} \dots\dots\dots 3.93$$

$$\text{where } r_1 - r_0 = h_1$$

$$\text{and } r_2 - r_1 = h_2$$

$$\therefore V_1 - V_2 = 2\pi r_0 (n_1 - n_2) H \left\{ Z_S + \frac{j\omega\mu_0}{(n_1 - n_2)} \left[(h_1 n_1 - h_2 n_2) + \frac{(n_1 h_1^2 - n_2 h_2^2)}{2r_0} \right] \right\} \dots\dots\dots 3.94$$

The quantity $\frac{1}{(n_1 - n_2)} \left[(h_1 n_1 - h_2 n_2) + \frac{(n_1 h_1^2 - n_2 h_2^2)}{2r_0} \right]$

may be conveniently expressed as h' . Thus equation 3.94 now becomes

$$V_1 - V_2 = 2\pi r_0 (n_1 - n_2) H \left[Z_S + j\omega\mu_0 h' \right] \dots\dots\dots 3.95$$

It may be seen from equation 3.95 that by careful control of the quantities n_1 and n_2 , the number of probe coil turns, it is possible to make the quantity h' become small, or in principle zero, and thus allow the term $j\omega\mu_0 h'$ to be neglected when compared to Z_s , provided the frequency is low enough.

The term \underline{H} is also a quantity which may be evaluated, see section 3.6, page 58, and hence equation 3.95 represents the outline of a powerful method for the evaluation of the surface impedance of a cylindrical metallic conductor, providing the principles established above may be controlled. Detailed measurements for this method may be found in Chapter 4.

3.6 Magnetic Field Strength Determination; Theory

The magnitude of the magnetic field strength between the metallic bar and the large outer magnetising coil requires accurate measurement in order that the term Z_s , the surface impedance, given in equation 3.95 may also be accurately evaluated. The magnitude of the magnetic field strength will also be required for any extension of the eddy current theory to include the evaluation of distance to the probe coils from the metallic surface. The magnitude of the magnetic field strength may be determined using the following method.

For two probe coils, situated close to the metallic surface, and being mounted one on top of the other, both having the same number of turns, the difference voltage between them will be given using equation 3.91.

$$\therefore V_2 - V_1 = j\omega\mu_0 H_z n \pi (r_1^2 - r_2^2) \dots\dots\dots 3.96$$

$$\text{for } r_1 < r_2$$

$$\therefore V_2 - V_1 = H_z j \omega \mu_0 n 2 r_1 \pi \left(h + \frac{h^2}{2 r_1} \right) \dots\dots\dots 3.97$$

$$\text{for } h = r_2 - r_1$$

$$\therefore H_z = \frac{(V_2 - V_1)}{j \omega \mu_0 n 2 \pi r_1 \left[h + \frac{h^2}{2 r_1} \right]} \dots\dots\dots 3.98$$

There will be a phase difference between V_1 and V_2 which will depend upon the value of h , the radial distance between the coils. For h small, ie the two coils being in close proximity, then the quantity $h^2/2r_1$ from equation 3.98 will be small when compared to h , thus this term may be neglected with only minimal loss of accuracy.

From equations 3.92, 3.95 and 3.98 it is now in principle possible to determine, by measurement, a sufficient number of the parameters of the eddy current system, to enable an accurate measurement to be made of the height of a probe coil above the surface of a metallic conductor. It is also evident, from the preceding section, that this type of eddy current gauging should, in principle, be possible for both ferrous and non-ferrous materials.

It is considered advisable, for ferrous materials, that the material should be driven into magnetic saturation. This will prevent any rapid change in the relative permeability, and will also eliminate any unwanted effects due to stray magnetic fields, external to the eddy current gauging system, or to localised magnetic fields within the material of the metal bar itself.

The result of implementing this type of system using a magnetically saturated bar is to make de-gaussing necessary if a dc system is

employed, or if ac magnetisation is used, as shown in Chapter 4, the whole eddy current system will of necessity be much more complex. However by the use of modern electronic techniques, described in Chapter 5, the complexities of the system may be readily handled.

CHAPTER 4 MEASUREMENT OF MODEL PARAMETERS

4.1 Introduction

In order to utilise the principles outlined in the previous chapter, with the objective of constructing a practical eddy current gauge, it is necessary to verify the accuracy and validity of the mathematical models which have been developed. To this end, it is considered necessary to measure the parameters associated with the mathematical models and also to consider any other quantities, for example the phase angle of the surface impedance, which may prove to be necessary for the construction of a practical eddy current gauge.

A practical eddy current gauge, based on the principles thus developed, will normally operate at a single frequency, apart from the low frequency stimulation introduced to obtain magnetic saturation and described in section 4.5, page 88. Conceivably there may be advantages in multi-frequency derived signals, but it was decided that studies in this field would not be included in the programme of research reported on in this thesis, but would be included in recommendations for further work in Chapter 6. For operation at a single frequency, with the proviso quoted above, it is necessary to exercise great care in the selection of that frequency of operation, as the determination of this frequency is not as straight forward as it may first appear.

From consideration of equation 3.92, page 55, it may be seen that voltage induced in the probe coil will be dependent upon two frequency determined factors:

- i) the surface impedance, Z_s , which will vary as $\sqrt{\omega}$, and
- ii) the term corresponding to the height of the probe coil above the surface, which will vary as ω provided $h_1^2/2r_0$ is small.

For a relatively high frequency of operation, the height term will predominate, whilst for lower frequency operation Z_s the surface impedance will be comparable with this height term. Consequently it may be seen that a relatively high frequency of operation may be advantageous since the magnitude of the surface impedance will be small when compared with the contribution of the impedance due to the height of the probe coil above the metallic surface. For the preceding condition to be satisfied, the frequency of operation would need to be rather more than hundreds of kilohertz.

If, however, a microprocessor aided, automatic eddy current gauging system is designed, using for example, sample and hold circuits, with acquisition time of the order of 12 μ s and a successive approximation type of analogue to digital convertor with a conversion time of the order of 6 μ s, and a microprocessor with a cycle time of 0.32 μ s, the above criterion would imply that the operating frequency for the eddy current gauge would need to be in the kilohertz range. Details of this type of system may be found in Chapter 5.

A frequency of operation for an eddy current gauging system in the kilohertz range would be suitable for use with a microprocessor

based system; and in principle eddy current gauging could be carried out at these frequencies, but it would have the considerable disadvantage of requiring a measurement of the surface impedance of the metal under consideration. If, however, measurement of the surface impedance can be made, then a lower frequency of operation will be rather easier to implement than the higher frequency operation, but for initial measurement purposes, a range of frequencies will be considered.

In order to measure the parameters associated with the surface impedance and contribution made by the height of the measuring coil above the metallic surface, the magnitude and phase angle of relatively small voltages will need to be measured. These voltages will be in the micro to milli volt range for frequencies of the order of kilohertz. Hence some amplification will be necessary in order to make the eddy current gauge compatible with the type of micro^oprocessor aided measuring system envisaged.

4.2 Experimental Apparatus

The experimental apparatus used for the basic measurement of surface impedance and of the height of the small probe coil(s) from the metallic surface is shown in Figure 3.1, page 19, and Figure 4.1. The large outer coil is wound with 30 SWG wire and is a nominal 50.95 mm (2.006 in) in diameter. The coil is supported by a perspex former, which was turned down to a nominal diameter of 50.8 mm, (2.00 in). The centre of this perspex former was drilled out to a nominal diameter of 38.1 mm (1.50 in) to allow a smaller probe coil holder to slide into it. Several small probe coils, using 34 SWG wire,

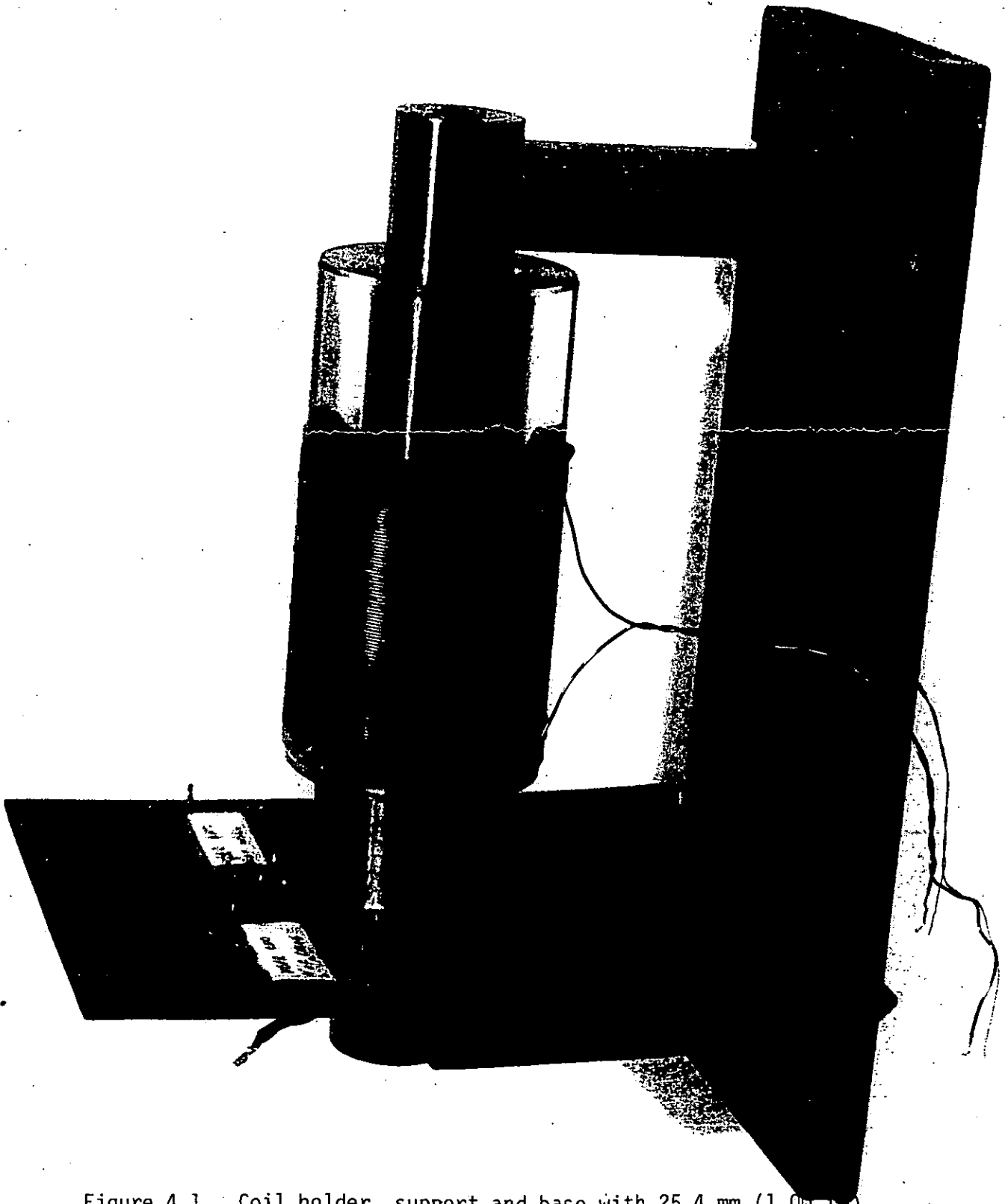


Figure 4.1 Coil holder, support and base with 25.4 mm (1.00 in.) diameter mild steel bar .

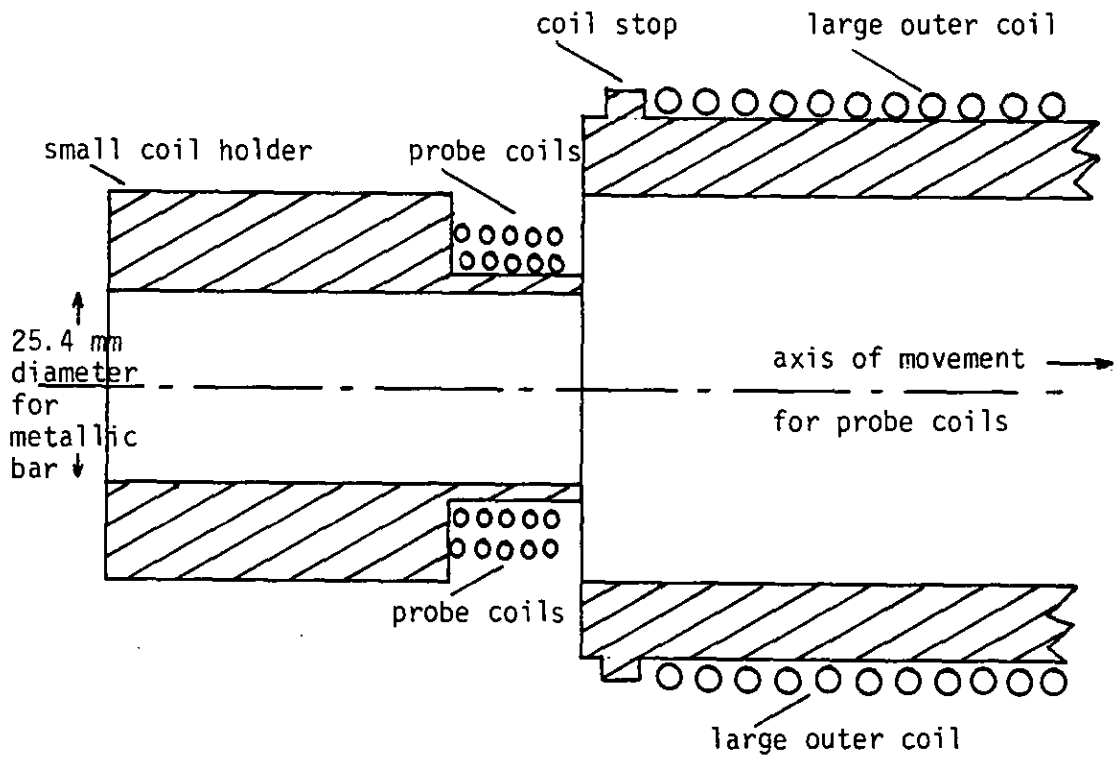


Figure 4.2 Sectional view of probe coils and large outer coil

and of varying diameter, were wound on this smaller probe coil holder. The smaller probe coil holder also has a nominal 25.4 mm (1.00 in) diameter hole drilled through it, to accommodate the various metallic bars. The whole coil arrangement is supported by a wooden base, together with appropriate connectors for the termination of the various coils. The arrangement is shown pictorially in Figure 4.1 and diagrammatically in Figure 4.2.

A first attempt at constructing a set of probe coils of differing diameter employed a stepped type of structure for the probe coil holder. This led to a simple assembly procedure, but of course the coils were not precisely at the same longitudinal position in the magnetic field, and this led to difficulties for the more accurate measurements. It was considered necessary to devise a constructional technique with exact probe coil location in longitudinal position, and the construction method finally chosen was as follows.

The small probe coils, wound on the coil holder, are mounted precisely one on top of the other. This precise longitudinal positioning is necessary in order to eliminate any contribution to the induced voltage in the probe coils by the small, but inevitable, variation in the magnetic field strength in the direction at right angles to the axis of the coil. If the large outer coil was infinite in length, then the assumption made when developing the rigorous mathematical model would be correct. However for practical implementation, a coil of finite length must be introduced. This could result in problems when measurements of the magnetic field strength are made, but these problems may be controlled by careful positioning of the small probe coils.

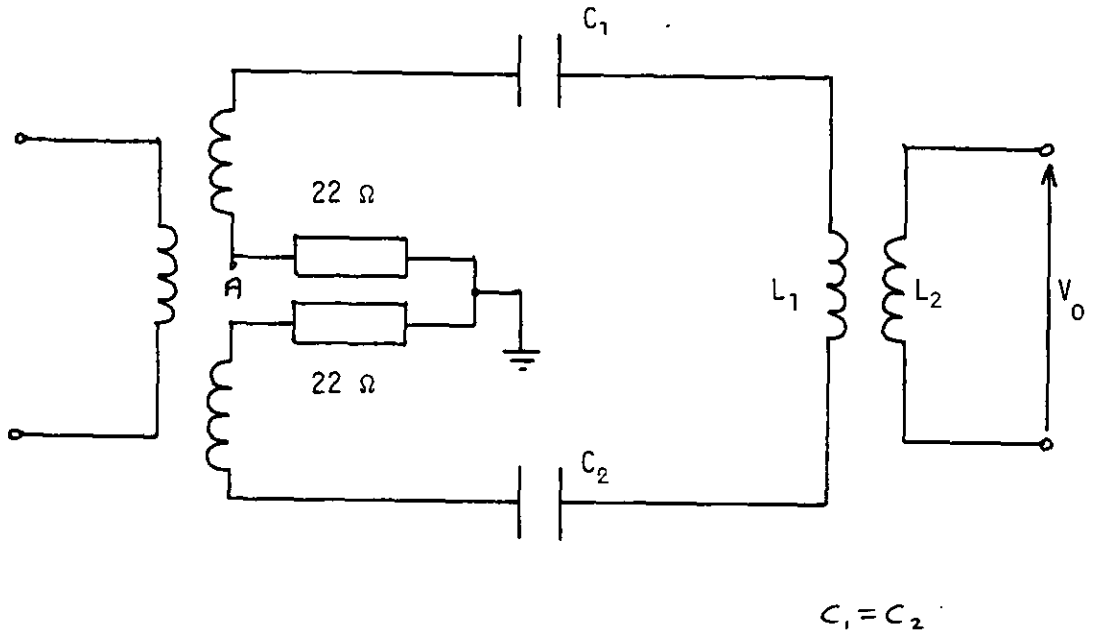


Figure 4.3 Circuit diagram showing the relationship between the probe coil and the external drive for the inducing coil

The first small coil was wound directly on the perspex coil holder, and held securely in place by a quick-setting epoxy resin type of adhesive, which when dry was turned down on a lathe, resulting in a firm base of known diameter. This is the base for the next coil. The process was then repeated for each coil in turn. The coil ends were formed into a twisted pair and then held in a groove on the top of the coil holder, terminating on connectors to facilitate the measurement of the appropriate coil voltages.

4.3 Measurements

4.3.1 Measurement of Probe Coil Voltage

In order to use the measurement of the voltage induced in the probe coils for the implementation of a practical eddy current gauge, an accurate measurement of the voltage is necessary. Initially it was observed that a stray capacitance of the order of 5 pF existed between the large outer coil and the small probe coils. This stray capacitance resulted in severe difficulties in the interpretation of the measurements at the higher end of the frequency range considered.

This stray capacitance is very difficult to eliminate completely, but the problem may be controlled to a great extent by use of the circuit shown in Figure 4.3. The capacitors C_1 and C_2 are chosen such that the circuit will have a reasonably high value of Q . The split supply results in the centre of the large outer coil, L_1 , effectively being at earth potential. This circuit does not eliminate the stray capacitance, but it does eliminate the capacitance current in the capacitance. By the use of this arrangement it is now possible to measure the induced probe coil voltages, without measuring an appreciable contribution from the stray capacitance between the coils.

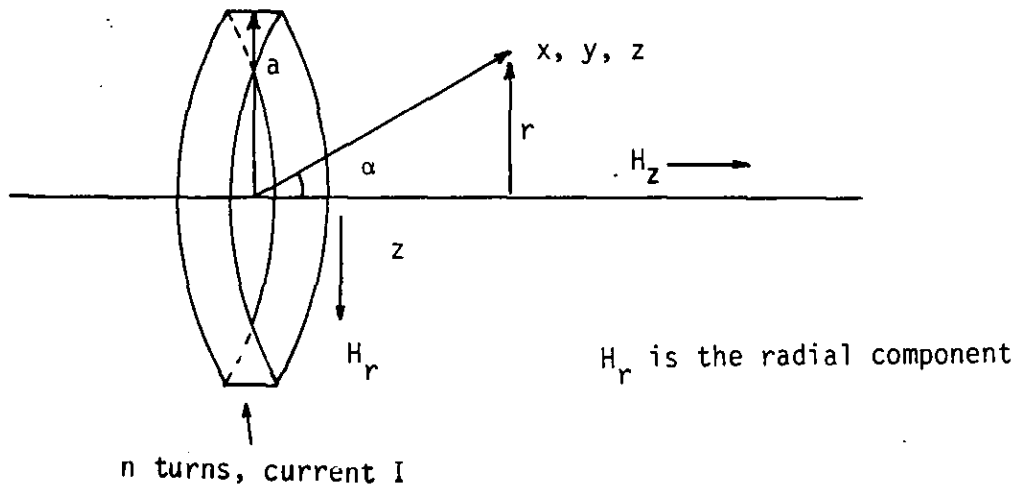


Figure 4.4 Concentrated coil for magnetic field strength determination

4.3.2 Measurement of Magnetic Field Strength

Once a method has been established for the accurate measurement of the voltages induced in the probe coils over an acceptable range of frequencies, it is then necessary to consider the measurement of the magnetic field strength between the metallic bar and the large outer coil, preferably using the small probe coils as the basis for this measurement.

The measurement of the magnetic field strength was achieved by the use of the two inner probe coils, connected in opposition. Thus using the voltage measured and from equation 3.98, page 59, a value for the magnitude of the magnetic field strength, which is dependent upon the number of turns on each coil and the distance, height, between the coils, may be evaluated. The phase difference between the voltages induced in these two coils was relatively small because the coils are close together.

It was considered necessary at this stage to devise an independent method, in order that the validity and accuracy of the magnetic field strength measurement, described above, may be checked. The following method is thought to satisfy that requirement.

From Stratton, reference 77, and Appendix 6 the magnetic field strength H_z and H_r at any point, given by the coordinates x, y, z , as shown in Figure 4.4, for n concentrated turns of wire, may be found by using the following expressions.

$$H_r = \frac{n I z}{2\pi r [(a+r)^2 + z^2]^{\frac{3}{2}}} \left[-K(k) + \frac{(a^2 + r^2 + z^2)E(k)}{(a-r)^2 + z^2} \right] \dots\dots\dots 4.1$$

MEAN RADII OF PROBE COILS USED FOR THE MAGNETIC FIELD STRENGTH MEASUREMENT

R(1)	:	14.74 mm
R(2)	:	15.09 mm
R(3)	:	15.44 mm
R(4)	:	15.79 mm
R(5)	:	16.13 mm
R(6)	:	16.52 mm
R(7)	:	16.93 mm

S.W.G. 34 wire used for all the above coils

TABLE 4.1

$$\text{and } H_z = \frac{nI}{2\pi[(a+r)^2 + z^2]^{\frac{3}{2}}} \left[K(k) + \frac{(a^2 - r^2 - z^2)}{(a-r)^2 + z^2} E(k) \right] \dots\dots\dots 4.2$$

$$\text{where } k^2 = \frac{4ar}{[(a+r)^2 + z^2]}$$

and $K(k)$ and $E(k)$ are complete elliptic integrals of the first and second kind.

From equations 4.1 and 4.2 it may be seen that for $z = 0, H_r = 0$ ie there is no radial component of the magnetic field strength at $z = 0$. The function for H_z will then give the total H field in the plane of the concentrated turns.

The magnetic field strength measurement will give a value for the field strength over the distance between the probe coils concerned. The theory quoted above will give the value of the magnetic field strength for various radii. As a result, several probe coils were wound on the probe coil holder using the method outlined in section 4.2, page 63. The mean radii of the probe coils thus wound are given in table 4.1. Seven probe coils in total, each of 20 turns using 34 SWG wire, were wound one on top of the other. This arrangement gave six measured values for the magnetic field strength, providing each adjacent pair of coils are connected in opposition in turn.

The theory presented above is for the determination of the magnetic field strength for a number n of concentrated turns. For a small number of concentrated turns, necessary for the theory to be valid, the change in the magnitude of the magnetic field strength, as the probe coil is moved along the axis of the outer coil is quite rapid.

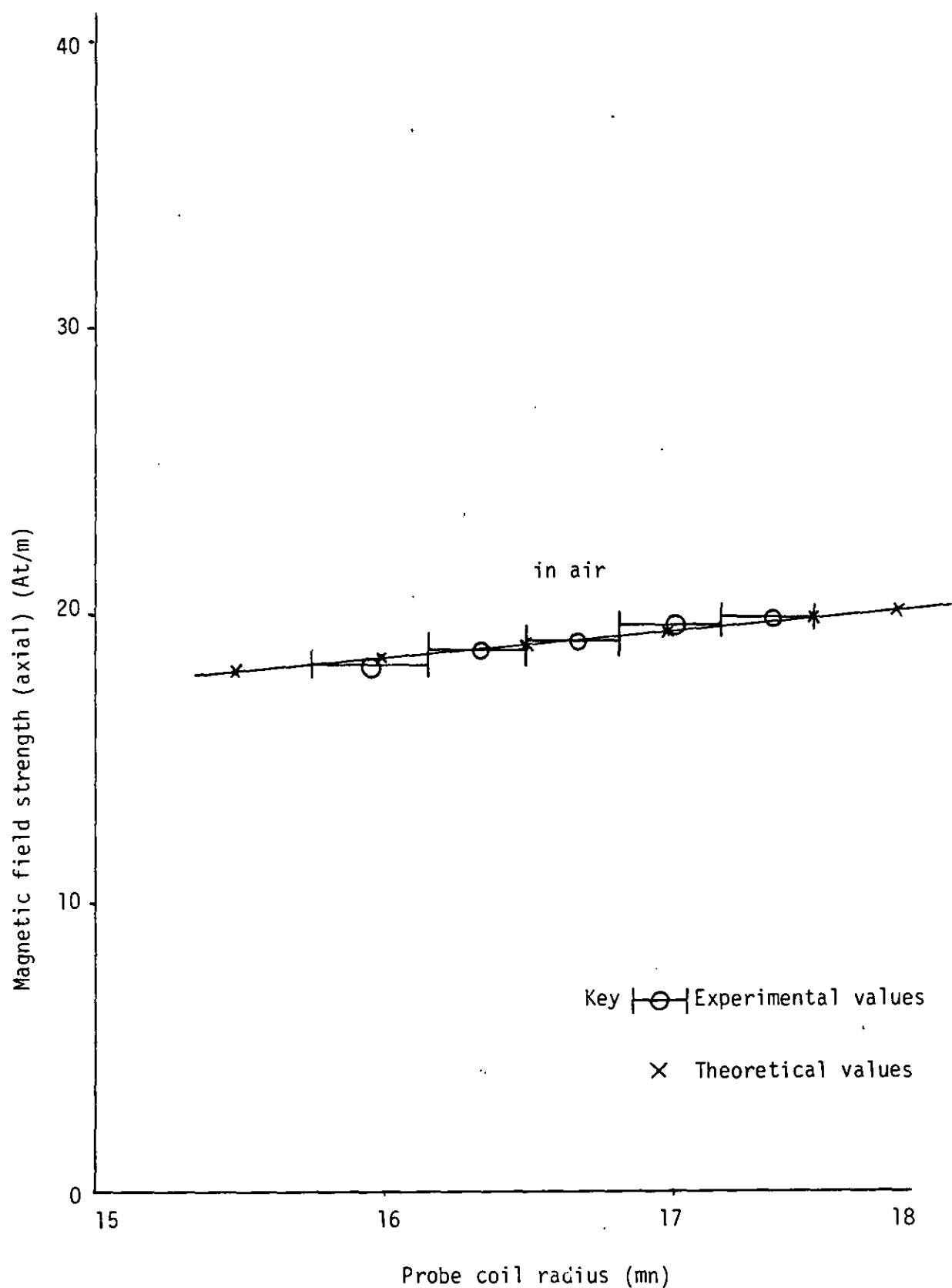


Figure 4.5 Graph to show magnetic field strength measurements using probe coils with close spacing, compared with theoretical values

Thus it was considered necessary to devise a method which would let the magnetic field strength remain constant over a larger axial distance. Such a suitable method is to use a Helmholtz coil arrangement.

In this case the Helmholtz coil arrangement consisted of two concentrated outer coils, each of diameter 50.8 mm (2.00 in) and 4 turns. The outer coils are separated by a distance equal to the radius of the outer coils. This method will ensure that the change in magnetic field strength, in the axial direction, will not introduce large errors into the measurement. Each turn of the probe coils will thus be subject to the same magnetic field strength.

The predicted results given by equation 4.2 and the measured values given according to equation 3.98, page 59, are compared in the graph of Figure 4.5. It may be seen that there is good agreement between theory and practice.

It should be noted at this stage that no direct comparison may be made between the method described above, and the measurements made to determine the magnetic field strength when the metallic bar is inserted. It may, however, be concluded that if the method for magnetic field strength determination is acceptable using the above method, then it must also give acceptable measurement with the metallic bar inserted. The above conclusion may be justified as correct because the variation in the magnetic field strength as a function of radius is small both in the case quoted above and also for the case when the metallic bar is inserted; the only difference being a change in the magnitude of the measured field.

There now remains one more parameter which it is necessary to evaluate, in order that an accurate measurement of surface impedance and hence distance, initially using non-ferrous material, may be completed.

4.3.3 Measurement of Conductivity

The conductivity of the metallic bars used in the experimental work reported in this thesis was measured by passing a large current of the order of 80 A dc, through the bars and the corresponding voltage across a known length of bar measured on a digital voltmeter, using a twisted pair of wires to eliminate unwanted effects due to stray 50 Hz magnetic fields. The results thus recorded were as follows:

- (i) For aluminium bar, length 152.4 mm (6.00 in) 25.4 mm (1.00 in) diameter

$$I = 70.0 \text{ A} \quad V = 0.7060 \text{ mV}$$

$$\therefore \sigma = 2.97 \cdot 10^7 \text{ S/m}$$

This compares with quoted values, reference 78, of

$$\sigma = 3.53 \cdot 10^7 \text{ S/m for pure aluminium}$$

$$\sigma = 2.13 \cdot 10^7 \text{ S/m for aluminium alloy}$$

- (ii) For brass bar, length 152.4 mm (6.00 in) 25.4 mm (1.00 in) diameter

$$I = 70.0 \text{ A} \quad V = 1.375 \text{ mV}$$

$$\therefore \sigma = 1.53 \cdot 10^7 \text{ S/m}$$

- (iii) Mild steel, length 152.4 mm (6.00 in) 25.4 mm (1.00 in) diameter

$$I = 70.0 \text{ A} \quad V = 5.740 \text{ mV}$$

$$\therefore \sigma = 7.35 \cdot 10^6 \text{ S/m}$$

compares with quoted values of 10^7 S/m, but this depends on the composition of the mild steel.

4.3.4. Measurement of Surface Impedance, Non-Ferrous

By consideration of equation 3.95, page 57, it may be seen that it is now possible to measure the quantity $(V_1 - V_2)$ and hence determine the magnitude of the surface impedance. However, it is first necessary to consider equations 3.94 and 3.95 to ensure that the quantity h' is small, hence ensuring that the imaginary term in equation 3.94 becomes negligible. From equation 3.94, page 57:

$$h' = \left[(n_1 h_1 - n_2 h_2) + \frac{(n_1 h_1^2 - n_2 h_2^2)}{2r_0} \right] \frac{1}{(n_1 - n_2)} \quad \dots\dots\dots 4.3$$

For the term $(V_1 - V_2)$ to give a measurement of the magnitude of surface impedance, equation 4.3 should ideally be zero hence

$$n_1 h_1 - n_2 h_2 + \frac{n_1 h_1^2 - n_2 h_2^2}{2r_0(n_1 - n_2)} = 0 \quad \dots\dots\dots 4.4$$

rearranging gives

$$\frac{n_1}{n_2} = \frac{h_2 [2r_0 + h_2]}{h_1 [2r_0 + h_1]} \quad \dots\dots\dots 4.5$$

Hence for $r_0 = 12.7$ mm

and $r_0 + h_1 = 14.84$ mm

$r_0 + h_2 = 16.88$ mm

gives $\frac{n_1}{n_2} = 2.10$

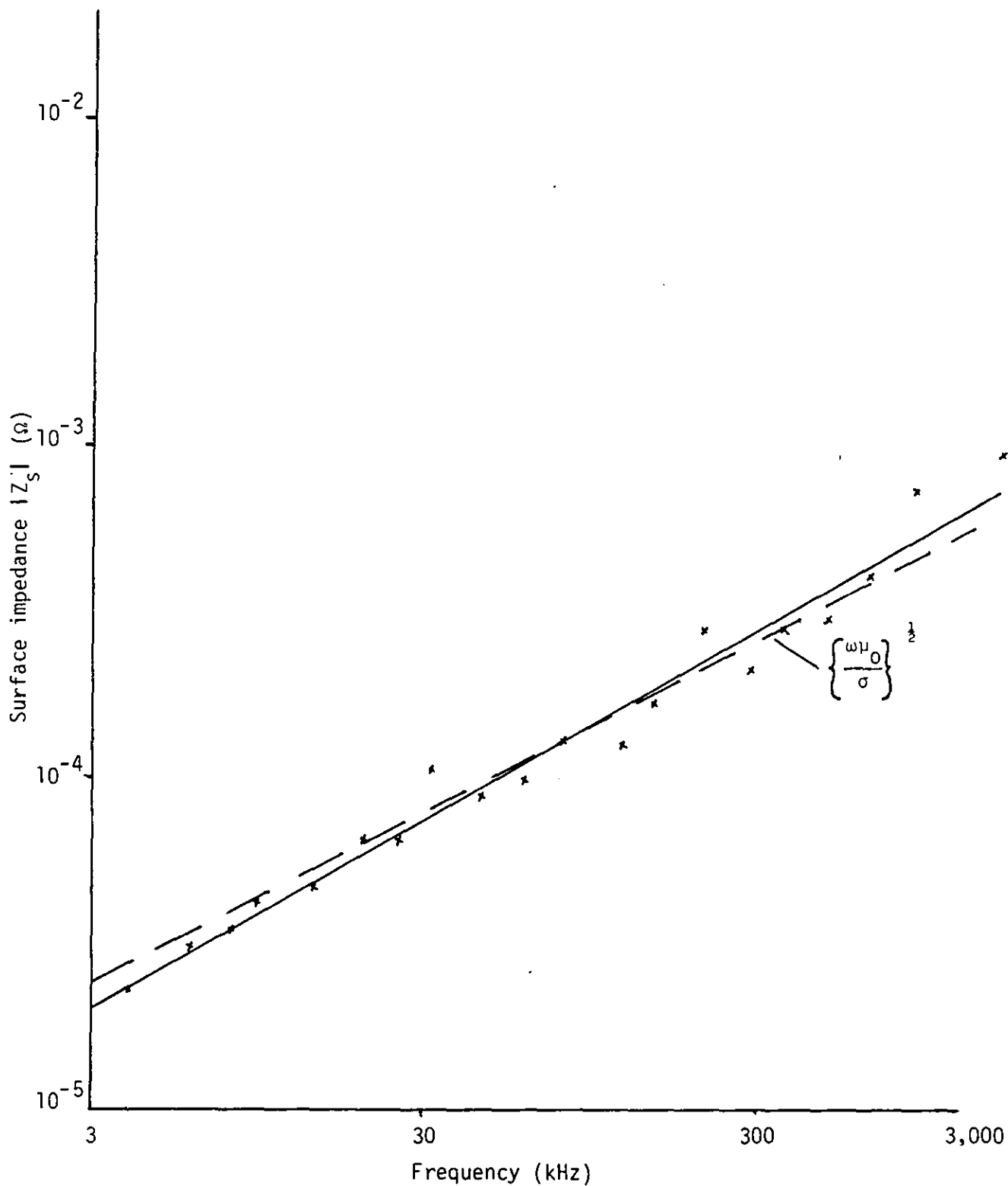


Figure 4.6 Graph of surface impedance against frequency, measured for an aluminium bar of diameter 25.4 mm (1.00 in)

which indicates that the surface impedance may be measured to a good degree of accuracy by using a ratio of n_1/n_2 of 2.

Using this ratio over a frequency range of 3 kHz to 3 MHz, gave the results shown in Figure 4.6. It should be noted that at the higher range of frequency the results will be increasingly in error due to the fact that the term h' is not zero. At the lower frequency end the results will be rather more accurate, however the actual voltages measured become rather small, ie less than $1 \mu\text{V}$ and hence spurious interference and noise become increasingly more of a problem.

4.3.5 Measurement of Surface Impedance, Phase Measurement

In the previous section it has been shown that by careful consideration of the number of turns wound on the pick-up coils, an accurate measurement of the magnitude of the surface impedance over a comparatively wide range of frequency may be achieved. It is also evident, from the principles outlined in the previous chapter, that there is a phase angle associated with the measurement of surface impedance.

The phase angle of the surface impedance will need to be considered with reference to either the \underline{E} field or the \underline{H} field. It would seem from the previous section that it would be convenient to measure the phase of the surface impedance with respect to the \underline{H} field, as a voltage which gives information regarding both the magnitude and phase of the \underline{H} field is readily available.

When the voltage proportional to the \underline{H} field was considered it was found that its magnitude was small. Hence when phase measurement was attempted using a digital phase meter, it was evident that the

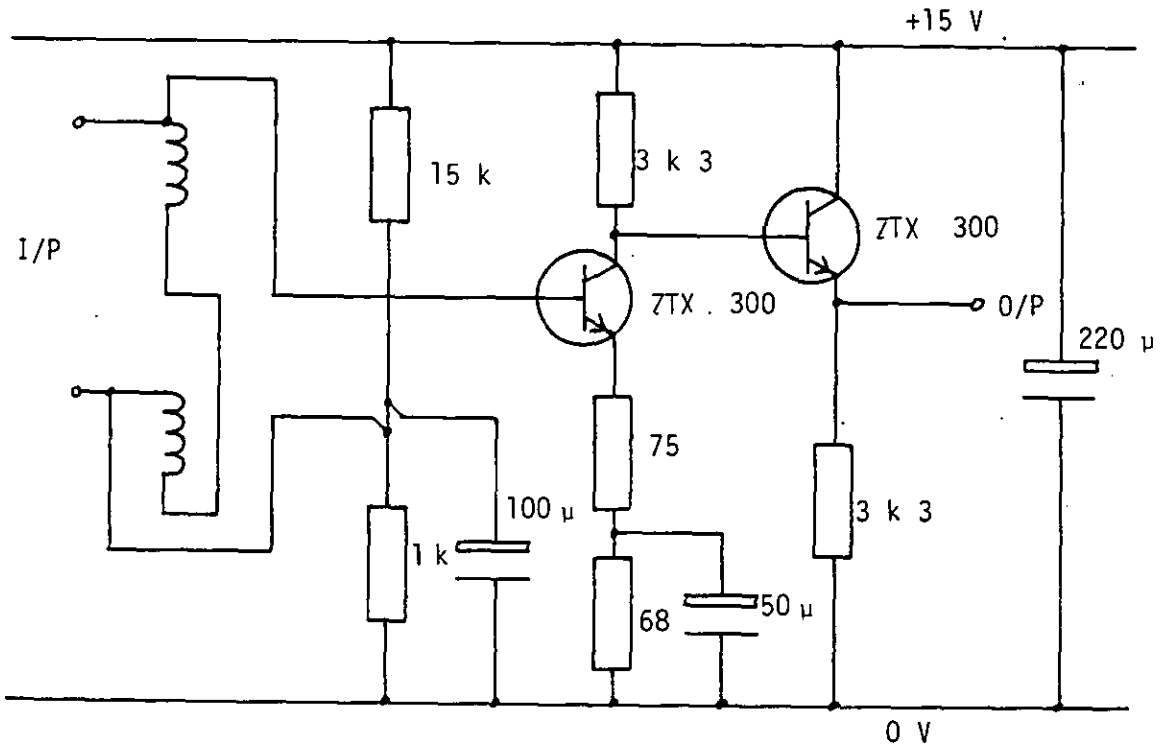


Figure 4.7a

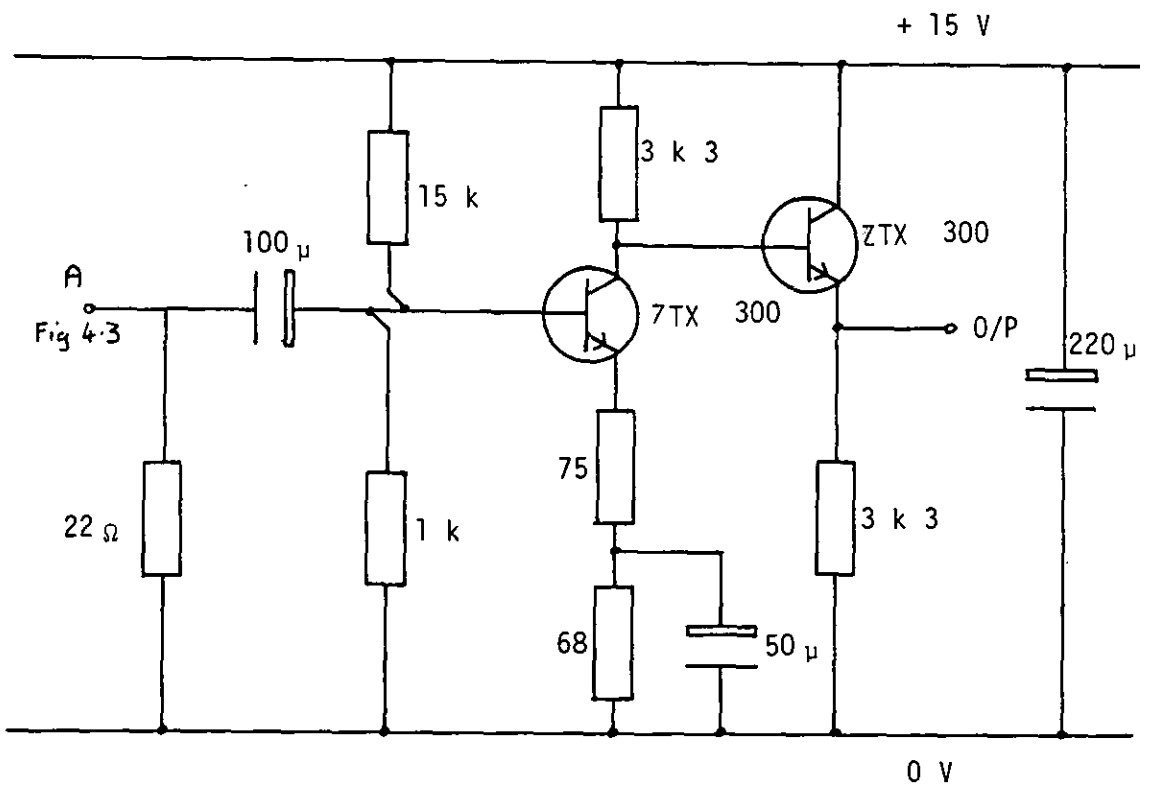


Figure 4.7b

Circuit diagrams for probe coil amplifiers

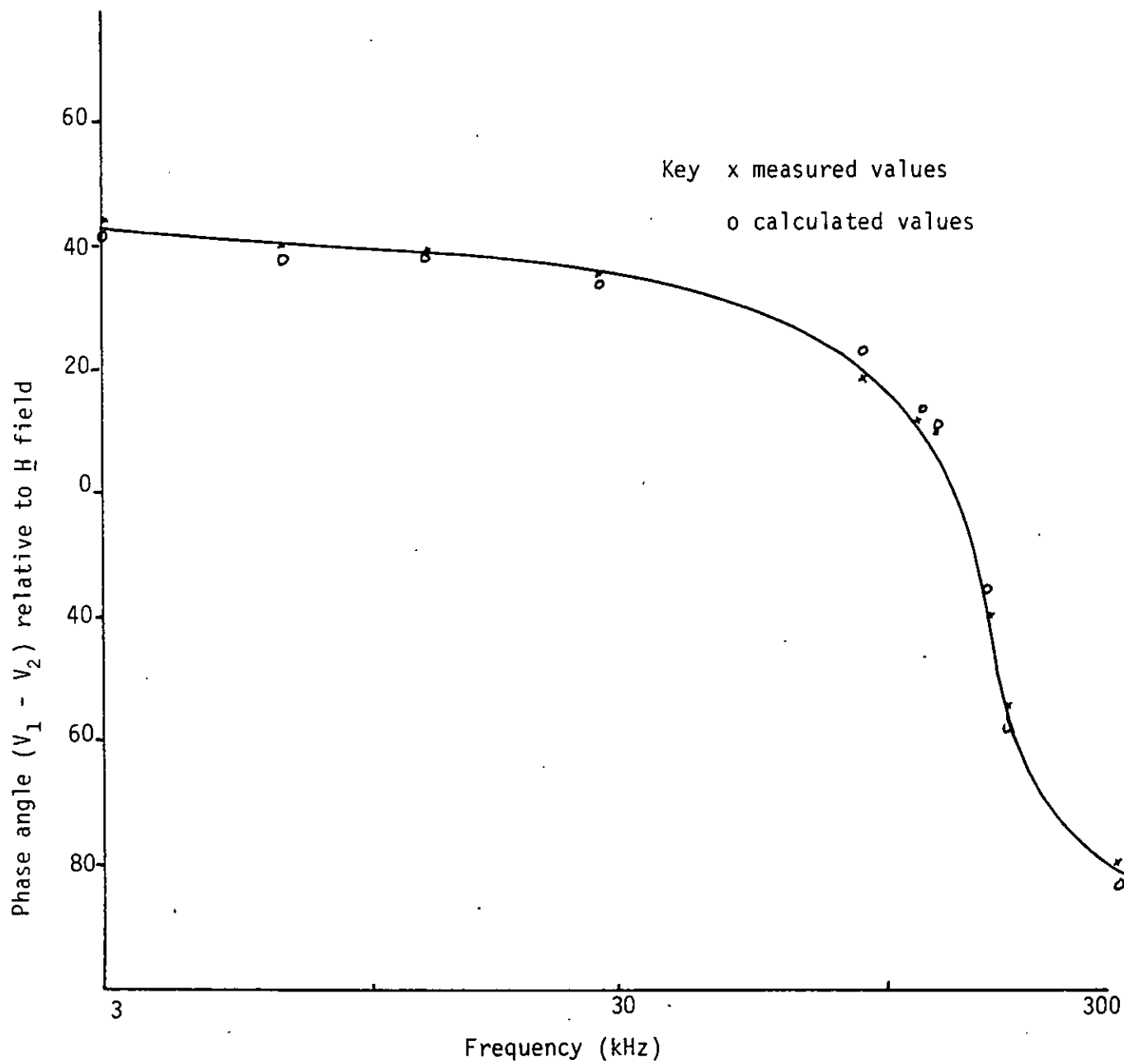


Figure 4.8 Graph to show phase variation, error, with frequency for the voltage proportional to surface impedance for a 25.4 mm (1.00 in) diameter aluminium bar

response of the phase meter became increasingly unreliable as the voltages decreased to 10 mV or less. It was noted however, that the current through the large outer coil was in phase with the H field and hence for phase measurement at the higher frequencies, a voltage derived from the resistor in the circuit of the large outer coil, may be used as part of the phase measurement system.

For lower frequency phase measurement however, the system described above could not be used. It was found that the voltages used for the phase measurement were both of insufficient magnitude for the reliable operation of the digital phase meter. As a consequence the circuits of Figure 4.7a and 4.7b were devised to overcome this difficulty. The circuit of Figure 4.7a was used to amplify the voltage proportional to the surface impedance, whilst the circuit of Figure 4.7b was used to amplify the voltage proportional to the magnetic field strength.

The phase measurements resulting from this system are shown in Figure 4.8. It may be seen from Figure 4.8 that for relatively low frequencies, the phase measurement for the surface impedance does in fact approach 45° . The variation in the measured phase angle from 45° for higher frequencies is a direct result of the term $j\omega\mu_0 h'$ of equation 3.95, page 57, becoming comparable with the surface impedance. It may be seen from Figure 4.8 that the measured values of phase angle and those calculated using equation 3.95 give a broad measure of agreement.

It should be noted that the phase angle measurement for the surface impedance, using the method outlined in section 4.3.4, page 76, departs significantly from 45° for frequencies of more than a few hundred

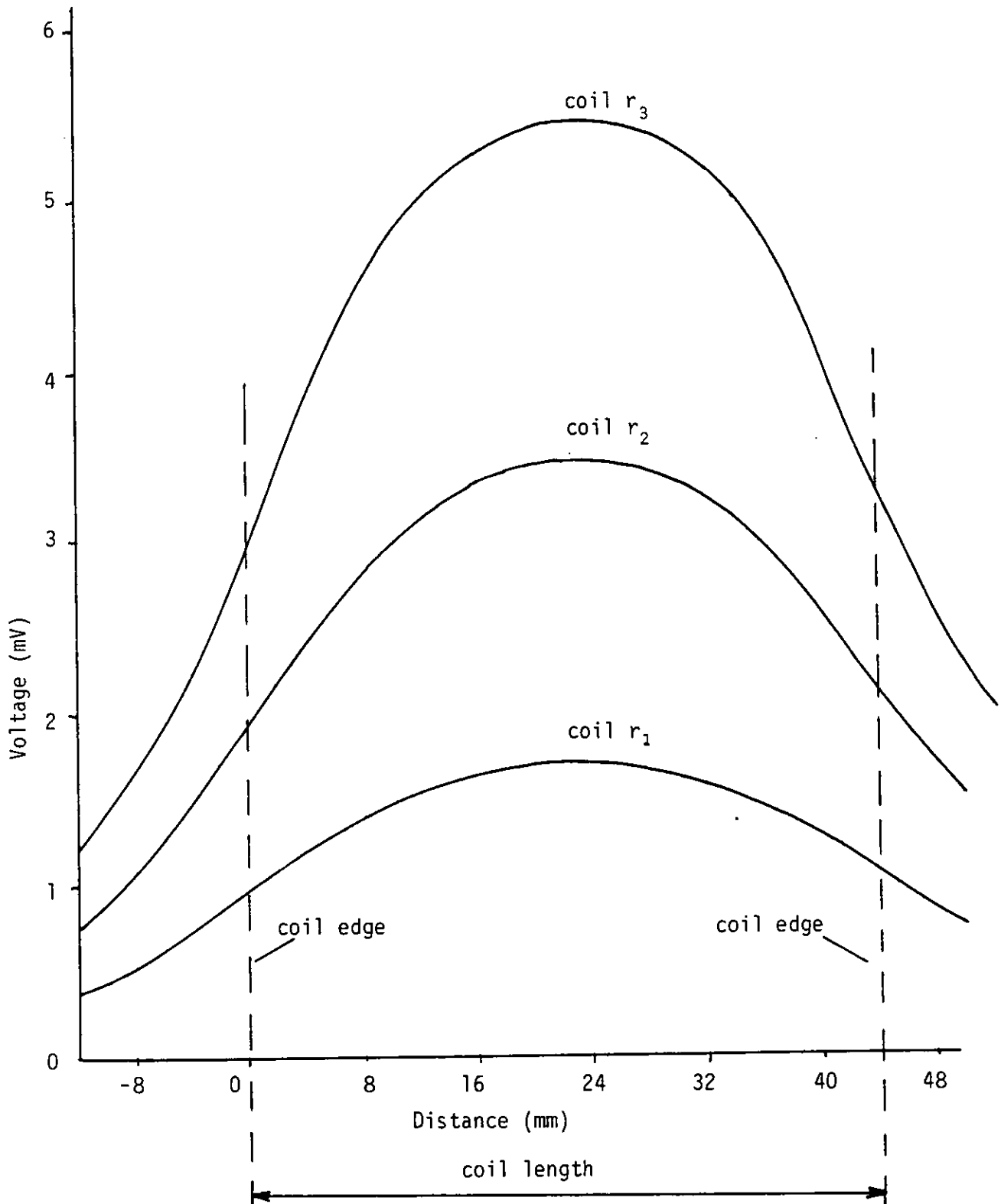


Figure 4.9 Graph to show variation of probe coil voltage with axial displacement

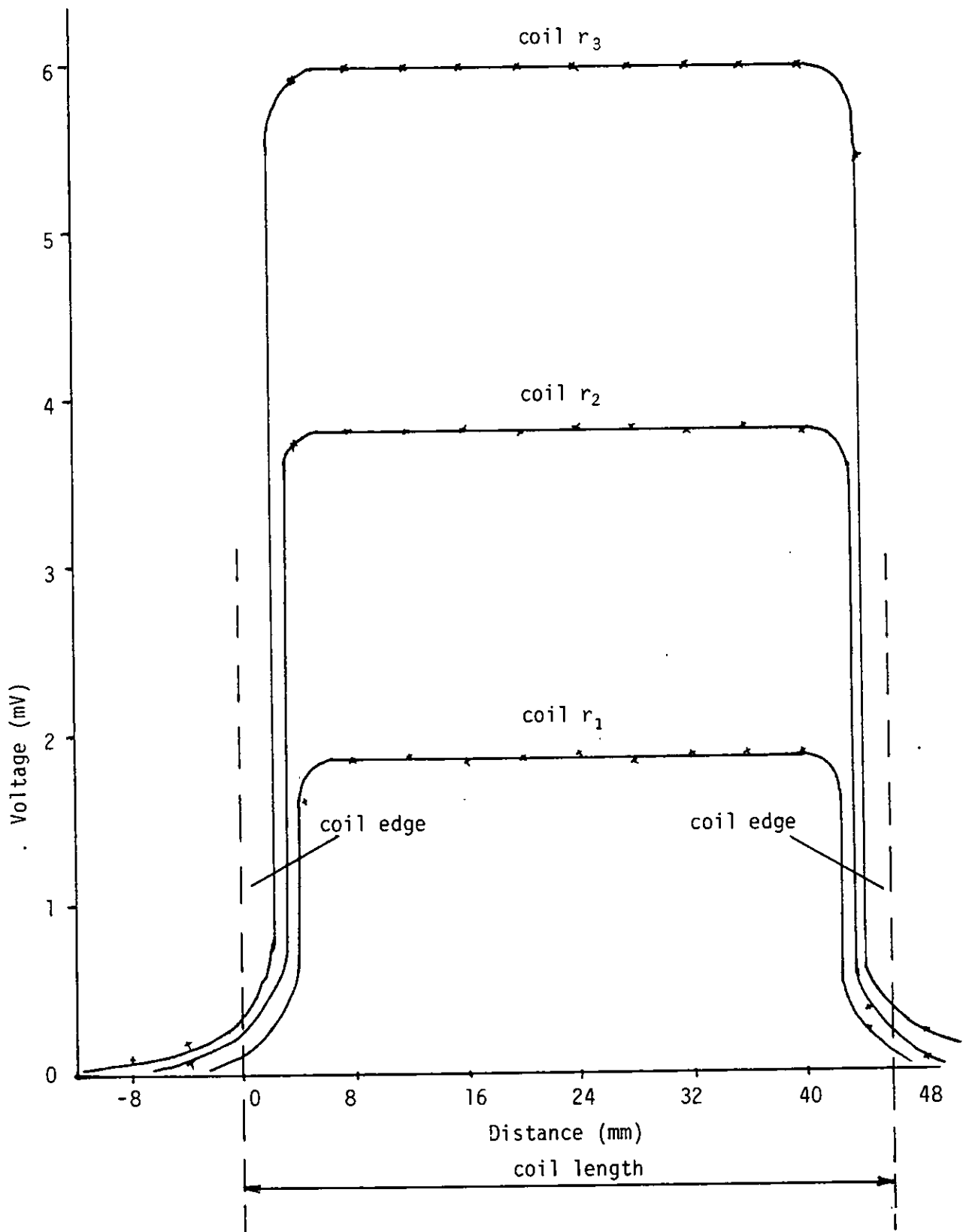


Figure 4.10 Graph to show variation of probe coil voltage with axial displacement after modification of outer coil

kilohertz. . If however it subsequently becomes necessary to measure the phase angle of the surface impedance at this higher frequency, this problem may be controlled by changing the ratio of the number of turns on the probe coils involved in the measurement of the surface impedance.

The implementation of an eddy current system, which is described in detail in Chapter 5, utilizes the relatively low frequency of 10 kHz. At this frequency the phase measurement for the surface impedance is quite acceptable, and thus the turns ratio for the probe coils will be as determined in section 4.3.4, page 76, and set at 2:1.

4.4 Mathematical Model Verification

The mathematical model given in equation 3.25, page 28, was produced by the assumption of an infinitely long outer coil. The infinitely long outer coil is almost impossible to approximate to in practice and hence verification is not practical. However, it is possible to verify the modified mathematical model given by equations 3.43, 3.44, page 32, and equations 3.53 and 3.54, page 33.

In order that verification of this modified mathematical model may proceed, certain changes were made to the coil system shown in Figure 3.1, page 19, and Figure 4.1, page 64. The nature of these changes are such that the axial distribution of the \underline{E} and \underline{H} field are made to approximate to a square wave, which is radically different to the distribution which would normally result from a current flowing through the coil, Figures 4.9 and 4.10 may be seen to illustrate these differences.

The square wave distribution, or in fact any required distribution, was produced by splitting the large outer coil in to segments of six turns

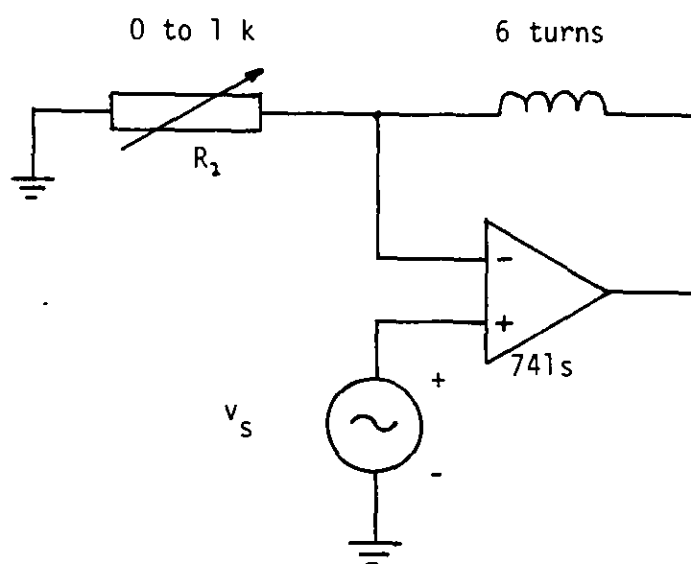


Figure 4.11 Circuit diagram for constant current source for coil segments

each, that is giving six discrete steps in differing values of coil current per quarter wave length. Thus giving twenty five steps for the whole coil length. Each segment is then driven separately from a current source at a fixed frequency. Figure 4.11 gives the circuit details for the type of current source used.

The input impedance seen by the oscillator in Figure 4.11 is high, hence one oscillator may be used to drive all twenty five circuits. This results in the signal current to each segment being at precisely the same frequency and phase as all the other segments.

Careful adjustment of the current flowing in each segment of the coil was made by adjustment of the resistor R. The maximum current for each segment in this case at a frequency of 10 kHz was ≈ 6.8 mA. A check was then made on the axial distribution of induced voltage in the probe coils to ensure a square wave distribution of the type given in Figure 4.10.

The last two segments of the coil, at the coil edge, have the current flowing in the opposite direction. This is to enable the 'good' square wave approximation of Figure 4.10 to be achieved without there being any appreciable voltage picked up by the probe coil, after the coil edge has been passed.

Measurements of the surface impedance, both in phase and magnitude, give similar values to those outlined in the previous section. Hence it may be concluded that the mathematical model thus produced and using the square wave approximation gives an adequate representation of the system described, but at this stage only for non-ferrous materials. Ferrous materials are dealt with in detail in the following section.

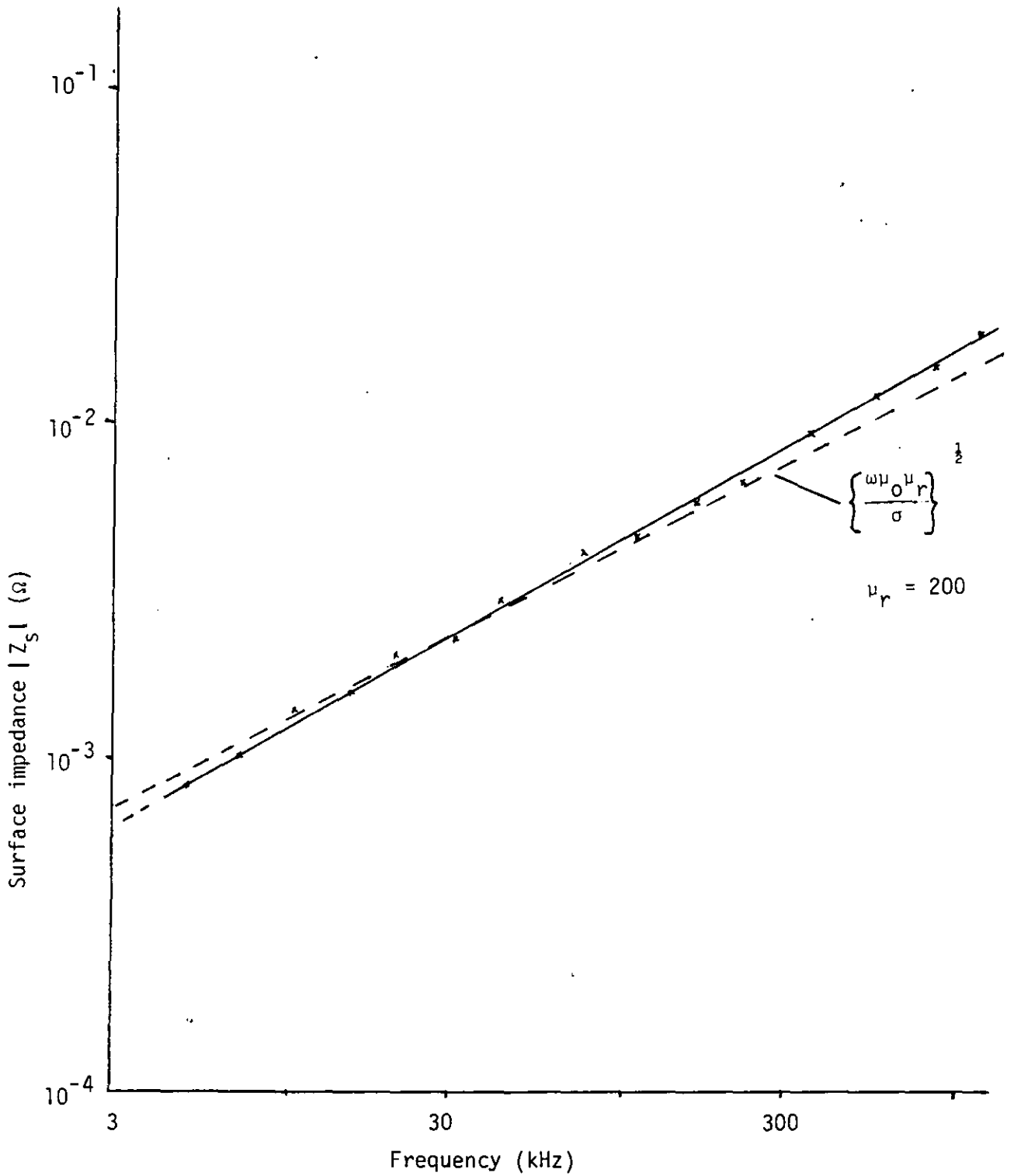


Figure 4.12 Graph of surface impedance against frequency measured for a 25.4 mm (1.00 in) diameter mild steel bar

4.5 Measurement of Surface Impedance, Mild Steel

The measurement of the surface impedance for ferrous material, in this case a 25.4 mm (1.00 in) diameter mild steel bar; was initially carried out in a similar manner as was the case for the non-ferrous material. However as the magnitude of the surface impedance for ferrous material may be much greater, for a given frequency, than for a similar non-ferrous sample, the measured values of induced voltage proportional to the surface impedance are also larger. Thus in principle it should be possible to measure the surface impedance for much lower frequencies for the ferrous material. In practice the lower limit was much the same for both types of material. The lower limit, in the case of the ferrous material, was determined by the problems associated with radio interference and noise and the magnitude of the voltages induced in the coils.

These initial measurements on a mild steel bar, are reproduced in Figure 4.12. It should be noted however that no direct comparison, at the moment, may be drawn from these measurements and the mathematical models produced in the previous chapter. This is as a consequence of the magnitude of the surface impedance being proportional to the value of the square root of the permeability of the material. For the case of the mild steel bar, unlike the non-ferrous case, the permeability may not be assumed to have a value close to unity. A value of 200 has been assumed for comparison purposes in Figure 4.12. It is also clear that the value of permeability will change with the magnitude of the current in the outer coil. It is also conceivable that stray magnetic fields will permanently magnetise the bar. This will also have the effect of changing the measured value of the surface impedance.

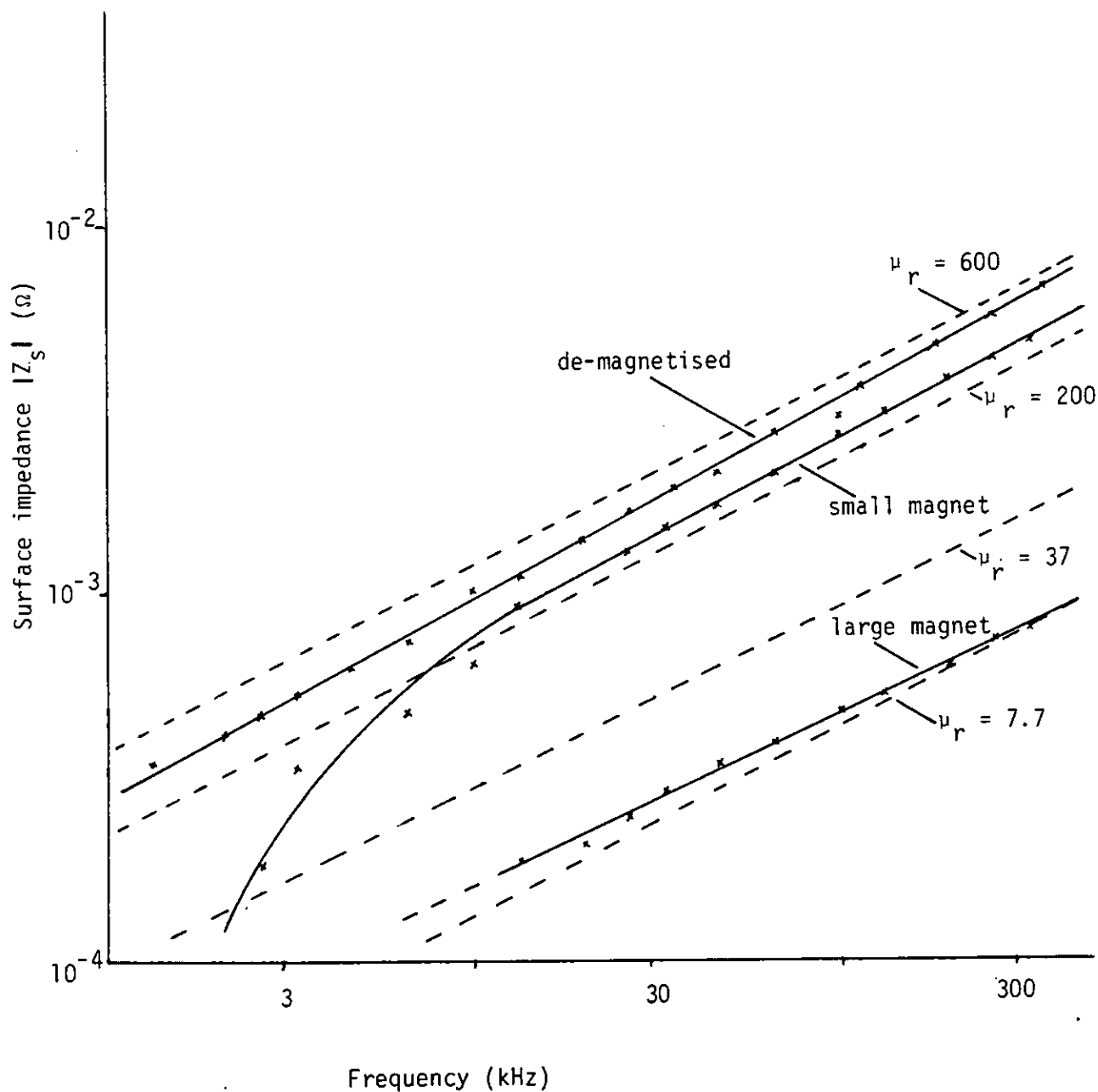


Figure 4.13 Graph of surface impedance against frequency measured for a 25.4 mm (1.00 in) diameter mild steel bar, for various magnetic states

It is as a result of the above considerations that it was thought necessary to devise a method of controlling, ie reducing, the permeability of the mild steel bar. Such a system would reduce, by external means, the permeability of the mild steel bar, to a value which will be much closer to that of the non-ferrous case.

Three possible ways of approaching this problem were considered.

- (i) Use of a large permanent magnet.
- (ii) Use of a large direct current supply to magnetise the mild steel bar.
- (iii) Use of 50 Hz supply derived from the 'standard mains' in order to magnetise the mild steel bar.

The first approach was rejected as a result of the difficulty of producing a uniform field of sufficient magnitude over a relatively large volume. However initial results, using large permanent magnets, and the measurements for which are presented in Figure 4.13, indicate that even though the magnetic field produced by these magnets was not uniform over a large part of the mild steel bar, the magnitude of the surface impedance was in fact reduced to a considerable extent over a wide frequency range.

The second approach was also rejected on the grounds that a large dc supply was not readily available and that the availability of such a dc supply would certainly be a problem for any practical eddy current gauge.

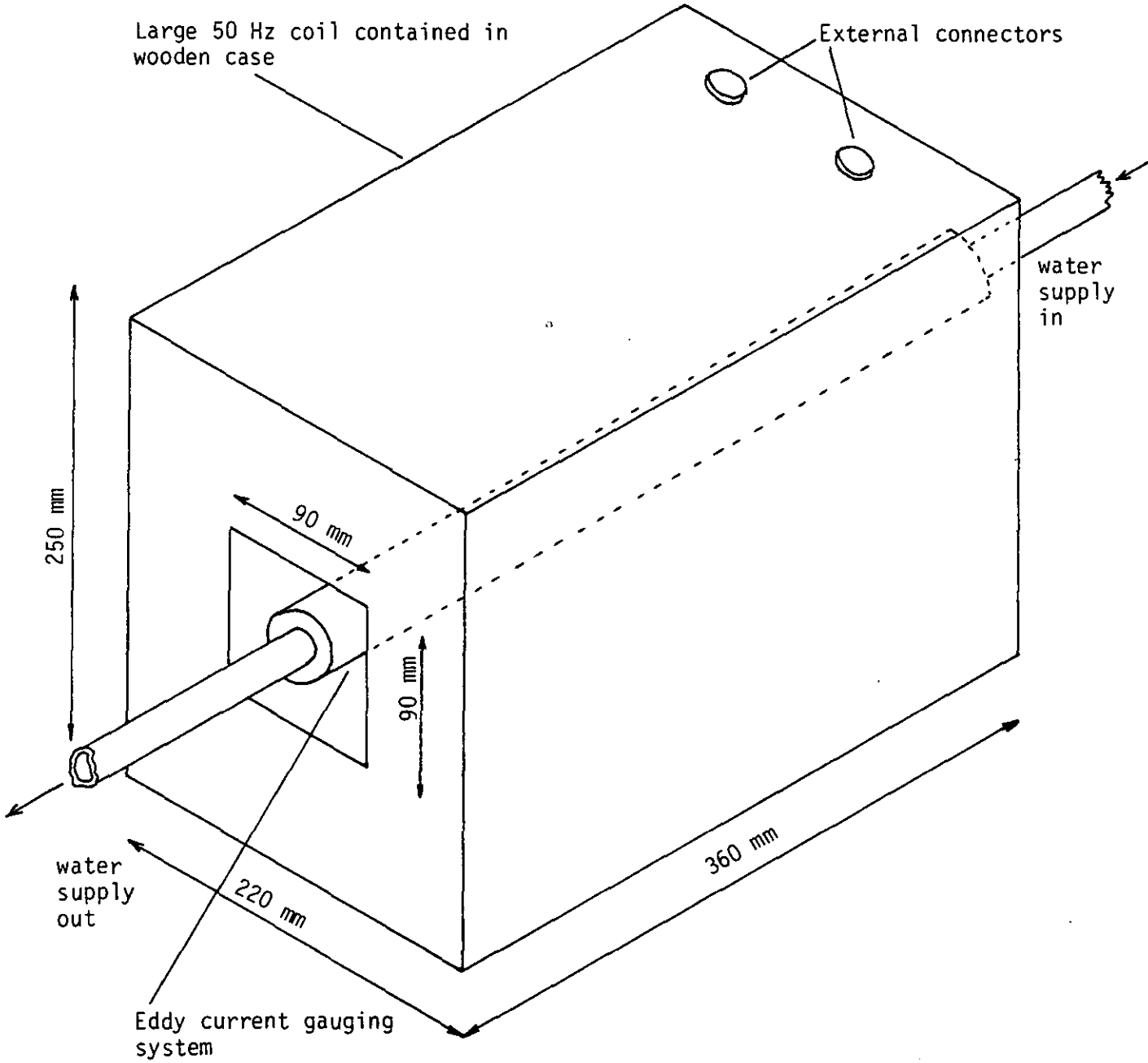


Figure 4.14 Magnetic saturation and water cooling system

A further problem associated with methods (i) and (ii) above is that with a dc or permanent magnet method of magnetisation of the mild steel bar, the mild steel bar will retain a certain amount of magnetism after any measurements have been made. This effect may present additional problems. As a consequence, any practical eddy current gauge which employs either of these two methods will need a de-gaussing system in order to ensure that the mild steel returns to its original de-magnetised state.

The third approach was considered to be the only feasible solution despite the inherent difficulty of dealing with a changing magnetic field. It was thought that by the use of certain electronic systems and techniques, which are outlined in Chapter 5, the difficulties of using this approach could be largely overcome. It should, however, be noted that one advantage of using the 50 Hz magnetic field is that the mild steel bar is automatically de-gaussed when the 50 Hz field is reduced to zero.

The basic approach to the problem of saturating the mild steel bar using the 50 Hz magnetic field was as follows. The entire eddy current gauging system was contained within a large coil, see Figure 4.14. When a current of up to 20 A at 50 Hz was passed through this large coil a magnetic field, which was measured at over 27,000 At/m, was produced.

This large field had two effects. The mild steel bar became hot very quickly and the resistors in the primary signal coil also became very hot very quickly. These problems were overcome as follows.

The power dissipated in the mild steel bar may be calculated approximately as follows:

For mild steel at 50 Hz the skin depth, using

$$\delta = \sqrt{\frac{2}{\omega \mu_0 \mu_r}} \quad \dots\dots\dots 4.6$$

will not be more than 1.5 mm. Hence the mild steel bar of 25.4 mm (1.00 in) diameter may be regarded as a 'thick slab' and then using the equations given in reference 51 as:

$$P/\text{unit area} = \frac{H^2}{\sigma \delta} \quad \text{W/m}^2 \quad \dots\dots\dots 4.7$$

and the value of H measured at I = 19 A was 27,430 At/m.

Using the Frohlich curve for mild steel⁵¹

$$B = \frac{H}{270 + 0.577 H} \quad \dots\dots\dots 4.8$$

gives B = 1.70 T

hence $\mu_r = 49.3$

From equation 4.5

$$P/\text{unit area} = 2.35 \cdot 10^4 \text{ W/m}^2$$

Hence for a mild steel bar of 203 mm (8.00 in) in length the total power dissipated was 380 W.

The 380 W of power dissipated, result in the bar becoming so hot that the perspex coil holder would be damaged if this rate of power dissipation was maintained for more than approximately 90 s. In order to prevent any damage to the coil holder, a 15 mm hole was drilled through the centre axis of the mild steel bar. A supply of fresh water was then allowed to pass through the hole in the bar at the rate of 4380 ml/min or 0.963 gal/min. Adequate cooling of the bar was thus achieved, with this rate of flow.

With water flowing through the mild steel bar at the rate quoted above, there was no subjective increase in the surface temperature of the bar, and the temperature of the water leaving the bar, measured by a thermocouple probe, showed a steady 1.40°C increase above the temperature of the water entering the bar. This magnitude of temperature increase indicates that the actual power dissipated in the metal of the bar is the same as that calculated above to within 10%.

It should be noted that the drilling of the mild steel bar does not represent the final solution to the problem of heat dissipation in the metal bar, as this is hardly a practical solution for anything other than short metal bars. It is felt that the problem of heat dissipation may not be evident for the case when high speed production methods are employed. However this problem is still rather serious for the study reported on in this thesis, Chapter 5 gives an alternative acceptable solution to this problem.

The next difficulty arising is that concerning the large power dissipation in the resistors connected to the primary side of the

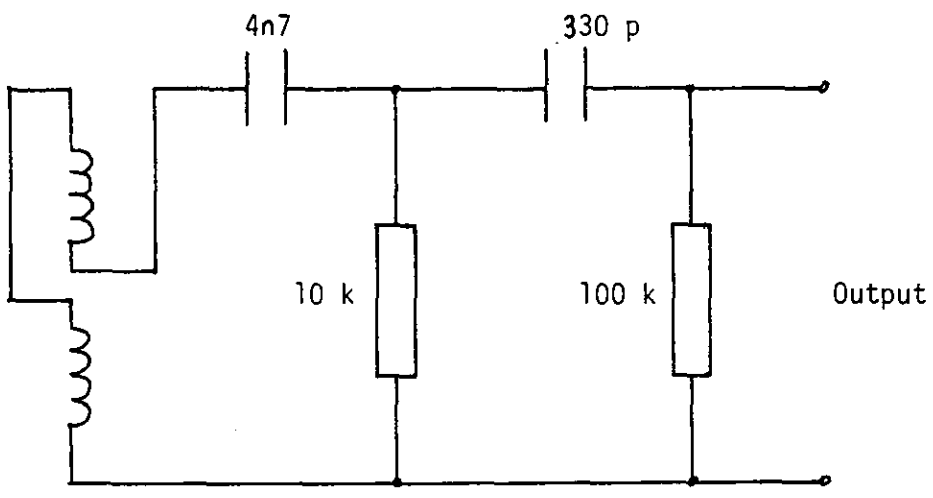


Figure 4.15 Cascaded R-C filters

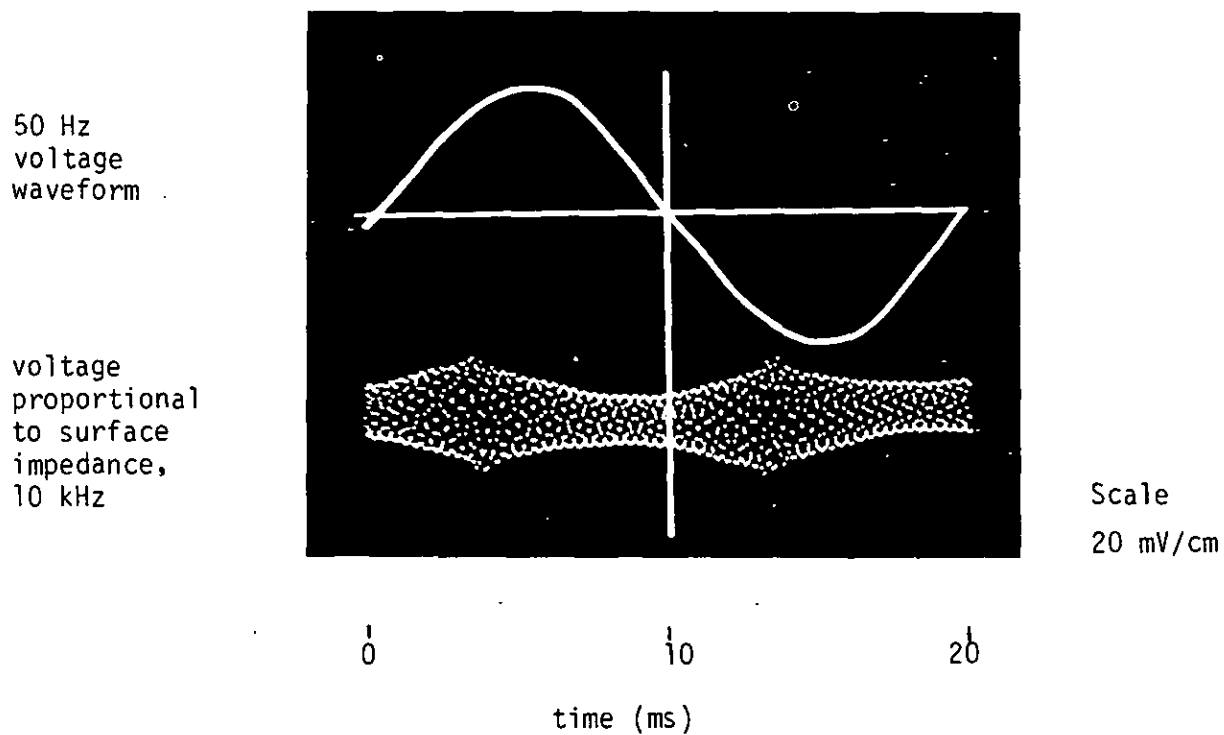


Figure 4.16 Variation of the voltage proportional to surface impedance, for a mild steel bar, compared with the voltage producing the 50 Hz magnetic field

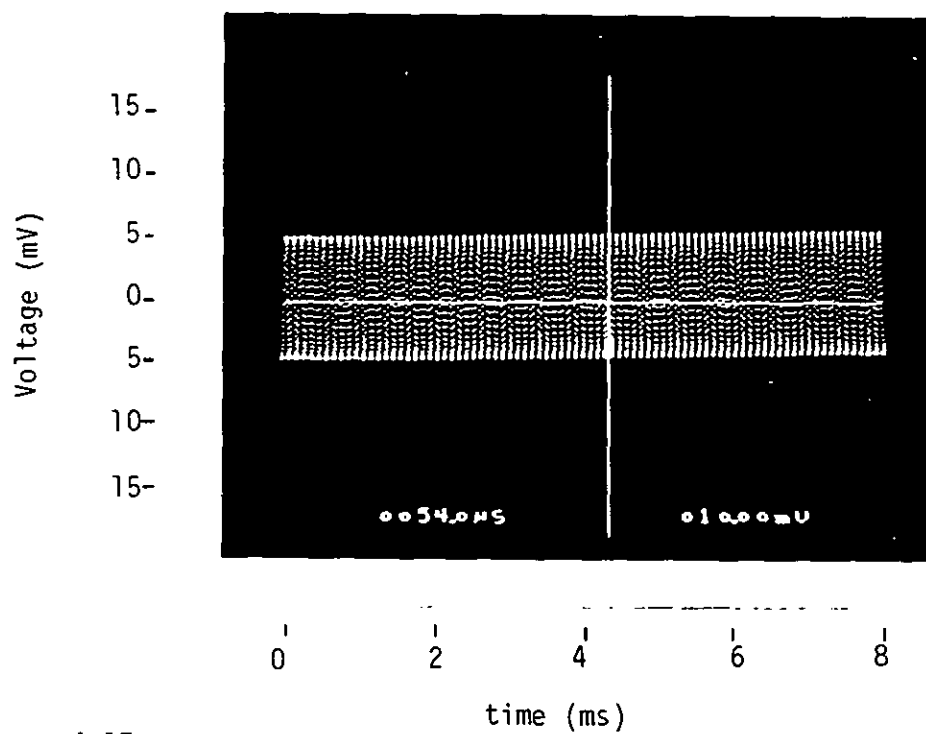


Figure 4.17a

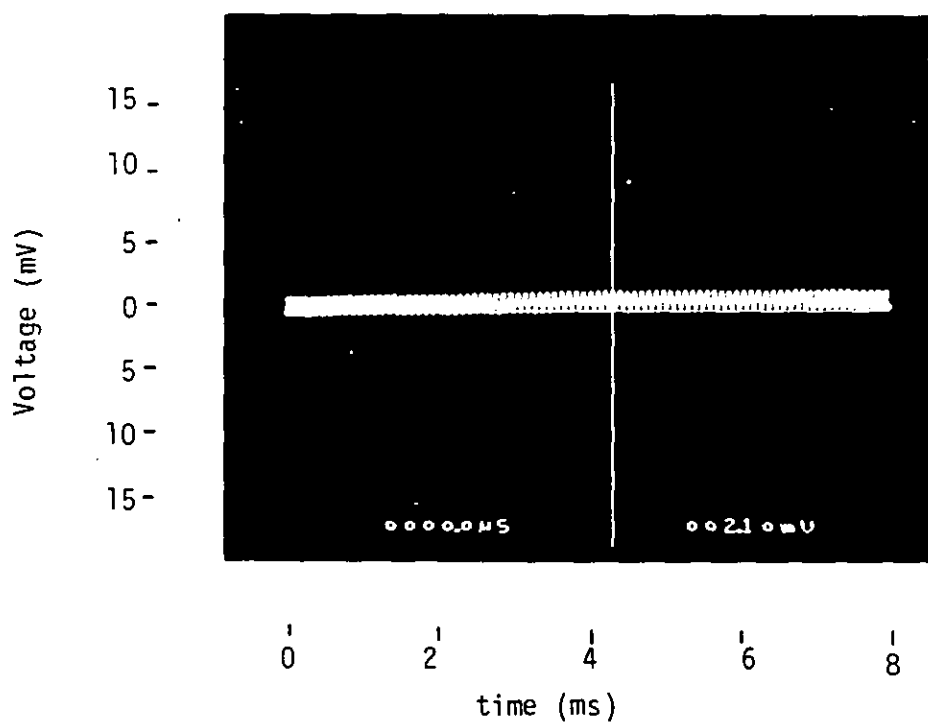


Figure 4.17b

Variation of voltage proportional to surface impedance for
 (a) non-metallic bar (b) aluminium bar when subject to the 50 Hz

signal coil. The resistors in question are the 22Ω types shown in Figure 4.3, page 67. This problem was adequately controlled by the use of an elementary form of high-pass filter, placed in series with the resistors. By calculation and experiment it was found that using capacitors of $2.5 \mu\text{F}$, in the high-pass filter, achieved the required blocking of the 50 Hz signal.

The resulting waveforms, for the voltage proportional to surface impedance, using a frequency of 10 kHz and two RC filters to eliminate the unwanted 50 Hz wave form see Figure 4.15, are shown in Figure 4.16 for the mild steel bar and in Figure 4.17a and 4.17b for the non-metallic and aluminium bars respectively, for comparison purposes.

It is now possible to consider the phase of the surface impedance as a result of the influence of the external magnetic field. It is not possible to measure the phase of the voltage proportional to Z_s in the manner which was used previously. This is because the amplitude of the signal is changing and this will cause errors in the digital phase meter. A Nicolet digital storage oscilloscope with a $5\frac{1}{2}$ inch floppy disc type of memory was used. The results obtained are shown in Figure 4.18 and Figures 4.19, 4.20a and 4.20b. This shows that there is no apparent phase change as the magnetisation of the mild steel bar increases.

Using the above constraints, the measurements at 10 kHz of the magnitude of the surface impedance for the unmagnetised specimen was found to be $1.85 \cdot 10^{-3} \Omega/\text{sq}$, and for the case of a relatively large magnetic field it falls to $2.80 \cdot 10^{-4} \Omega/\text{sq}$ or less depending on the intensity of the magnetising field.

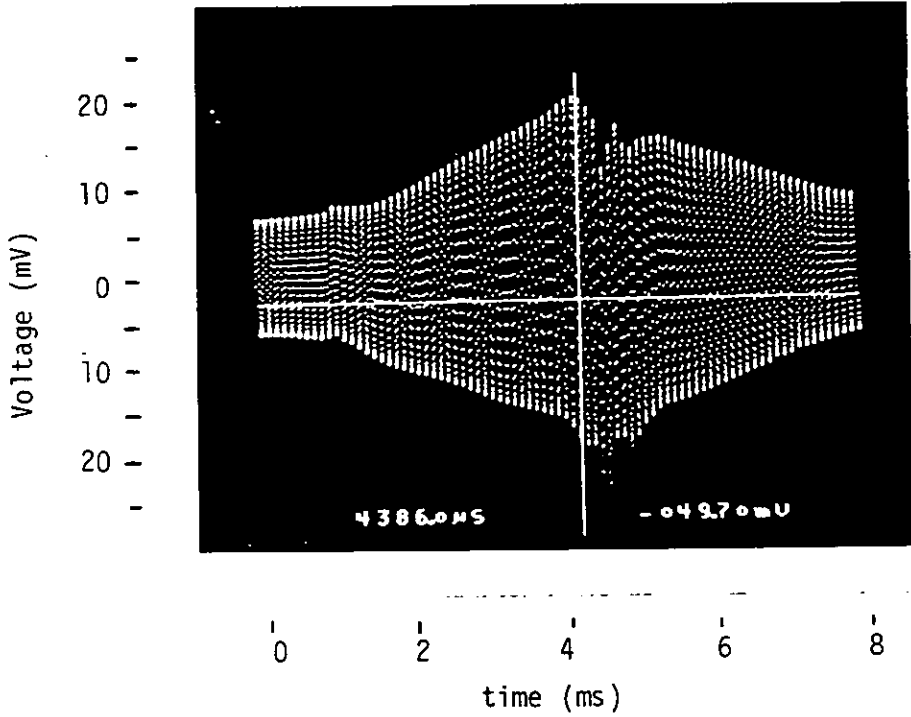


Figure 4.18

Variation of voltage proportional to surface impedance for a mild steel bar subject to a 50 Hz magnetic field

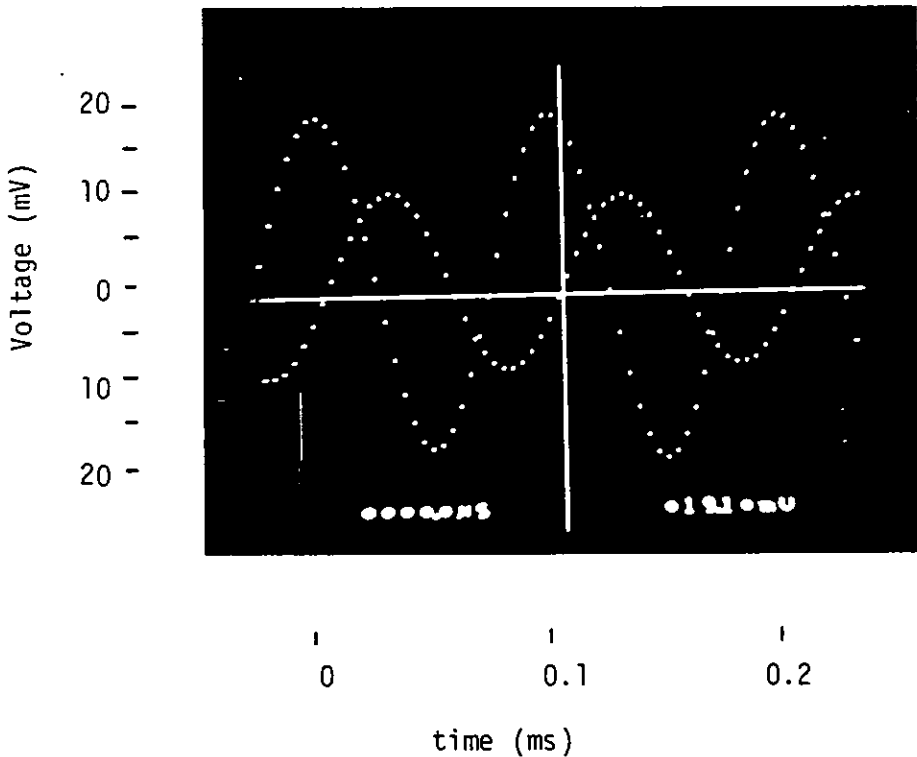


Figure 4.19

Representation of the phase angle of the voltage proportional to surface impedance for the mild steel specimen in its demagnetised state

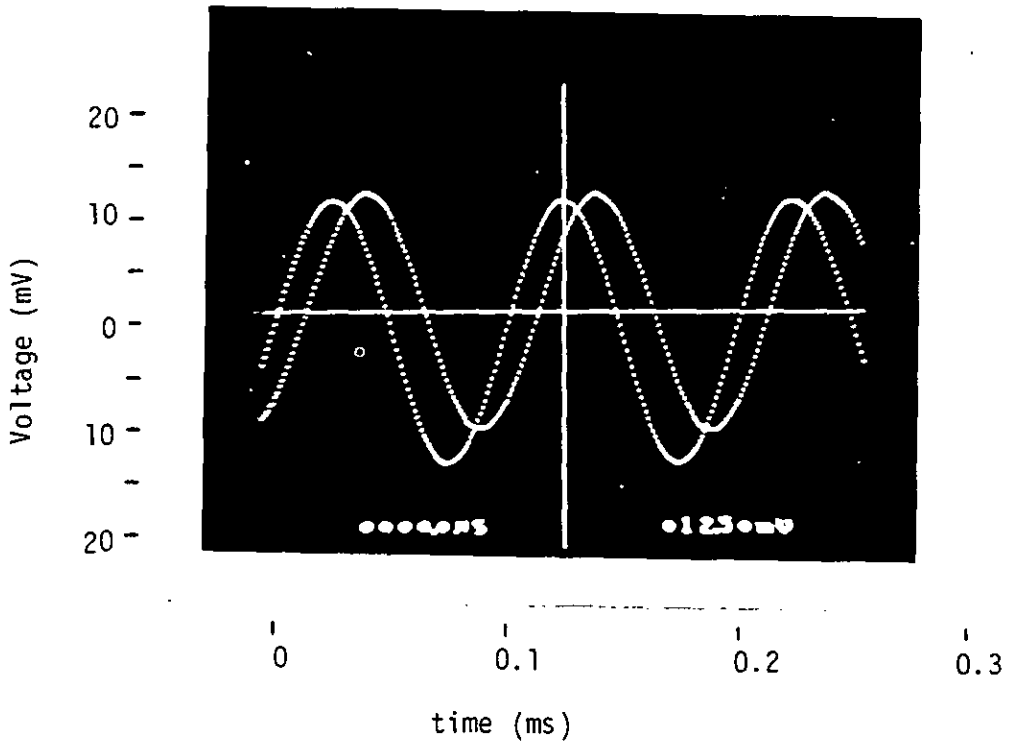


Figure 4.20a

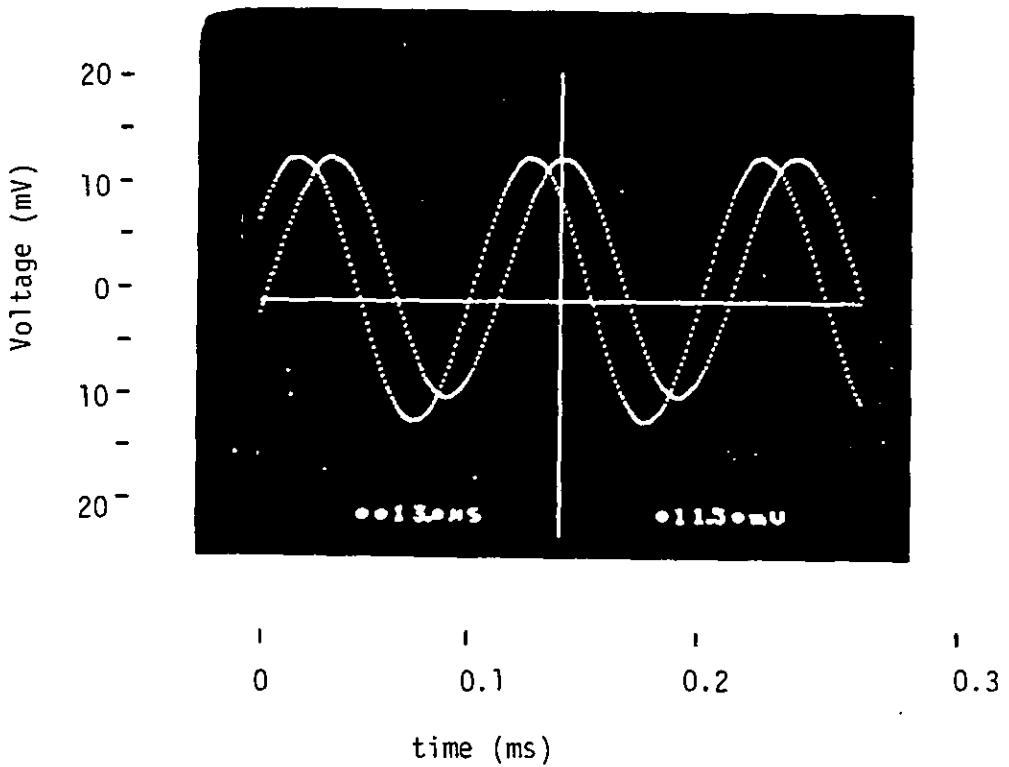


Figure 4.20b

Measurement of the phase angle of the voltage proportional to the surface impedance for a mild steel bar of maximum magnetisation

It may be observed from Figure 4.16 that the minimum measured value for the surface impedance would seem to occur before the maximum and minimum of the external 50 Hz magnetising field. This effect is thought to be as a result of hysteresis in the mild steel, with the maximum values of surface impedance occurring at the point of the minimum magnetisation of the specimen.

It is now possible to compare the results obtained in this section with the mathematical model which was developed in Chapter 3.

4.6 Mathematical Model Verification

The verification of the mathematical model produced in Chapter 3, for an eddy current gauging system with a metallic conductor, may be performed for the case of a square wave distribution of the \underline{E} and \underline{H} field in an axial, or longitudinal direction, with respect to the large outer coil or inducing coil. The type of distribution is shown in Figure 3.4, page 37, and approximated to in Figure 4.10, page 83.

The measurements of surface impedance and other parameters, recorded in the previous sections, produce a good, but inevitably not an exact fit to the mathematical model developed in section 3.2, page 21. The errors between the mathematical model thus produced and the practical measurements, is a result of the unpredictability of some of the model parameters. For example the relative permeability of mild steel, may not in fact be unity even when acceptable saturation techniques are used.

It is however clear from the mathematical model evaluation of section 3.3, page 34, that the model is valid for various heights of the probe coil above

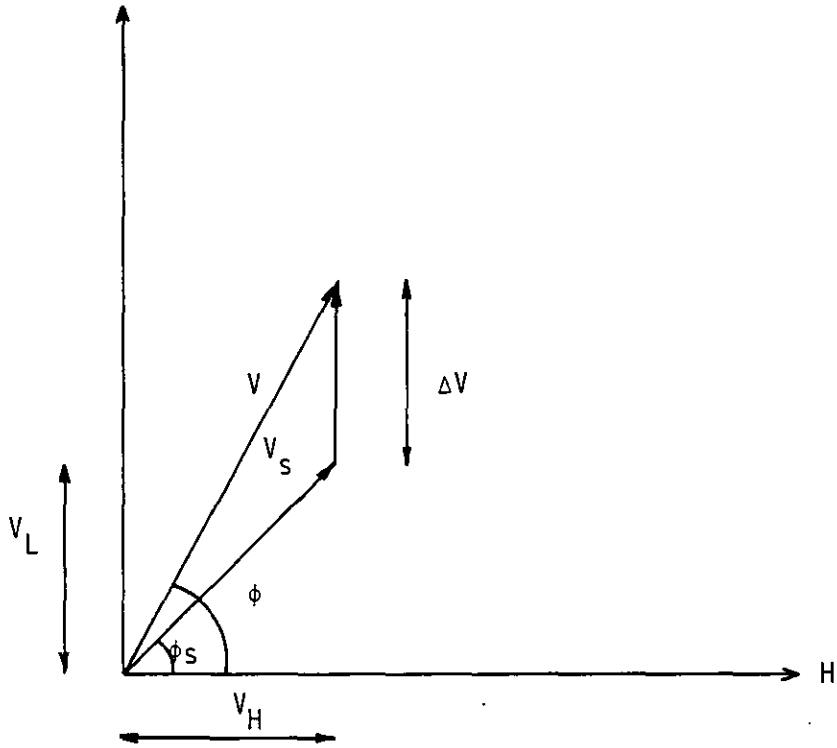


Figure 4.21 Phasor diagram for the eddy current gauging system

the metallic surface. Thus distance (height) measurements may be made, and the results compared directly with micrometer measurements of the heights of the probe coils above the metallic surface.

It will be shown in the next section that this type of measurement gives good agreement between theory and practice, for both ferrous and non-ferrous metallic bars, over a comparatively wide range of frequency.

4.7 Distance Measurement

Consider now the phasor diagram shown in Figure 4.21 for an eddy current gauge with a mild steel bar and a probe coil at a height 'h' above the metallic surface. From the phasor diagram:

$$V_s \sin \phi_s = V \cos \phi \quad \dots\dots\dots 4.9$$

for $\phi_s = 45^\circ$

$$\text{Hence } V \sin \phi = \Delta V + V_s \sin \phi_s \quad \dots\dots\dots 4.10$$

combining equations 4.9 and 4.10 yields

$$\Delta V = V(\sin \phi - \cos \phi) \quad \dots\dots\dots 4.11$$

From equation 3.92, page 55, and for $\Delta V = V_1$, gives

$$\Delta V = 2\pi r_0 n_1 \underline{H} \omega \mu_0 \left(h_1 + \frac{h_1^2}{2r_0} \right)$$

substituting for \underline{H} from equation 3.98, page 59, yields:

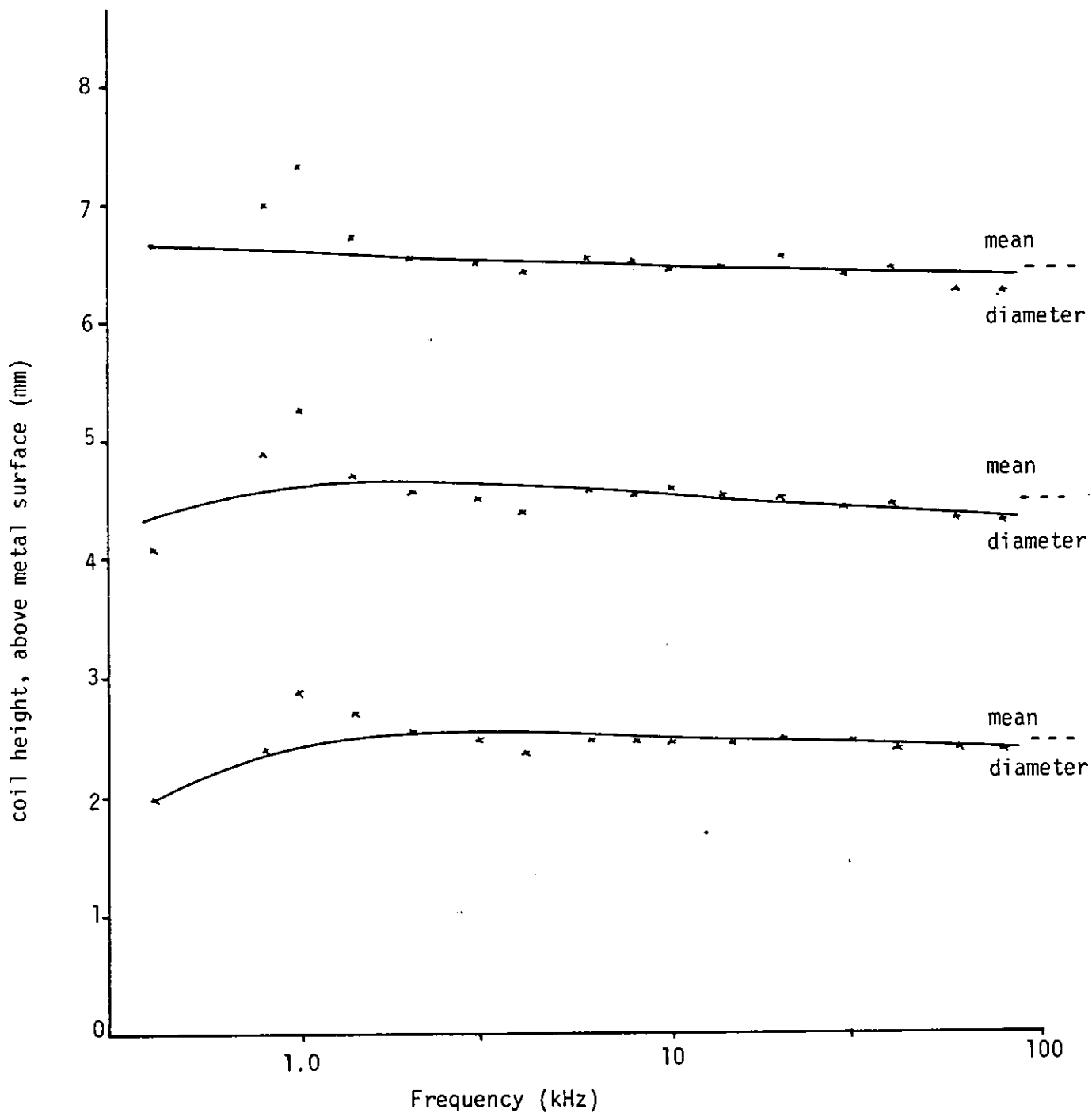


Figure 4.22 Graph of measured coil height against frequency for a 25.4 mm (1.00 in) diameter mild steel bar

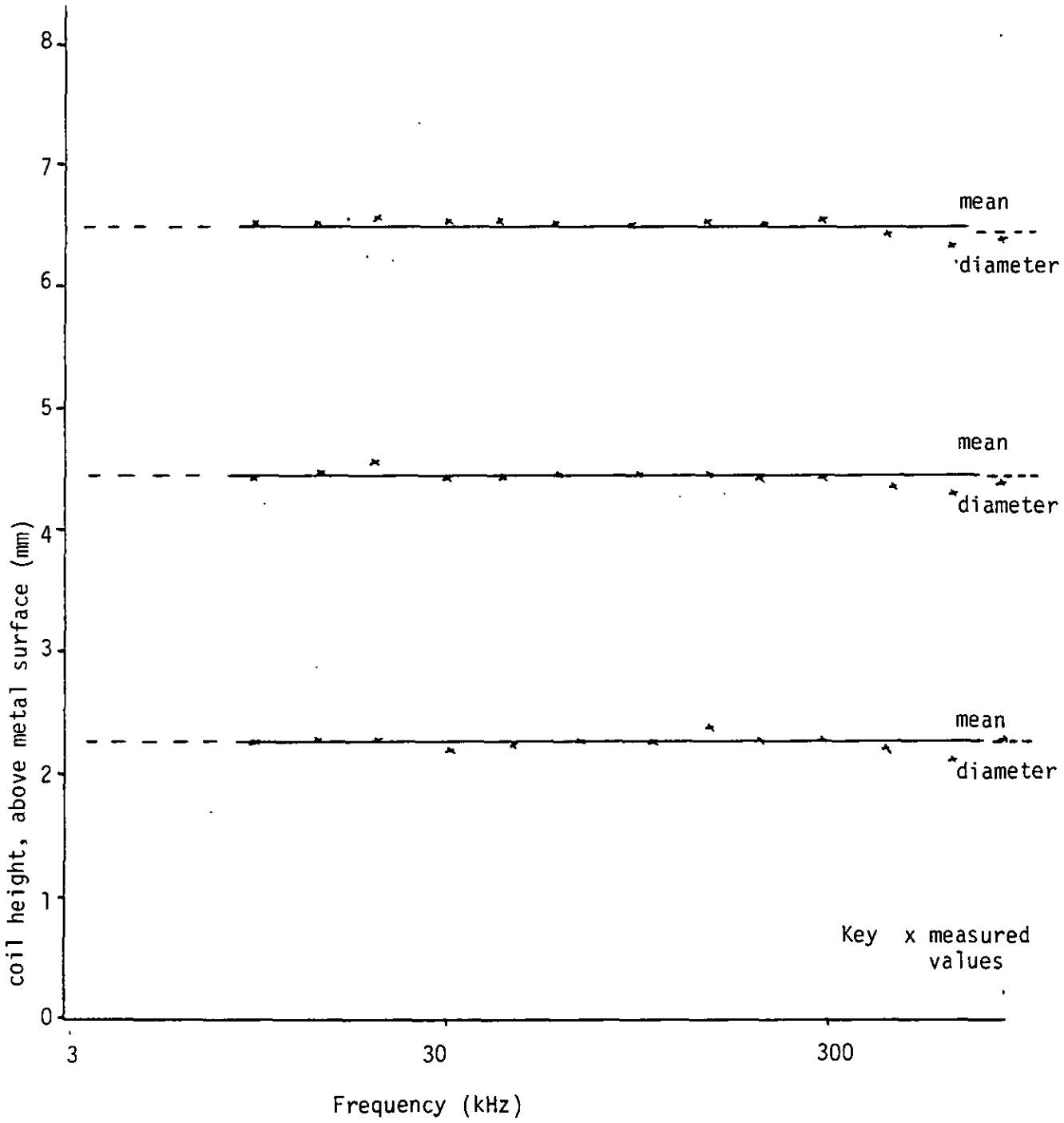


Figure 4.23 Graph of measured coil height against frequency for a 25.4 mm (1.00 in) diameter non-ferrous aluminium bar

$$\Delta V = \frac{2\pi r_0 n_1}{h \ell n_2} (V_1 - V_2) \left(h_1 + \frac{h_1^2}{2r_0} \right) \dots\dots\dots 4.12$$

where V_1 and V_2 are the voltages measured for the probe coils n_1 and n_2 respectively.

$$\therefore h_1 + \frac{h_1^2}{2r_0} = \frac{V(\sin\phi - \cos\phi)h \ell n_2}{(V_1 - V_2) 2\pi r_0 n_1} \dots\dots\dots 4.13$$

$$h_1^2 + 2r_0 h_1 - \frac{V(\sin\phi - \cos\phi)h \ell n_2}{(V_1 - V_2) 2\pi r_0 n_1} = 0 \dots\dots\dots 4.14$$

Solving equation 4.14 for h_1 gives:

$$h_1 = -r_0 \pm \sqrt{r_0^2 + V \frac{(\sin\phi - \cos\phi)h \ell n_2}{(V_1 - V_2) 2\pi r_0 n_1}} \dots\dots\dots 4.15$$

By using the *positive* value in equation 4.15 and employing the elements outlined in the previous section it is now possible to predict the heights of the various probe coils above the mild steel and non-ferrous (aluminium) surfaces. The results of these measurements are given in Figure 4.22 and Figure 4.23.

It may be seen from Figure 4.22 that the computed heights, derived from the probe coil voltage measurement, compare well with the height derived from micrometer measurements of the diameters of the probe coils.

It is evident from Figures 4.22 and 4.23 that the accuracy of measurement, of distance for the eddy current gauging system, is to within 0.1 mm for the largest diameter coil and to within 0.05 mm for the two smaller diameter coils. The accuracy quoted is over three decades of frequency in each case.

4.8 Conclusion

From the previous sections it is apparent that the basic principles of eddy current gauging, and in particular the distance measurement quoted in the previous section, are sound, and with respect to the system used, produce results of acceptable accuracy. From the graphs reproduced in Figures 4.22 and 4.23 it may be seen that using the principles outlined previously, distance may be measured to within 0.05 of a mm ie to within 2 thousandths of an inch. The limit on the accuracy of this system would seem to be determined by the thickness of the wire used to wind the probe coils and by the accuracy to which the probe coils may be wound.

The accuracy quoted above at ± 0.05 mm is considered too inaccurate for most distance gauging applications, however the eddy current gauge described is merely a stage in the modelling of this type of system. Any practical type of distance gauge will incorporate a calibrating procedure which would eliminate the errors due to the thickness of the probe coil wire, location of the probe coils and other similar effects. Thus accuracies of considerably less than 0.02 mm could reasonably be expected from a gauge of this type.

It is on the basis of the work presented in the previous sections that the eddy current gauging system may be extended to produce a gauge which will reduce the labour involved in taking measurements on the system. That is, to all intents and purposes, the eddy current gauging system should automatically take, store, and if possible process, any measurements taken.

The measurements recorded in this thesis are for the most part rather laborious to take and collate. It is with this problem in mind that the principles thus far outlined should be extended to produce an eddy current gauging system which would achieve these measurements in an automatic manner.

It is now worth considering the type of signal which has to be measured and is shown in Figure 4.16. The measurement to be made on the signal reproduced in Figure 4.16, is in the region which corresponds to the time when the mild steel bar is in its magnetic saturation state, that is in the region when the signal is at its minimum. Hence for any automated measuring system, there must be an element of timing to enable the system to identify and select the points of interest, and to record the voltage at specified points in the cycle.

To achieve this end it was thought necessary to utilize a digital measuring and storage system, as the analogue equipment available was considered unsuitable for the accurate measurement of the type of signal represented in Figure 4.16.

It is with this end in view that the implementations of an automatic microprocessor-aided measuring system is described in the next chapter, together with its principle of operation.

CHAPTER 5 IMPLEMENTATION OF A MICROPROCESSOR-AIDED MEASURING
SYSTEM

5.1 Introduction

The principles of eddy current gauging outlined in the previous chapters of this thesis are, on the whole, rather complex, and as a result the measurements which need to be taken are of necessity both difficult and tedious. In particular measurements taken for the ferrous bar, when it is subjected to an alternating magnetic field, were found to be impossible unless some method of storage was used. Thus in order to implement a practical and automatic eddy current measuring system, without recourse to the rather expensive storage system as described in Chapter 4, a microprocessor based measuring system was thought to be a solution which would be both cheap and easy to operate.

The microprocessor based system would be used as an aid to measurements taken within the system. It would not, however, be a complete eddy current gauge. The implementation of a complete eddy current gauge of the type described here, must await the development of much faster processors, of the type which are not currently available. In Chapter 6 this anticipated development is discussed in more detail.

The microprocessor aided measuring system, for use as part of an eddy current gauging system described in this chapter is based on a microprocessor system which is designed to automatically measure and record the probe coil voltage which is proportional to the magnitude of the surface impedance. This measurement is made for the case of

the 25.4 mm (1.00 in) diameter mild steel bar when it is subjected to an external magnetic field of such an intensity that the bar will be saturated over a considerable part of the 50 Hz waveform. The measurements of the voltage, which is proportional to the surface impedance, will only be taken when the mild steel bar is in the saturated state.

The measurements presented in Chapter 4 indicate that for the eddy current gauging system under consideration, and using the external 50 Hz magnetic field, the following system design criteria should be met in order to allow the system to operate correctly.

- (i) The measuring system will be required to select that part of the probe coil voltage signal which corresponds as closely as possible to the saturated state of the mild steel bar, ie the range over which the probe coil voltage is at its minimum value, as shown in Figure 5.1, page 113, and Figure 4.16, page 96.
- (ii) The mild steel bar must not be subjected to the 50 Hz magnetising field for more than 90 seconds. This is because the heating effect in the magnetically saturated mild steel bar when subject to the 50 Hz magnetic field, is such that the heat dissipated will cause damage to the equipment after 90 seconds, as discussed in section 4.5. One consequence of this 90 second limitation on the mild steel bar would be for the case where the system was used in association with continuous bar production. The 90 second limit would set a minimum for the speed of travel of the bar through the gauge.

(iii) As a consequence of (i) and (ii) above an automatic means of recording the measurements thus taken will be required. The probe coil voltage to be measured will be changing twice over the 50 Hz cycle, and thus the voltage will be difficult if not impossible to measure using simple analogue equipment.

As suggested in previous chapters, it would appear that some type of computer controlled system needs to be developed for all the above criteria to be satisfied.

Further, the computer/microprocessor will need to operate in real time, as opposed to using a time sharing system. A time sharing system, such as the Prime 750 computer used for the mathematical model evaluation of Chapter 3, would be impractical, as for this eddy current gauging system to operate successfully, great care is needed with the timing of the various operations. It would present an insoluble extra problem if the time sharing system stopped running the program during one of the critical timing phases, see section 5.3, page 116, and 5.4, page 118. A mini-computer or microprocessor, operating in real time, would seem to be best able to overcome the constraints detailed above.

The selection of a processor to be used for the implementation of a prototype gauging system was of necessity given careful consideration in order to satisfy the constraints listed above. Other relevant points were that the processor should be:

(i) convenient to operate

(ii) small in size

(iii) inexpensive to buy and to operate.

For the reasons listed above a microprocessor, rather than a mini computer was selected. The type of microprocessor used for this eddy current gauge was the Intel 8085. The Intel microprocessor system was used on the grounds that the Intel system is relatively simple to operate, the corresponding microprocessor development system (MDS) is readily available, and the internal clock frequency for the Intel 8085 is 6.125 MHz. This frequency is, at the moment, higher than most other easily available microprocessors.

A high clock frequency leads to fast processing times, the cycle time for the 8085 CPU is $0.32 \mu\text{s}$. Fast processing is a requirement for a system which has to sample, measure and process a 10 kHz signal voltage. All the processing for each measurement of the 10 kHz probe coil voltage, for this system, is completed within less than one period of the 10 kHz probe coil signal, ie within 0.1 ms, in order that the processor system may be re-set for the measurement of the next peak of the 10 kHz signal as shown in sections 5.3, page 116, and 5.4, page 118. For the processing to be complete within 0.1 ms it is a basic requirement that the processor must be fast. It is envisaged by the author that as the cycle times for future microprocessors decrease, ie clock frequencies increase, then rather more ambitious processing for eddy current gauging systems may be attempted, this development is discussed in some detail in Chapter 6.

The basic eddy current gauging system described in this chapter, samples the 10 kHz probe coil voltage, as given by equation 3.95, which

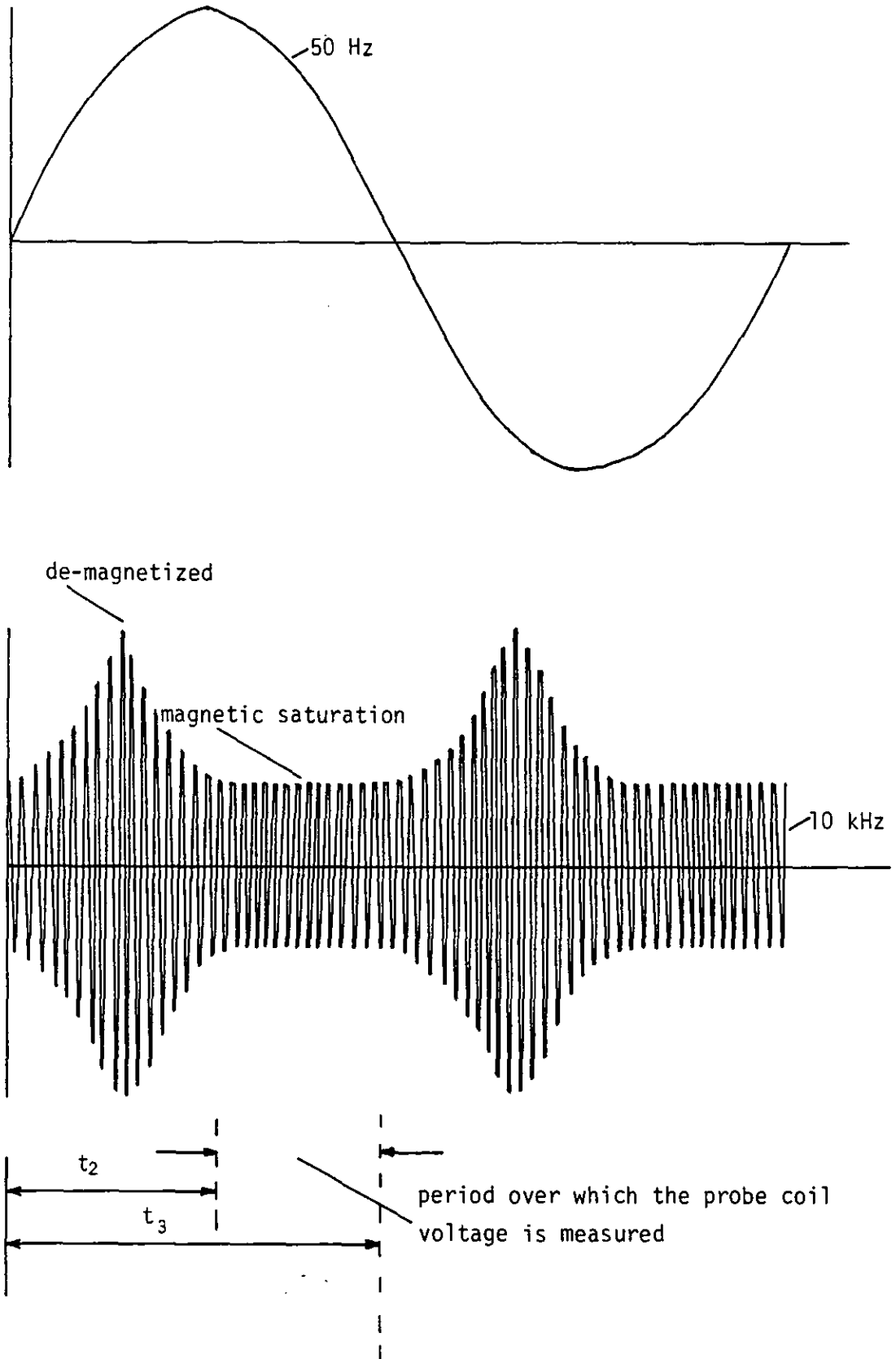


Figure 5.1 Diagram showing the measurement period for the 10 kHz probe coil waveform

is proportional to the magnitude of the surface impedance and then either records or displays the value thus determined. Once this probe coil voltage has been accurately measured and recorded, it is then possible to produce, with a certain amount of mathematical manipulation and further measurement, values for the height of the coil above the metallic surface, or the surface impedance or any other parameter which the eddy current system has been shown to be capable of measuring and that the operator may require.

5.2 Basic System

The basic microprocessor system is required to sample the 10 kHz probe coil voltage at a pre-determined point in the 50 Hz magnetization cycle, and then measure the voltage thus sampled. The sample point or points is at a time during the 50 Hz magnetizing field period when the mild steel bar is as close to magnetic saturation as possible. This sample point must be synchronized with the 50 Hz magnetic field and is in the interval during which the envelope of the 10 kHz waveform is smallest in magnitude as shown in Figure 5.1.

The point at which saturation occurs can and does vary, and hence it is a system requirement that the starting point of the measurement and the time over which it is possible to make this measurement, must both be variable and of course be synchronized to the 50 Hz magnetic field. The 10 kHz probe coil voltage is sampled using a sample and hold circuit and is then converted to digital form using a standard A/D converter* to enable storage of the measurements and then conversion to enable the results to be displayed on a line printer or an LED display. Justification for the use of this hardware is given in the next section.

* ZN427, conversion time 10 μ s (typ)

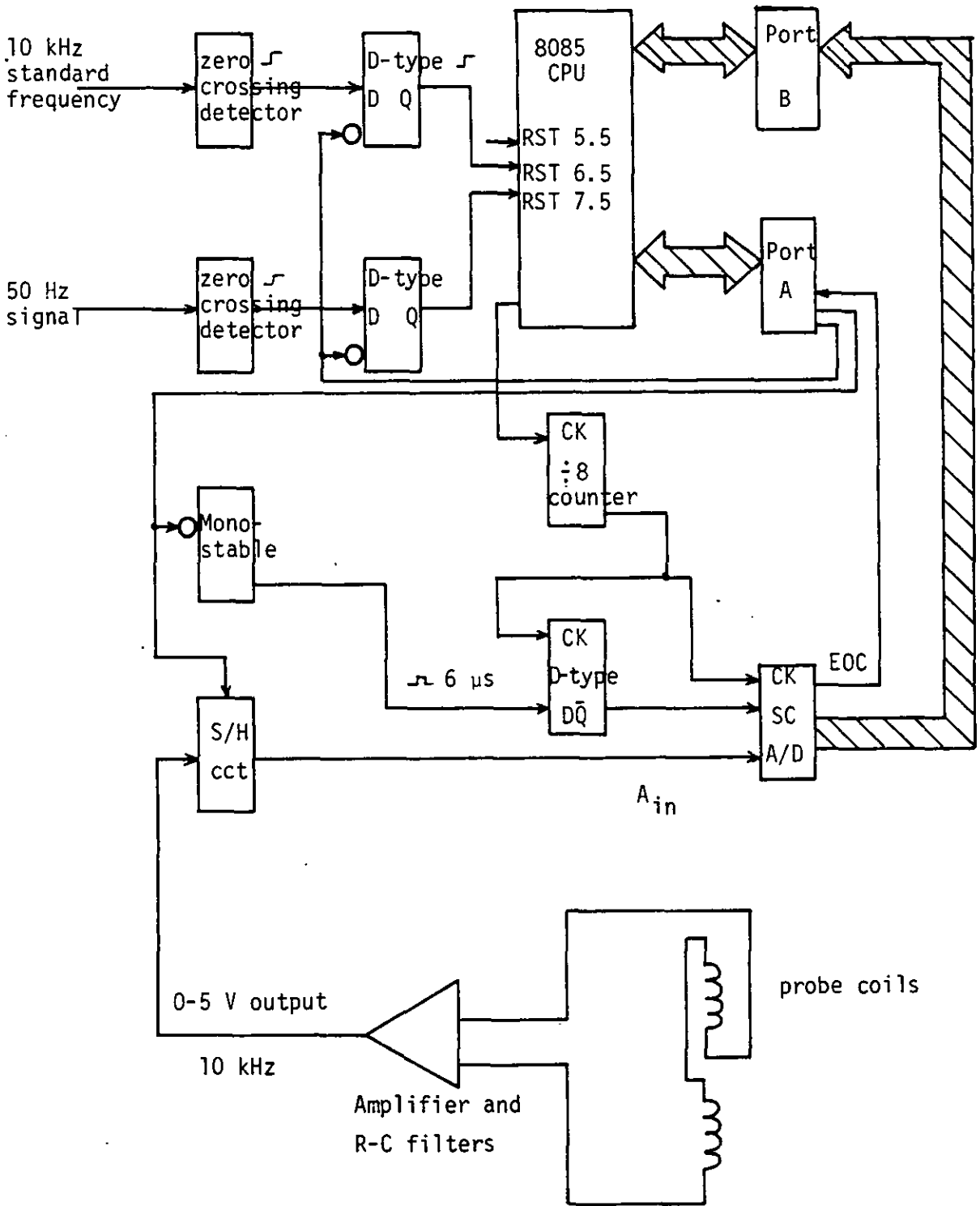


Figure 5.2 Block diagram for the microprocessor aided measuring system

5.3 System Hardware

The block diagram of Figure 5.2 shows the basic hardware required for the probe coil voltage measurement of the eddy current gauging system. The probe coil amplifier and R-C filter used is that shown in Figure 4.7a, page 79, and 4.15, page 95, which for reliable operation of the sample and hold circuit, will need to be pre-adjusted to give an output in the range 0-5 V. This adjustment may be achieved at the same time as the voltage corresponding to the H field is measured; this measurement is described in section 4.3.2.

The system shown in the block diagram of Figure 5.2 functions in the following manner.

It is assumed that the Intel 8085 central processing unit (CPU) and all its ancillary equipment has been initialized correctly and that it is ready for operation, see section 5.4, page 118, for details. As the 50 Hz magnetic field first passes zero, the zero crossing detector, using a simple Schmitt trigger circuit, produces a pulse with a leading positive edge. This pulse is sent to the D-type flip flop, which produces one and only one positive edge, which is sent to the interrupt RST 7.5 input of the CPU. A second positive edge can not occur until the D-type flip flop is re-set by the CPU. Similarly the 10 kHz standard frequency, synchronized with the probe coil voltage, will also produce a high level input to the RST 6.5 input via its own D-type flip flop. As a result of the signals to the interrupt, RST inputs, a signal is then sent from port A of the CPU to the sample and hold circuit, causing this circuit to enter its hold mode, and also to set its associated monostable. The sample and hold circuit used in this system has an acquisition time of 6 μ s, required to

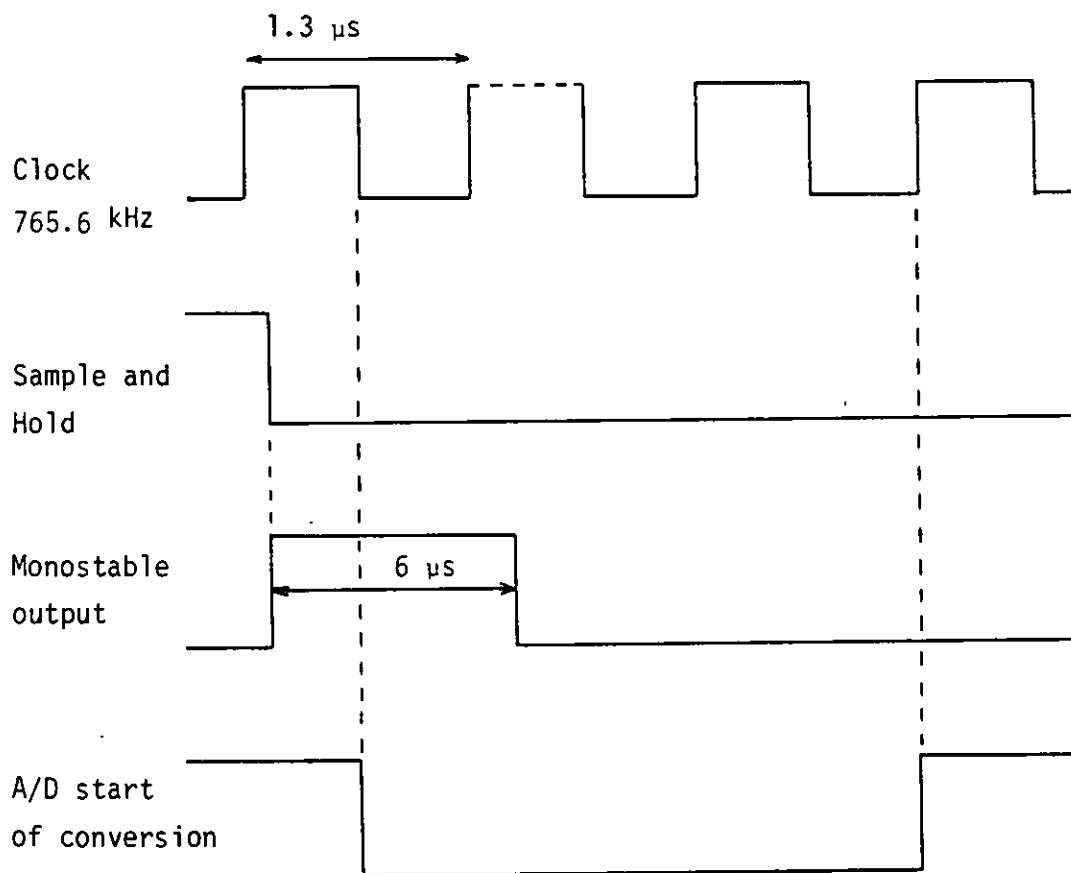


Figure 5.3 Waveforms for the microprocessor aided measuring system hardware

'read' the peak value of the 10 kHz signal from the probe coil amplifier. After the 6 μ s acquisition time has elapsed, the monostable associated with the sample and hold circuit, will re-set, and thus send a signal, called the start conversion signal to the A/D converter. A D-type flip flop is used as a buffer between the monostable and the A/D converter, as the positive edge of the start conversion pulse should not occur within a negative transition of the A/D clock pulse, shown in Figure 5.3. The D-type flip flop is hence used to synchronize the start conversion pulse with the positive edge of the A/D clock pulse.

The 'end of conversion' pulse is fed into the CPU via port A. Upon receipt of this pulse the digitised value of 10 kHz probe coil voltage, held by the A/D converter, is fed into the CPU of the processor via port B. Detailed timing considerations for the block diagram of Figure 5.2 together with the timing constraints for the software are given pictorially in Figure 5.4 and the software details are discussed in detail in section 5.4.

5.4 System Software

When developing an initial prototype for a microprocessor system, for example the eddy current gauging system described in this project, it is often convenient to use a development board. The type of development board used with this eddy current gauging system was the Intel SDK-85 board. This development board contains the following system: a 8085 CPU, 8155 RAM, 8355 ROM, I/O ports and a keyboard/display unit which is used as an interface to facilitate the initial programming of the system. It is also possible to use extra RAM, EPROM and I/O ports to allow expansion for a larger system^{79,80,81}.

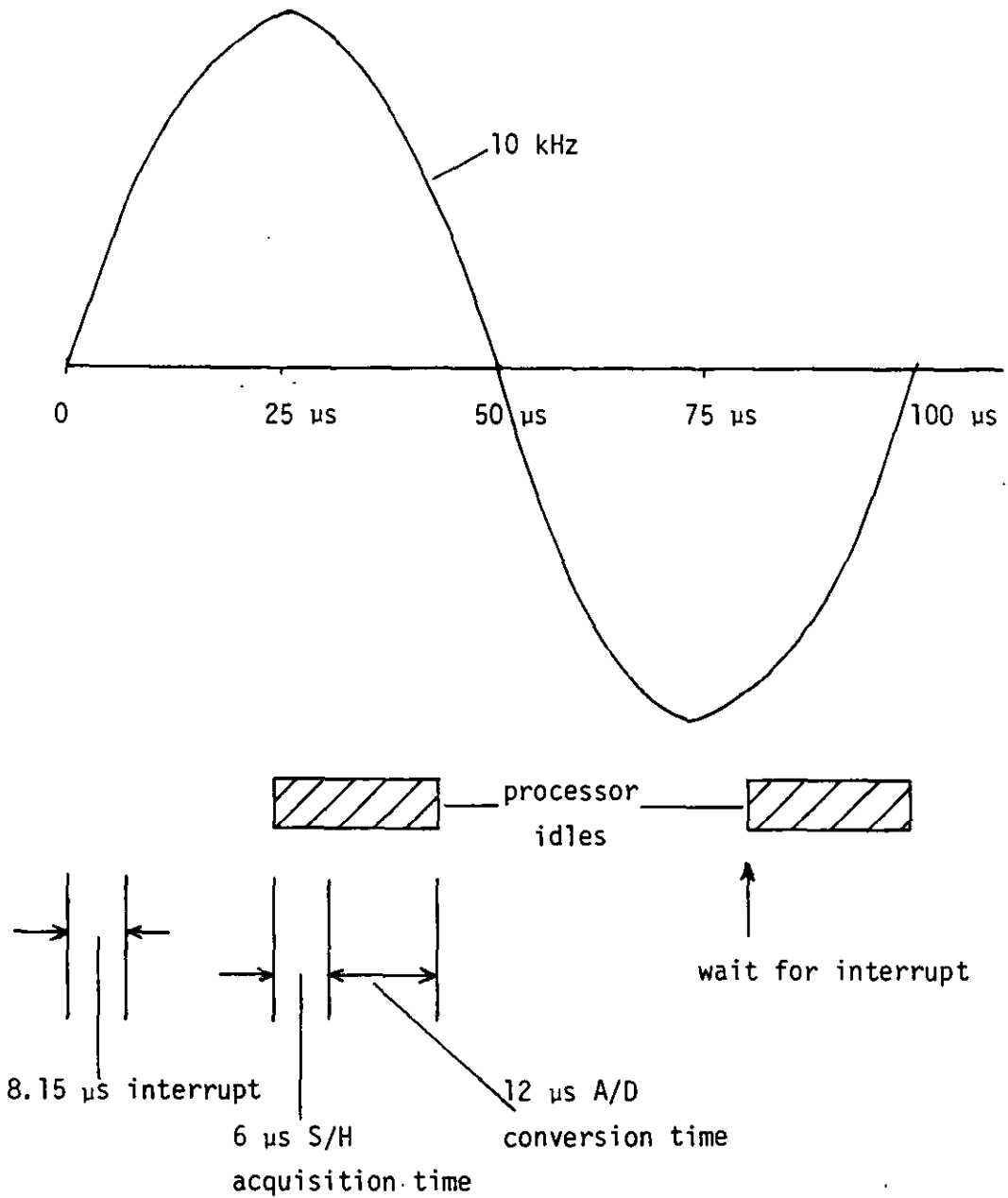


Figure 5.4 Eddy current gauging system timing relative to the 10 kHz waveform

It is important, when a program containing interrupt routines is written, to consider the frequency at which the interrupts may be generated, and also the associated processing time required to service each interrupt. For the program associated with the eddy current gauging system, all the processing has been designed to take place within the 10 kHz interrupt cycle. Details are given in Figure 5.4.

All the vector interrupt addresses are located in the SDK-85 monitor ROM, hence an extra instruction is required to allow each interrupt address to be located in the RAM. In this case the extra instruction will be a jump instruction, see reference 79 for the jump addresses.

The 8085 uses the SIM instruction to selectively enable or disable each vector interrupt. There are two basic machine instructions, EI (enable interrupt) and DI (disable interrupt). These interrupts are used to determine when the interrupts are recognized and hence when they should be serviced during the program. It should be noted, however, that all interrupts are sampled by the processor on the descending, ie negative going, edge of the clock cycle, one clock cycle before the end of the instruction in which the interrupt has been activated.

The maximum possible time taken for the processor to recognise an interrupt, after the receipt of the enable interrupt instructions, is 150 ns, plus one cycle time before the end of the instruction in which the interrupt was activated. Hence the maximum time before the main program recognises an interrupt for this eddy current gauging program, may be obtained by adding together the processing times for each of the interrupt routines. This means a maximum of two jump instructions

together with one halt instruction, plus the 150 ns period as stated previously. The processor cycle time is 0.32 μs . Hence the maximum time before the main program recognizes an interrupt is 8.18 μs .

The timing for the main body of the program may be calculated in a similar manner to that above. The results of this computation are given in a pictorial manner in Figure 5.4. The 10 kHz interrupt occurs every 100 μs , and the peak value of the sine wave will occur after 25 μs . All the processing is designed to be complete in the remaining 75 μs from this point in the 10 kHz signal. Hence it is clear that at this frequency, 10 kHz, with a time period of 100 μs , and for this processor the time available for processing is rather short. The main program, in consequence must be written and due allowance taken, for the short processing time available.

The operator may select, at the commencement of the program, the period over which the measurements of the 10 kHz probe coil voltage are made by selecting the measurement start time, t_2 from the point of the zero crossing of the 50 Hz signal, 50 Hz interrupt and the time t_3 from the time t_2 . This third time t_3 determines the time over which the measurements are made. This third period t_3 will usually correspond to the period over which the metal is in its saturated state, but this restriction need not always apply. The final timing point, t_1 , which will be entered first by the operator, allows for a number of 50 Hz interrupt to pass before a measurement is made, thus allowing the system to settle down before any measurement is recorded.

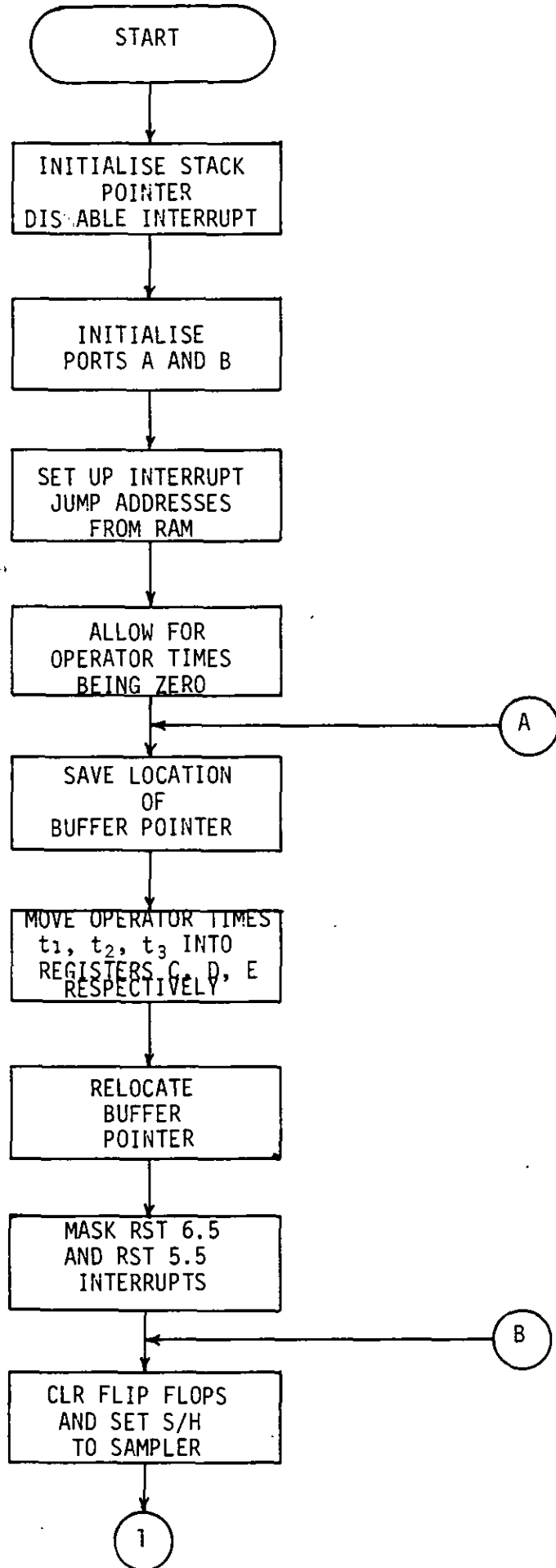


Figure 5.5a

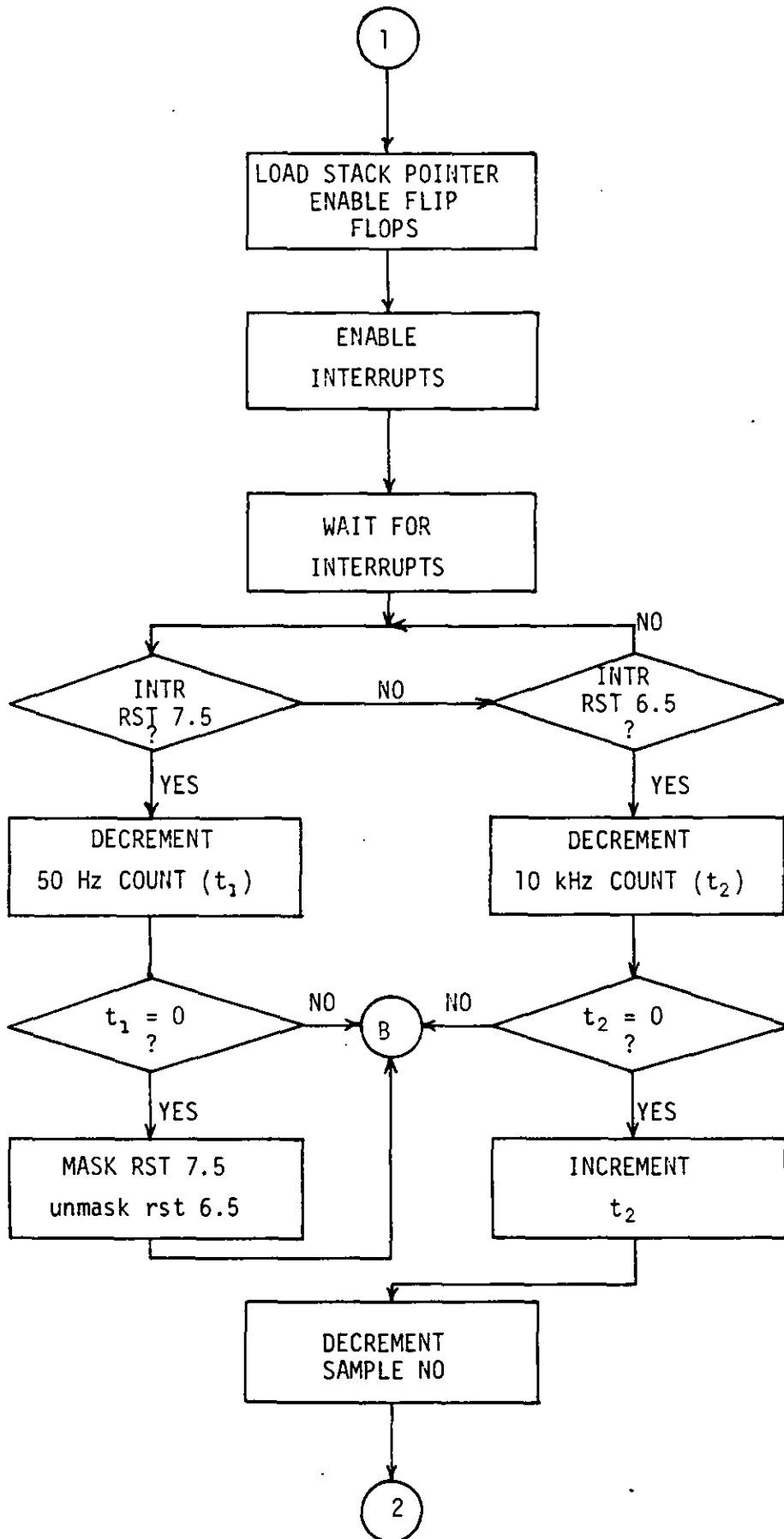


Figure 5.5b

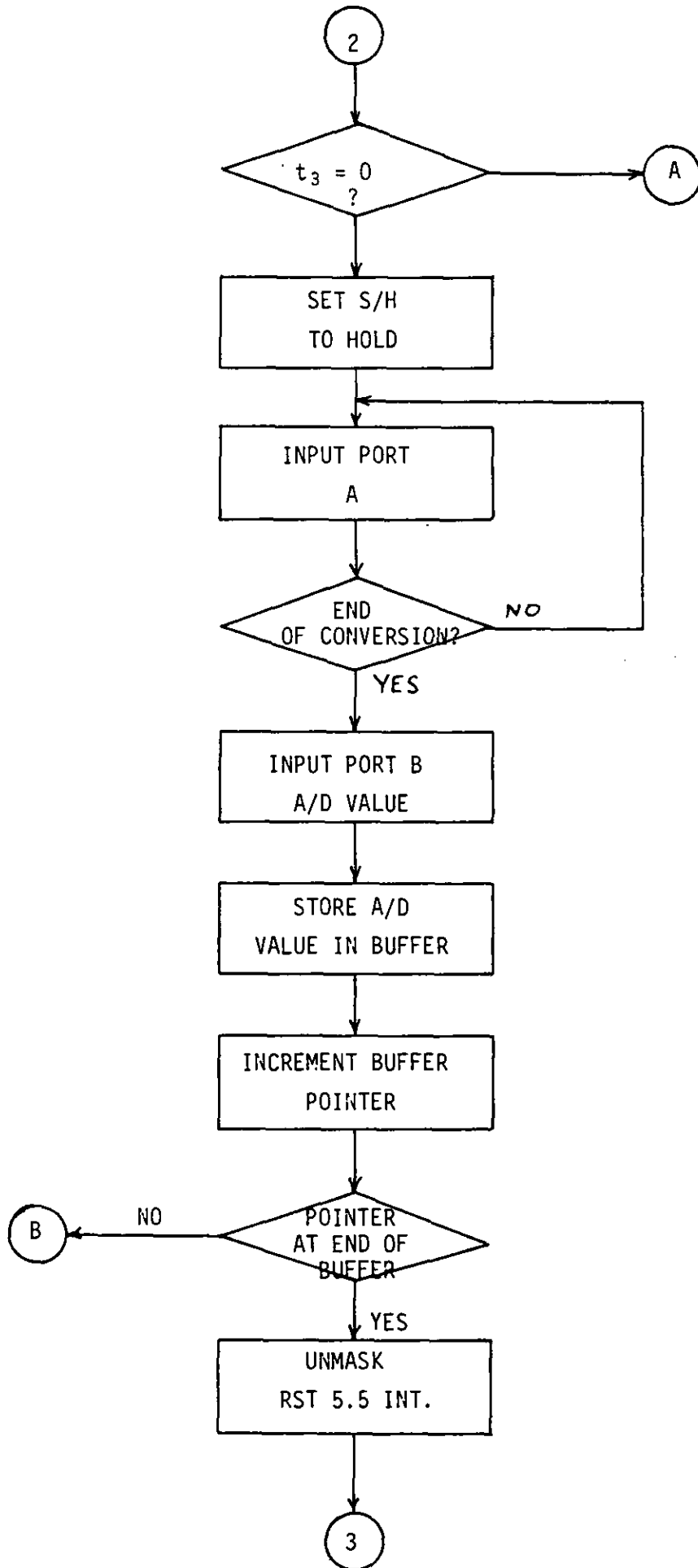


Figure 5.5c

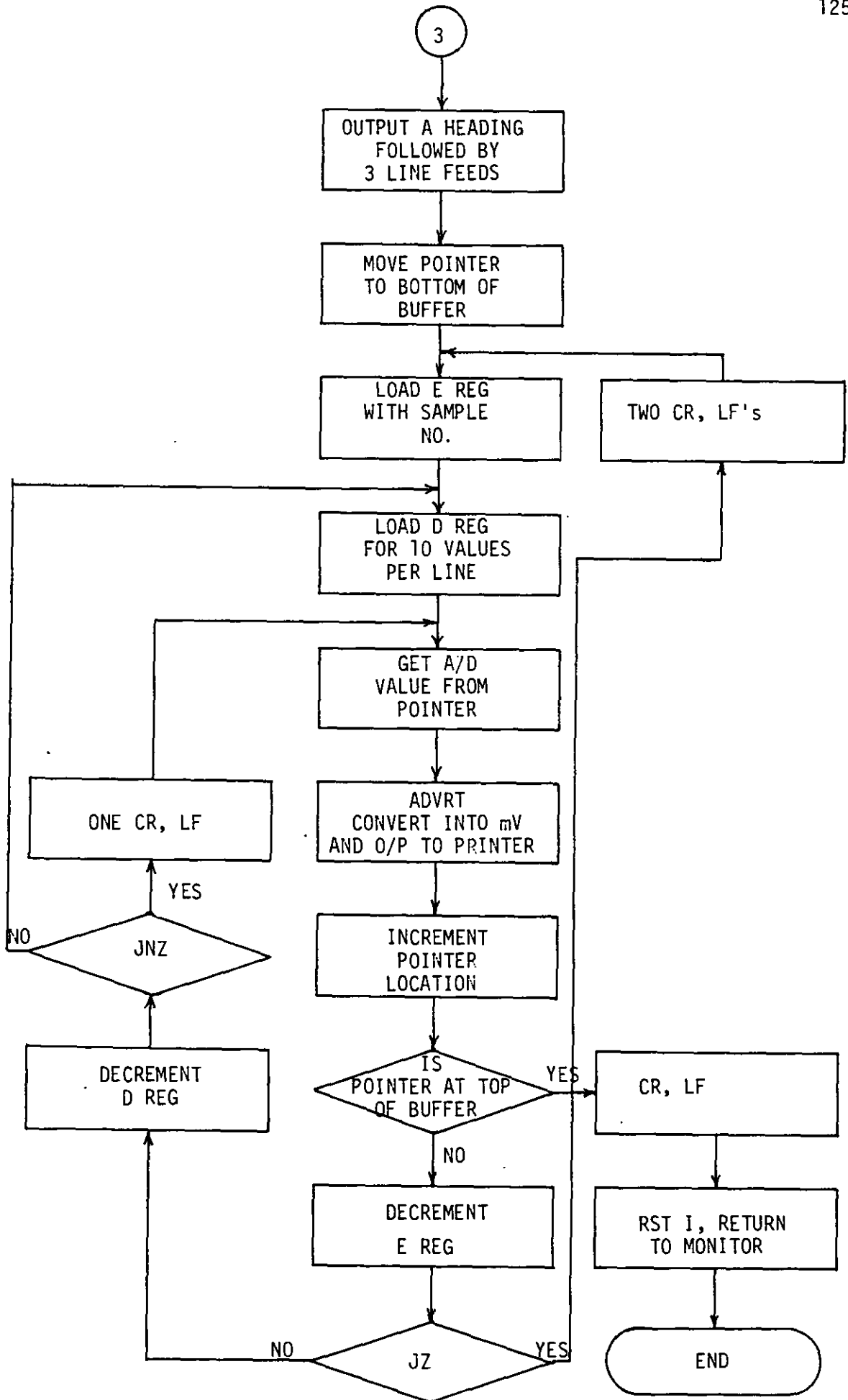


Figure 5.5d

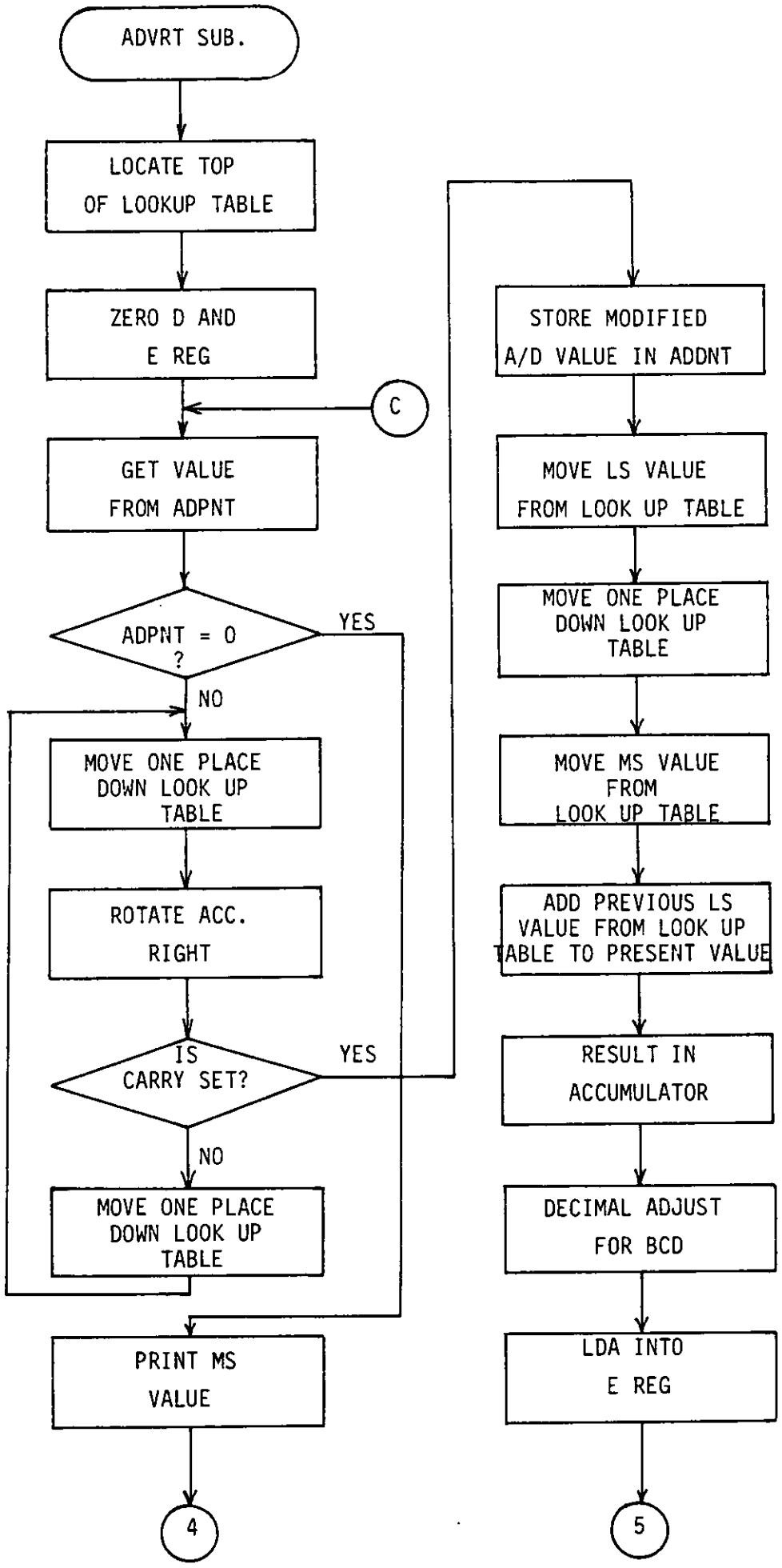
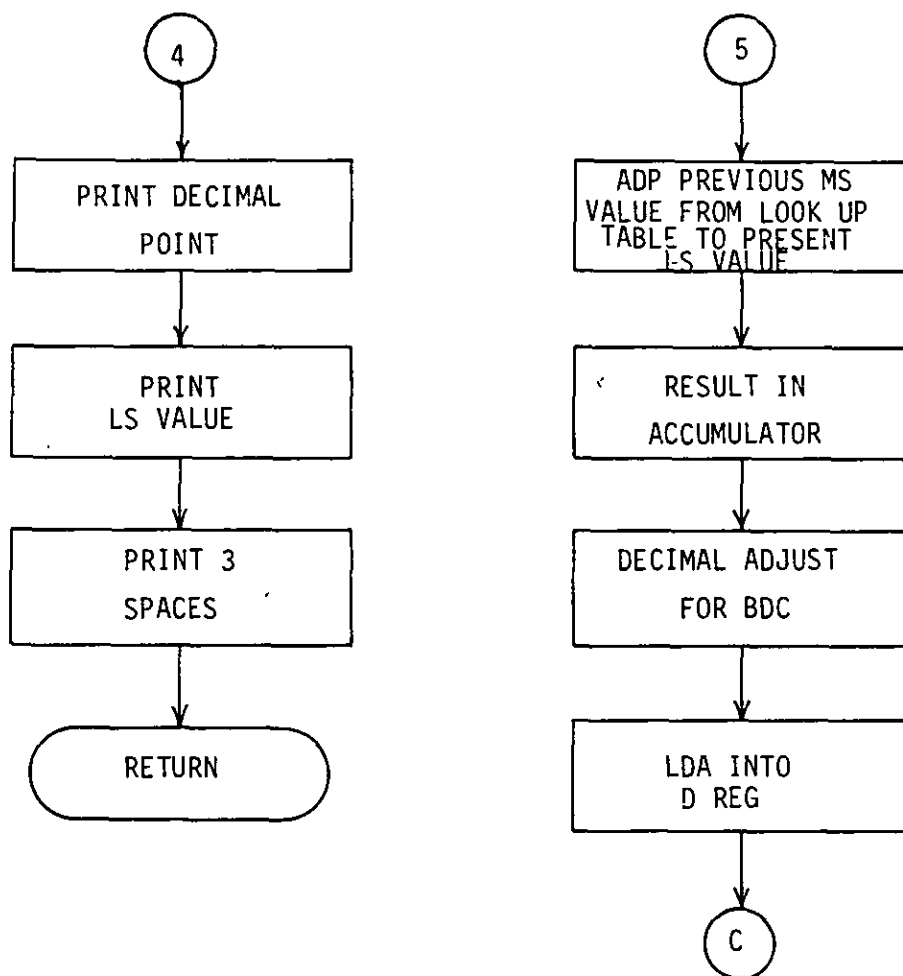


Figure 5.5e



Flow chart for the microprocessor aided measurement system

Figure 5.5f

The times t_1 , t_2 and t_3 are selected by the operator at the start of the program either on the key board of the SDK-85 monitor or on a line printer.

5.5 Software Operation

The flow chart for the eddy current gauging microprocessor aided system is shown in Figures 5.5a to 5.5d with associated subroutines shown in Figures 5.5e to 5.5f. The program listing, which was produced during assembly using the microprocessor development system (MDS) may be found in Appendix 7. The operation of the program is as follows.

The program is started as a result of the operator issuing the command $GO\ 2000_{16}$. Operation of the program beginning by the disabling of all the interrupts, the stack pointer is initialized and the input/output (I/O) points A and B are also initialized. Lines 41-50 are concerned with the setting up of the main program interrupt jump addresses in an area of RAM, where the vector interrupts RST 6.5 and RST 7.5 are sent from the monitor ROM. Lines 54-66 are concerned with the prevention of the times t_1 , t_2 and t_3 , as selected by the operator, being set to less than zero. Any zero times set at the start of the program are incremented to prevent these times being decremented through zero. It is obvious that negative time is not possible, but zero time for either t_1 or t_2 is possible. The buffer is then shifted to the bottom of the buffer store in readiness for the acceptance of the first A/D value.

The 50 Hz interrupt is unmasked at line 86 in order to prepare for the enable interrupt (EI) instruction at line 92. In readiness for the EI instruction at line 92, the 50 Hz and 10 kHz D-type flip flops are

Table 5.1 Memory Map of RAM

Memory address	Contents
2000 2002	t_1 , t_2 and t_3 to be entered by operator
2003 20AD	Buffer area for storing A/D data
20AE 20AF	ADPNT, temporary location for the buffer pointer address. ADPNT is also used for storing the data undergoing conversion to BCD
20BD 20C2	STACK area is used for storing return address when subroutines are called
20C8 20CA	RST 6.5 (10 kHz) vector interrupt jump address for main program
20CE 20D0	RST 7.5 (50 Hz) vector interrupt jump address for main program
20D1 20FF	Reserved RAM locations for use by the SDK-85 monitor

cleared, and the sample and hold device is set to the sample mode. The stack pointer is also redefined at line 89. This is so that it retains its usual memory location, as on receipt of a vector interrupt, the stack pointer position is decremented by two places on each occasion.

At line 95 or 101 the main program encounters a halt (HLT) instruction, depending upon which interrupt has previously been unmasked. This instruction allows the processor to idle until interrupted. For lines 95 to 102 the program will mask interrupt RST 7.5 and unmask interrupt RST 6.5 on receipt of the t_1 interrupt, (50 Hz interrupt). t_1 is decremented as a result of every RST 6.5 interrupt (10 kHz interrupt). When t_2 reaches zero the program control will move to line 103.

From line 103 to 107 is denoted the time period ie t_2 over which the measurements of the probe coil voltage are completed. The value of t_2 is decremented after each RST 6.5 interrupt and continues up to line 107. When t_2 is decremented to zero, program control is transferred to line 75, where the operator, if necessary, may re-enter the three times, t_1 , t_2 and t_3 for the measurement to be repeated.

Line 108 corresponds to the time where the 10 kHz probe coil voltage reaches its maximum value. Lines 110 to 112 are a programming loop to allow the A/D converter to finish its operation and then send the end of conversion signal to the CPU via port A. At lines 113 to 117 port B is allowed to input the digitized value of the probe coil voltage to the buffer. The buffer pointer is then incremented, and the program control will pass to line 87, if and only if the pointer has not reached the top of the buffer.

TABLE 5.2

10 KHZ PEAK SAMPLED VALUES <MILL VOLTS>

08.12 08.14 08.10 08.09 07.88 08.30 08.08 08.02 08.15 08.79
 08.13 08.12 08.15 07.99 08.11 07.56 08.15 08.20 08.14 08.09
 08.03 08.05 08.13 08.17 08.09 08.04 08.00 08.11 08.13 08.13
 07.89 07.98 07.90 08.13 08.16 08.20 08.10 08.12 08.15 08.11

08.15 08.10 08.20 08.10 08.30 08.00 08.12 08.14 08.10 08.04
 07.90 07.98 07.99 08.01 08.20 08.05 08.08 08.20 08.15 08.13
 08.01 07.95 07.91 07.80 07.88 07.79 07.90 07.50 07.87 07.97
 08.03 08.01 07.98 07.90 07.98 07.88 07.76 07.85 07.85 07.95

07.90 07.95 07.98 07.89 07.97 08.03 08.01 08.09 08.10 08.13
 08.10 08.13 08.14 08.20 08.15 08.25 08.16 08.01 08.16 08.09
 08.12 08.20 08.16 08.14 08.09 08.25 08.60 08.18 08.17 08.05
 08.09 08.30 08.14 08.18 08.08 08.18 08.24 08.21 08.19 08.26

08.20 08.21 08.24 08.26 08.20 08.31 08.25 08.02 08.04 08.24
 08.21 08.23 08.24 08.19 08.27 08.30 08.32 08.19 08.13 08.14
 08.12 08.14 08.34 08.25 08.26 08.26 08.17 08.34 08.32 08.15
 08.32 08.53 08.32 08.28 08.29 08.32 08.19 08.26 08.20 08.32

Typical data for T1=4 and T2 and T3 respectively 6 ms and 4 ms

Typical measurements for the microprocessor aided eddy
 gauging system

When the buffer is full, both the RST 7.5 and the RST 6.5 interrupts are masked and the RST 5.5 interrupt is unmasked. This is in the way of preparation for the value of the probe coil voltage being sent to the line printer (if required). At this point in the program the value of the probe coil voltage may be displayed on the SDK-85 monitor display should this be required.

The data displayed by the line printer will have the following format. A heading is printed, see line 190. The data output to the line printer is formatted into data blocks of 10 columns per line. The time selected for t_3 , the time period over which the measurements are taken, will determine the size of each block: Each column is separated by one space, and every block by a row of spaces. Hence each block of data on the line printer, will represent values taken over each 50 Hz period stated.

A subroutine (ADVRT), converts each byte from the buffer into a four figure decimal value, which will be in millivolts. An 8 x 2 byte, 'look up table' is used to convert each bit of the data byte, from the buffer, into its appropriate decimal value. Each assigned value of the data byte is then successively added together using the BC and DE register pairs in the (CUTBYT) subroutine. The most significant (MS) and least significant (LS) numbers are built up in the D and E registers respectively, where they are used by the monitor routine for an output of the converted value to the line printer. A decimal point is used to separate the MS and the LS values in the display. A typical print out produced by the program is shown in Table 5.2. It should be noted however that the accuracy of the voltage measurement by the system is subject to certain limitation and errors.

(i) attenuation is produced by the R-C filters, which are necessary for the elimination of the unwanted 50 Hz signal which is fed back into the probe coils from the magnetizing field, see Chapter 4.

(ii) the sample and hold acquisition time is 6 μ s.

Over this period the 10 kHz signal will change its value. This change is only small, but the error is still produced.

(iii) the A/D converter is only accurate to + or - its least significant data bit.

The errors lists above may be easily allowed for, and hence the method is still acceptable in its present form.

5.6 Results

The program for reading the probe and voltage, which is proportional to the magnitude of the surface impedance was run successfully. However care must be exercised in the interpretation of the typical set of results given in table 5.2. Account has been taken of the errors quoted in section 5.5. It is necessary to allow for these errors before conversion of the measurement can be made to values of surface impedance. When allowance was made for the errors in the results, the magnitude of the values of the surface impedance were consistent with the values obtained and presented in Chapter 4.

It would be rather more convenient to use the processor for the conversion of the results to surface impedance, however preliminary

calculations suggest that for a processor cycle time of $0.32 \mu\text{s}$, there would be insufficient time available during the 10 kHz time period for any sizable operation to take place. It may however be possible to make some refinements to the main program or to use a faster processor to achieve this end. See Chapter 6 for details.

CHAPTER 6 CONCLUSIONS AND RECOMMENDATIONS FOR FURTHER WORK6.1 Conclusions

It is appropriate now to consider the theme of this project; this was to classify and then test concepts relating to eddy current gauging in general and to the control of certain types of magnetic flaws during the gauging process in particular. The classification and testing of concepts relating to eddy current gauging were carried out in the following manner.

The literature survey indicated that there is a large body of knowledge relating to eddy current gauging, dating back to 1822. However a large proportion of this literature relates to eddy current gauging from an empirical point of view, that is the works contained no apparent sound mathematical basis.

The work reported on in this thesis used the basic magnetic field relationships to develop a sound mathematical model, which is rigorous in its treatment, as a foundation for subsequent eddy current gauging application. Concepts relating to surface impedance and eddy current considerations were important factors in the rigorous field analysis of Chapter 3. The mathematical model resulting from the exact field equation was shown to be rather cumbersome when related to the actual system configurations used for eddy current gauging.

The rigorous mathematical model of Chapter 3 was subsequently modified step by step in order to give a much simpler model. An extensive test programme was undertaken to ensure that each simplification introduced did not result in an unacceptable loss of

accuracy. The outcome of this simplification of the mathematical model was to produce a model of acceptable accuracy and simplicity whilst retaining the concepts of the original field analysis.

It was also shown that the simplified mathematical model could be used in an eddy current gauging system where the metal under test contained certain types of magnetic defects. The results of test carried out on this type of system indicated that the simplified mathematical model could be used as a basis for the design of an eddy current instrumentation system, for use with metal which may contain this type of magnetic flaw. The system was also shown to give adequate performance for both ferrous and non-ferrous materials.

The eddy current instrumentation system was based on an INTEL microprocessor. This system was designed to automatically record and then display measurements made on the eddy current gauging system, based on the principles and experimentation reported previously. This system reported on in Chapter 5 produced adequate results, whilst allowing some scope for further development.

6.2 Recommendation for Further Work

The work reported on in this thesis is an extension of the work on eddy current gauging reported on in the literature by a number of research workers. The work reported here presents a range of theoretical and practical arguments, and also an eddy current gauging instrumentation system. Whilst the arguments and instrumentation system reported on in this thesis are complete, there are a number of ways in which extensions and improvements may be made.

- i) The rigorous mathematical model using the infinitely long coil may be tested experimentally providing an infinitely long solenoid may be simulated. The author feels that whilst this option may be possible, little practical benefit will result.
- ii) The rigorous mathematical model may also be extended to allow the inclusion of the many non-magnetic defects which occur from time to time in both ferrous and non-ferrous metallic samples.

The application of the eddy current instrumentation system described in Chapter 5, may also be extended and improved in the following manner:

- i) All measurements and all subsequent calculations on the eddy current gauging system could be done automatically. This would require a faster processor than the one currently available. However faster processors may become available in the near future.
- ii) A hardware dedicated system could be implemented. This would reduce processing time, and enable more ambitious processing to be attempted.
- iii) Temperature sensing could also be included to prevent damage to the measurement system. This would be for ferrous materials only.
- iv) An extension of the area of RAM, to increase the number of

measurements taken and an automatic system for switching on and off for the 50 Hz magnetic field, would enable the system to perform more reliably.

It would seem from the suggestions above that there is still a large area of research still to be carried out in this area of eddy current gauging, and surely any resulting improvement in eddy current gauging techniques is worthwhile. It is to this end that the work presented in this thesis is dedicated.

CHAPTER 7 BIBLIOGRAPHY

1. J. C. MAXWELL, "A treatise on electricity and magnetism", 1873
3rd edition 1904; Oxford Clarendon Press.
2. J. C. MAXWELL, "On the induction of electric currents in an
infinite plane sheet of uniform conductivity", Proc. Royal Soc.,
vol 20, pp 160-168, 1872.
3. MORECROFT, TURNER, "The shielding of electric and magnetic
fields", Proc. I.R.E., vol. 13, pp 477 - 506; August 1925.
4. KING, "Electromagnetic shielding at radio frequencies", Phil.
Mag., vol. 15, 1933.
5. LYONS, "Experiments on Electromagnetic shielding at frequencies
between one and thirty kilocycles", Proc. I.R.E., vol. 21,
pp 574-590; April 1933.
6. S. LEVY, "Electromagnetic shielding effects of an infinite plane
conducting sheet placed between circular coaxial coils", Proc.
I.R.E., vol 24, pp 923-941; June 1936.
7. C. W. MARCHANT, J. L. MILLER, "The loss of energy in metal
plates of finite thickness, due to eddy currents produced by
alternating magnetic fields", Proc. Royal Soc., vol III,
pp 604-614, 1926.
8. N. W. McLACHLAN, A. L. MEYERS, "Eddy current loss in a
cylindrical tube situated in an axial alternating magnetic
field", Phil. Mag 1934, pp 610-624.

9. N. W. McLACHLAN, A. L. MEYERS, "Eddy current loss in a cylindrical tube situated in an axial alternating magnetic field", *Phil. Mag* 1935, pp 846-849.
10. R. M. FOSTER, "Mutual impedance of grounded wires lying on the surface of the earth", *Bell Systems Technical Journal*, 1931, Vol 10, pp 408-419.
11. A. T. PRICE, "The induction of electric currents in non-uniform thin sheets and shells", *Quart. Journal Mech. and Applied Maths.*, Vol II Pt. 3, 1949, pp 283-310.
12. A.T. PRICE, "Electromagnetic induction in a semi-infinite conductor with a plane boundary", *Quart. Journal Mech. and Applied Maths.*, Vol 3, Pt. 4 1950, pp385-410.
13. J. R. WAIT, "The magnetic dipole over the horizontally stratified earth", *Canadian Journal of Physics*, 1951, Vol. 29 No 1, pp 577-592.
14. G. H. H. REUTER, E. H. SONDEIMER, "Theory of the anomalous skin effect in metals", *Proc. Royal Soc. A*, Vol 193, 1948 pp 336-364.
15. R. B. DINGLE, "The anomalous skin effect and the reflectivity of metals", *Applied Scientific Research*, 1953, Vol. 33, pp 69-99.

16. A. N. GORDON, E. H. SÖNDHEIMER, "The evaluation of the surface impedance in the theory of the anomalous skin effect in metals", Applied Scientific Research, 1953 Vol 3, pp 297-304.
17. F. FÖRSTER, K. STAMBKE, "Theoretische und experimentelle Grundlagen der zerstörungsfeien Werkstoffprüfung mit Wirbelstromverfahren", Zeitschrift für Metallkunde, 1954 Vol 45, pp 166-179 (In German).
18. W. A. CANNON Jr., "Industrial Applications of eddy current testing", Non-Destructive Testing, May 1953, pp 30-33.
19. A. BRENNER, J. GARCIA-RIVERA, "An electronic thickness gage", Plating and Surface Finishing, Nov. 1953, Vol. 40, pp 1238-1244.
20. W. A. YATES, J. L. QUEEN, "Sheet and plated-metal measurements with a phase-angle-type probe", Trans. AIEE, Comm. and Elect., 1954 May, No 12, pp 138-147.
21. R. HOCHSCHILD, "Eddy current testing by impedance analysis", Non-Destructive Testing, May-June 1954, Vol. 12, pp 35-44 and p 51.
22. R. HOCHSCHILD, "The theory of eddy current testing in one (not-so-easy) lesson", Non-Destructive Testing, Sept.-Oct. 1954, Vol. 12, pp31-40.
23. D. L. WAIDELICH, "Coating thickness measurements using pulsed eddy currents", Proc. Nat. Elec. Conf. 10, 1954, pp 500-507.

24. D. L. WAIDELICH, "Pulsed eddy currents gauge plating thickness", Electronics, 1955, Vol. 28 (II), pp 146-147.
25. D. L. WAIDELICH, "Measurement of coating thickness by use of pulsed eddy currents", Materials Evaluation, 1956, Vol. 14, pp 14-16.
26. C. J. RENKEN, R. G. MEYERS, "A double pulse eddy current testing system", Argonne National Laboratory Report ANL5935, 1959.
27. C. J. RENKEN, "A through transmission system using pulsed eddy current fields", Materials Evaluation 1960, Vol. 18, pp 234-236.
28. H. L. LIBBY, "Basic principles and techniques of eddy current testing", Non-Destructive Testing, Nov.-Dec. 1956, pp 12-18 and p 27.
29. G. O. McCLURG, "Flaw detection by eddy-current methods", Non-Destructive Testing, March-April, 1957, Vol. 15, pp 116-119.
30. J. W. ALLEN, R. B. OLIVER, "Inspection of small-diameter-tubing by eddy current methods", Non-Destructive Testing, March-April 1957, Vol. 15, Pt 2, pp 104-109.
31. J. B. C. ROBINSON, L. T. PERRIAM, "The inspection of tubes for flaws and variations in thickness", J. of the Institute of Metals, 1957-58, Vol. 86, pp 316-322.

32. P. GRANEAU, "The effect of sample movement in fault detection using eddy currents", IEE paper No 2945M, July 1959, pp 417-421.
33. P. GRANEAU, S. A. SWANN, "Electromagnetic Fault Detection on non-ferrous pipes", J. of Electronics and Control, 1960, Vol. 8, pp 127-147
34. R. HOCHSCHILD, "Testing metals 'on-the-fly' with eddy currents", Control Engineering, Aug. 1957, Vol. 4, pp 78-85.
35. F. FOERSTER, "Principles of eddy current testing", Metal Progress, Jan 1959, Vol. 75, pp 101-105.
36. G. O. McCLURG, "Non-destructive eddy current testing", Inst. of Radio Eng. Trans. on Nuclear Sci. Vol. 1E-11, Dec. 1959, pp 20-26.
37. P. HAMMOND, "The calculation of the magnetic field of rotating machines. Part 3 eddy currents induced in a solid slab by a circular current loop", Proc. IEE., 1962 109C, pp 508-512.
38. P. HAMMOND, "Electric and magnetic images", IEE Monograph No. 379, May 1960, pp 306-313.
39. C. V. DODD, "Applications of a phase sensitive eddy current instrument", Materials Evaluation, 1964, Vol. 22, No. 6, pp 260-263.
40. C. V. DODD, "A portable phase-sensitive eddy current instrument", Materials Evaluation, 1968, Vol. 26, No. 3, pp 33-36.

41. R. C. McMASTER, "A new eddy current non-destructive test", Met. Eng. Quart., American Society for Metals, 1966, Vol. 6, pp 32-49.
42. J. R. MOSER, "Low-frequency shielding of a circular loop electromagnetic field source", IEEE Trans on Electromagnetic Compatibility, 1967, Vol. EMC9, No. 1, pp 6-18.
43. C. M. RYAN, "Computer expression for predicting shielding effectiveness for the low-frequency plane shield case", IEEE Trans on Elect. Comp. 1967, Vol. EMC9, No. 2, pp 83-94.
44. P. R. BANNISTER, "New theoretical expressions for predicting shielding for the plane shield case", IEEE. Trans on Elect. Comp., 1968, Vol. EMC10, No. 1, pp 2-7.
45. P. R. BANNISTER, "Further rules for predicting shielding effectiveness for the plane shield case", IEEE Trans. on Elect. Comp., 1969, Vol. EMC11, No. 2, pp 50-53.
46. T. J. RUSSELL, V. E. SCHUSTER, D. L. WAIDELICH, "The impedance of a coil placed on a conducting plane", Communications and Electronics, Sept. 1962, pp 323-237.
47. J. VINE, "Impedance of a coil placed near to a conducting sheet", Journal of Electronics and Control Vol. 16, No. 5, May 1964, pp 569-577.
48. D. H. S. CHENG, "The reflected impedance of a circular coil in the proximity of a semi-infinite medium", IEEE. Trans on Inst. and Meas. Vol. IM-14, No. 3, Sept. 1965, pp 107-116.

49. C. V. DODD, W. E. DEEDS, "Analytical solutions to eddy-current probe-coil problems", J. of Applied Physics, Vol. 19, No. 6, May 1968, pp 2829-2838.
50. C. V. DODD, W. E. DEEDS, J. W. LUQUIRE, W. G. SPOERI, "Analysis of eddy current problems with a time sharing computer", Materials Evaluations, 1969, Vol. 27, pp 165-168.
51. P. HAMMOND, K. K. LIM, "Universal loss chart for the calculations of eddy-current losses in thick steel plates", Proc. IEE., Vol. 117, No. 4, April 1970, pp 852-864.
52. P. HAMMOND, K. K. LIM, "Numerical method for determining the electromagnetic field in saturated steel plates", Proc. IEE, Vol. 119, No. 11, Nov. 1972, pp 1667-1674.
53. D. O'KELLY, "Hysteresis and eddy current losses in steel plates with non-linear magnetisation characteristics", Proc. IEE., Vol. 119, No. 11, Nov. 1972 pp 1675-1676.
54. J. J. REGAN, B. J. POTSCO, "Eddy currents check aluminium strip", Metal Progress, 1970, Vol. 98, Pt. 5, pp 113-117.
55. P. M. REYNOLDS, "On-line strip thickness gauging of non-ferrous metals", Proc. of Symp. on Process. Inst. in the metals Industry, London 1971, pp 42-48.
56. R. HUTCHESON, "Electrical and electronic gauging", Engineers Digest, 1972, Vol. 33, No. 12, pp 33-36.

57. D. R. BIRCHENOUGH, M. J. MARSHALL, "Magnetic and electromagnetic methods of coating thickness measurement", Measurement and Control, Vol. 5, Dec. 1972, pp 509-512.
58. A. L. JONES, K. F. PEZDIRTZ, "Non-destructive eddy current testing", IEEE Trans. on Inst. and Measurement, Feb. 1972 Vol. IM-21 No. 1, pp 11-15.
59. D. SCHEIBER, "Transient eddy current in thin metal sheets", Trans. of IEEE on Magnetism, Dec. 1972, Vol Mag. 8 No. 4, pp 775-779.
60. R. C. CALLOROTTI, M. ALFONZO, "Measurement of the conductivity of metallic cylinders by means of an inductive method", J. of Applied Physics, Vol. 43, No. 7, July 1972, pp 3040-3047.
61. A. B. BIRTLES, "Closed-form expressions for the magnetic field due to a single-layer cylindrical coil", J. Phys: Appl. Phys., Vol 5, 1972, pp 1-5.
62. A. B. BIRTLES, "Magnetic field of an arbitrary array of circular coils", Proc. IEE, Vol. 119, No. 7, July 1972, pp 925-926.
63. H. SUTCLIFFE, "Image of a coil in relation to the gauging of distance of metal surfaces", Electronic Letters, 3rd Oct. 1974, Vol. 10, No. 20, pp 346-348
64. H. SUTCLIFFE, "Principles of eddy current distance gauging", Proc. IEE, Vol. 124, No. 5, May 1977, pp 479-484

65. E. BALL, "Principles of eddy-current gauging of sheet metals", Ph.D. Thesis Oct. 1979, University of Salford.
66. E. BALL, J. A. STANIFORTH, "Transfer impedance between circular coils separated by thick non-ferrous metal sheets", Proc. IEE, Vol. 128, Pt. A, No. 1, Jan 1981, pp 64-67.
67. M. J. BALCHIN, J. A.M. DAVIDSON, "Numerical method for calculating magnetic-flux and eddy-current distributions in three dimensions", Proc. IEE, Vol. 127, Pt. A, No. 1, Jan. 1980, pp 46-53.
68. J. A. M. DAVIDSON, M. J. BALCHIN, "Experimental verification of network method for calculating flux and eddy-current distributions in three dimensions", Proc. IEE, Vol. 128, Pt. A, No. 7, Oct. 1981, pp 492-496.
69. M. J. BALCHIN, J. A. M. DAVIDSON, "3-dimensional eddy-current calculation by the network method", Proc. IEE, Vol. 130, Pt. A, No. 2, March 1983, pp 88-92.
70. C. S. BIDDLECOMBE, E. A. HEIGHWAY, E. A. SIMKIN, C. W. TROWBRIDGE, "Methods for eddy current computation in three dimensions", IEEE Trans., 1982, MAG-18, pp 492-497.
71. N. W. McLACHLAN, "Bessel functions for engineers", Clarendon Press Oxford, 1955.
72. S. A. SCHELKUNOFF, "Electromagnetic waves", Van Nostrand, 1943.

73. J. E. LEWIS, T. K. SARKAR, P. O. O'KELLY, "Generation of Bessel functions of complex order and argument (Computer Program Description)", Electronics Letters, 7th Oct 1971, Vol. 7, No. 20, pp 615-611.
74. E. JAHNKE, F. EMDE, "Tables of Functions", Dover New York, 1945.
75. E. KREYSZIG, "Advanced Engineering Mathematics", J. Wiley and Sons, 1967.
76. M. ABRAMOWITZ, I. A. STEGUN, "Handbook of Mathematical Functions", Dover, 1965.
77. J. A. STRATTON, "Electromagnetic Theory", McGraw Hill, 1941.
78. S. RAMO, J. R. WHINNERY, "Fields and waves in modern radio", J. Wiley and Sons, July 1962.
79. "SDK-85 Systems Design Kit Users' Manual", Intel Corporation, 1978.
80. "MCS-80/85 Family Users' Manual". Intel Corporation, Oct. 1978.
81. "8080/8085 Assembly Language Programming", Intel Corporation, 1979.

APPENDIX IList of Symbols

<u>Symbol</u>	<u>Name of Quantity</u>	<u>Units</u>
\underline{E}	Electric field strength	V/m
\underline{B}	Magnetic flux density	T
t	Time	s
\underline{H}	Magnetic field strength	A/m
\underline{J}	Current density	A/m ²
\underline{D}	Electric flux density	Q/m ²
ω	Angular frequency	rad/s
j	Imaginary unit $\sqrt{-1}$	-
μ	Permeability	H/m
σ	Conductivity	S/m
ϵ	Permittivity	F/m
x	Coordinates	m
y		m
z		m
r	Radius	m
ϕ	Angle for cylindrical coordinates	rad
A	Variable in terms of r only	
λ	Wavelength	m
$2\pi\ell$	Wavelength of E in the z direction	m
γ	Propagation coefficient	-
A_1	Constant	-
B_1	Constant	-
$I_n(r)$	Modified Bessel function of 1st kind	-

$K_n(r)$	Modified Bessel function of 2nd kind	-
L	Outer coil length	
Z_s	Surface impedance	Ω
d	Skin depth	m
r_o	Radius of metal bar	m
r_n	Radius of nth probe coil	m
n	number of coil turns	-
h_n	Height of nth probe coil above metal surface or between coils	m
I	Current flowing in large outer coil	A
ϕ_s	Phase angle of surface impedance	Deg
V_s	Voltage proportional to surface impedance	V
V_L	Out of phase component of voltage proportional to surface impedance	V
V_H	In phase component of voltage proportional to surface impedance	V
V_n	Voltage induced in the nth probe coil	V
$K(k)$	Complete elliptic integral of the 1st kind	-
$E(k)$	Complete elliptic integral of the 2nd kind	-
k	Elliptic variable	-
Z_w	Impedance of the Wave	Ω
N	Number of Harmonics	-

APPENDIX 2Basic magnetic field relationships and coordinate systems

$$\nabla \times \underline{E} = -\frac{\partial \underline{B}}{\partial t} \quad \text{-----1}$$

$$\nabla \times \underline{H} = \underline{J} + \frac{\partial \underline{D}}{\partial t} \quad \text{-----2}$$

$$\nabla \cdot \underline{D} = \rho \quad \text{-----3}$$

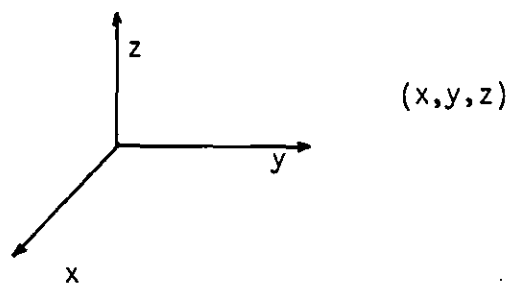
$$\nabla \cdot \underline{B} = 0 \quad \text{-----4}$$

$$\underline{D} = \epsilon_0 \epsilon_r \underline{E} \quad \text{-----5}$$

$$\underline{B} = \mu_0 \mu_r \underline{H} \quad \text{-----6}$$

$$\underline{J} = \sigma \underline{E} \quad \text{-----7}$$

Cartesian coordiantes



$$\nabla = \underline{u}_x \frac{\partial}{\partial x} + \underline{u}_y \frac{\partial}{\partial y} + \underline{u}_z \frac{\partial}{\partial z} \quad \text{-----8}$$

Hence
$$\nabla V = \underline{u}_x \frac{\partial V}{\partial x} + \underline{u}_y \frac{\partial V}{\partial y} + \underline{u}_z \frac{\partial V}{\partial z} \quad \text{-----9}$$

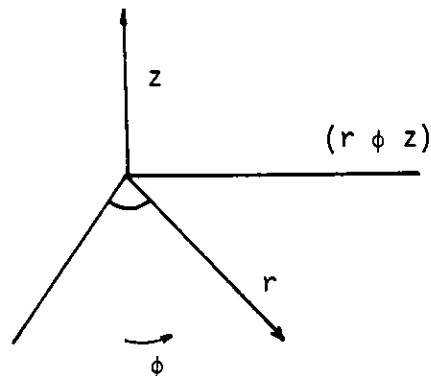
$$\nabla \cdot \underline{F} = \frac{\partial F_x}{\partial x} + \frac{\partial F_y}{\partial y} + \frac{\partial F_z}{\partial z} \quad \text{-----10}$$

$$\nabla \times \underline{F} = \begin{vmatrix} \underline{u}_x & \underline{u}_y & \underline{u}_z \\ \partial/\partial x & \partial/\partial y & \partial/\partial z \\ F_x & F_y & F_z \end{vmatrix} \quad \text{-----11}$$

$$\nabla^2 V = \frac{\partial^2 V}{\partial x^2} + \frac{\partial^2 V}{\partial y^2} + \frac{\partial^2 V}{\partial z^2} \quad \text{-----12}$$

$$\nabla^2 \underline{F} = \underline{u}_x \nabla^2 F_x + \underline{u}_y \nabla^2 F_y + \underline{u}_z \nabla^2 F_z \quad \text{-----13}$$

Cylindrical coordinates



$$\nabla V = \underline{u}_r \frac{\partial V}{\partial r} + \underline{u}_\phi \frac{1}{r} \frac{\partial V}{\partial \phi} + \underline{u}_z \frac{\partial V}{\partial z} \quad \text{-----14}$$

$$\nabla \cdot \underline{F} = \frac{1}{r} \frac{\partial (r F_r)}{\partial r} + \frac{1}{r} \frac{\partial F_\phi}{\partial \phi} + \frac{\partial F_z}{\partial z} \quad \text{-----15}$$

$$\nabla \times \underline{F} = \begin{vmatrix} \underline{u}_r/r & \underline{u}_\phi & u_z/r \\ \partial/\partial r & \partial/\partial \phi & \partial/\partial z \\ F_r & rF_\phi & F_z \end{vmatrix} \quad \text{----- 16}$$

$$\nabla^2 V = \frac{\partial^2 V}{\partial r^2} + \frac{1}{r} \frac{\partial V}{\partial r} + \frac{1}{r^2} \frac{\partial^2 V}{\partial \phi^2} + \frac{\partial^2 V}{\partial z^2} \quad \text{----- 17}$$

$$\begin{aligned} \nabla^2 \underline{F} = & \underline{u}_r \left(\nabla^2 F_r - \frac{2}{r^2} \frac{\partial F_\phi}{\partial \phi} - \frac{F_r}{r^2} \right) \\ & + \underline{u}_\phi \left(\nabla^2 F_\phi + \frac{2}{r^2} \frac{\partial F_r}{\partial \phi} + \frac{F_\phi}{r^2} \right) \end{aligned} \quad \text{----- 18}$$

APPENDIX 3Bessel Functions

Differential equation

$$\frac{d^2y}{dz^2} + \frac{1}{z} \frac{dy}{dz} + k^2y = 0 \quad \text{-----1}$$

gives solutions of the form:

$$y = A_1 J_0(kz) + B_1 Y_0(kz) \quad \text{-----2}$$

and $\frac{d^2y}{dz^2} + \frac{1}{z} \frac{dy}{dz} - k^2y = 0 \quad \text{-----3}$

gives solutions of the form:

$$y = A_1 I_0(kz) + B_1 K_0(kz) \quad \text{-----4}$$

and $\frac{d^2y}{dz^2} + \frac{1}{z} \frac{dy}{dz} - j^2 k^2 y = 0 \quad \text{-----5}$

gives solution of the form:

$$y = A_1 I_0(kzj^{\frac{1}{2}}) + B_1 K_0(kzj^{\frac{1}{2}}) \quad \text{-----6}$$

Bessel function relationships

$$I_n(z) = i^{-n} J_n(zj) \quad \text{-----7}$$

$$I_{-n}(z) = I_n(z) \quad \text{-----8}$$

$$I_n(-z) = (-1)^n I_n(z) \quad \text{-----9}$$

$$H_n^{(1)}(z) = J_n(z) + j Y_n(z) \quad \text{-----10}$$

$$H_n^{(2)}(z) = J_n(z) - j Y_n(z) \quad \text{-----11}$$

$$\therefore H_n^{(1)}(re^{j\theta}) = H_n^{(2)}(re^{-j\theta}) \quad \text{-----12}$$

From equation 7

$$I_n(z) = \frac{1}{2} j^{-n} \left[H_n^{(1)}(z_j) + H_n^{(2)}(z_j) \right] \quad \text{-----13}$$

$$\text{and } K_{-n}(z) = K_n(z) = \frac{1}{2} \pi j^{(n+1)} H_n^{(1)}(z_j) \quad \text{-----14}$$

substitute for $H_n^{(1)}(z_j)$ from equation 10

$$\text{Thus } K_n(z) = \frac{1}{2} \pi j^{(n+1)} \left[J_n(z_j) + j Y_n(z_j) \right] \quad \text{-----15}$$

$$K_n(z) = \frac{1}{2} \pi j^{(n+1)} \left[j^n I_n(z) + j Y_n(z_j) \right] \quad \text{-----16}$$

APPENDIX 4A

```

10 REM
20 REM          *****
30 REM EDDY CURRENT GAUGING, CYLINDRICAL
40 REM COORDS.FINAL FORM
50 REM          *****
60 REM
70 REM INITIAL INPUTS TO THE PROGRAM
80 REM
90 PRINT'ENTER LO IN MM'
100 PRINT'ENTER CO IN MM'
110 PRINT'ENTER F IN KHZ'
120 INPUT LO,CO,FZ
130 REM
140 F=FZ*1000
150 PRINT'ENTER CONDUCTIVITY IN UNITS'
160 PRINT'      OF 10↑(7)      '
170 PRINT'ENTER REL. PERMEABILITY'
180 INPUT SIG,MU
190 SIG=SIG*10↑(7)
200 PRINT'ENTER THE RADIUS OF METAL BAR IN MM'
210 INPUT AO
220 PRINT'ENTER HEIGHT OF THE PROBE COIL'
230 PRINT' ABOVE METAL SURFACE IN MM'
240 INPUT HO
250 H=HO/1000
260 L=LO/PI/1000
270 C=CO/1000
280 A=AO/1000
290 R=(2*PI*F*MU*4*PI*10↑(-7)/(2*SIG))↑(1/2)
300 GOTO 370
310 PRINT'DO YOU WISH TO CONTINUE Y/N'
320 INPUT AS
330 IF AS='Y' GOTO 220
340 IF AS='N' GOTO 9000
350 PRINT'PLEASE TYPE Y OR N !!!'
360 GOTO 310
370 REM
380 D1=0
390 D2=0
400 D3=0
410 D4=0
420 D5=0
430 D6=0
440 REM LOOP TO CALCULATE THE REAL AND

```

```

450 REM IMAGINARY PARTS OF THE E-FIELD'
460 REM ER AND EI AND THE REAL AND
470 REM IMAGINARY PARTS OF THE H-FIELD
480 REM HR AND HI. THIS DOES NOT INCLUDE
490 REM THE DC TERMS. FOR DC TERMS
500 REM LINES 1900 TO 2060
510 REM
520 PRINT'INPUT THE NUMBER OF HARMONICS'
530 INPUT Q1
540 Q=Q1
550 X=0
560 L1=0
570 J1=2/PI
580 REM          *****
590 REM START OF MAIN PROGRAM LOOP
600 REM          *****
610 REM
620 FOR N=1 TO Q STEP 2
630 REM
640 REM SIGN DETERMINATION FOR FOURIER
650 REM          SERIES
660 REM
670 B=(N-1)/4
680 B1=INT(B)
690 B2=B-B1
700 IF B2=0 THEN A1=1 : GOTO 730
710 IF B2>0 THEN A1=-1 : GOTO 730
720 REM
730 REM E-FIELD CALCULATION
740 REM
750 X=2*PI*F*4*PI*10†(-7)*L/N
760 L1=L/N
770 IF N=1 GOTO 790
780 J1=2*A1/PI/N
790 PRINT'X=',X
800 PRINT'L1=',L1
810 REM
820 REM
830 REM EVALUATION OF ALPHA*A (P1),
840 REM ALPHA*R (P2),ALPHA*C (P3).
850 REM AND THE CORESPONDING BESSEL
860 REM          FUNCTIONS
880 REM
890 P1=A/L1
900 P2=(H+A)/L1
910 P3=C/L1
920 REM PRINT OUT OF BESSEL FUNCTIONS
930 REM          ARGUMENTS
940 REM
950 PRINT'P1=',P1

```

```

960 PRINT'P2=',P2
970 PRINT'P3=',P3
980 GOSUB 3000
990 REM
1000 REM PRINT OUT OF BESSEL FUNCTIONS
1010 REM
1020 PRINT IAOP1,IBOP2,ICOP3
1030 PRINT ID1P1,IE1P2,IG1P3
1040 PRINT KAOP1,KBOP2,KCOP3
1050 PRINT KD1P1,KE1P2,KF1P3
1060 REM
1070 REM
1100 REM FOR THE OUTER COIL
1110 REM
1120 REM
1130 ECN=X*(1/((ICOP3/IG1P3)+(KCOP3/KF1P3)))*(J1)
1140 HCN=1/(1+(IG1P3*KCOP3)/(ICOP3*KF1P3))*(J1)
1150 REM AT THE BAR SURFACE
1160 REM
1170 EAN=(ECN)*(ID1P1)/(IG1P3)
1180 HAN=(HCN)*(IAOP1)/(ICOP3)
1190 REM
1200 REM REFLECTION AT THE BAR SURFACE
1210 REM
1220 R=(2*PI*F*MU*4*PI*109/((2*SIG))1/2)1/2
1230 I10A=(ID1P1)/(IAOP1)
1240 K10A=(KD1P1)/(KAOP1)
1250 CEJ=(1+R/(X*K10A))2+(R/(X*K10A))2
1260 KRER=((-1+R/(X*I10A))*(1+R/(X*K10A))+(R/X)2/(I10A*K10A))/CEJ
1270 K2EI=((-R/(X*I10A))*(1+R/(X*K10A))+(R/(X*K10A))*(-1+R/(X*I10A)))/CEJ
1280 E1APR=-EAN*K2EI
1290 E2API=EAN*KRER
1300 CHJ=R2+(R+X*K10A)2
1310 K3HR=(R2+(R-(X*I10A))*(R+(X*K10A)))/CHJ
1320 K4HI=R*X*(-I10A-K10A)/CHJ
1330 H1APR=HAN*K3HR
1340 H2API=HAN*K4HI
1350 REM
1360 REM TOTAL FIELD CALCULATION HA AND
1370 REM          EA
1380 REM
1390 H3AR=HAN-H1APR
1400 H4AI=-H2API
1410 E3AR=E1APR
1420 E4AI=EAN+E2API
1430 REM
1440 REM CALCULATION TO DETERMINE E AND
1450 REM H-FIELDS AT RADIUS R
1460 REM
1470 REM

```

```

1480 E5RPR=E1APR*KE1P2/KD1P1
1490 E6RPI=(E2API)*(KE1P2)/(KD1P1)
1500 E7RNI=ECN*IE1P2/IG1P3
1510 E8RNR=0
1520 PRINT'E7RNI=',E7RNI
1530 PRINT'E5RPR=',E5RPR
1540 PRINT'E6PRI=',E6RPI
1550 PRINT'E4AI=',E4AI
1560 H5RNR=HCN*IBOP2/ICOP3
1570 H6RNI=0
1580 H7RPR=H1APR*KBOP2/KAOP1
1590 H8RPI=H2API*KBOP2/KAOP1
1600 REM
1610 REM SUM OF FIELDS AT RADIUS R
1620 REM
1630 E9RR=E5RPR
1640 ERI=E6RPI+E7RNI
1650 H9RR=H5RNR-H7RPR
1660 PRINT'E3AR=',E3AR
1670 HRI=-H8RPI
1680 PRINT'KE1P2=',KE1P2
1690 PRINT'KD1P1=',KD1P1
1700 PRINT'IE1P2=',IE1P2
1710 PRINT'IG1P3=',IG1P3
1720 PRINT'E4AI=',E4AI
1730 PRINT'H3AR=',H3AR
1740 PRINT'H4AI=',H4AI
1750 E9RR=E9RR+D1
1760 ERI=ERI+D2
1770 PRINT'TOTAL E-FIELD ',E9RR '+J',ERI
1780 H9RR=H9RR+D3
1790 HRI=HRI+D4
1800 PRINT'TOTAL H-FIELD ',H9RR '+J',HRI
1810 E3AR=E3AR+D5
1820 E4AI=E4AI+D6
1830 D1=E9RR
1840 D2=ERI
1850 D3=H9RR
1860 D4=HRI
1870 D5=E3AR
1880 D6=E4AI
1890 PRINT'#####';N'#####'
1900 NEXT N
1910 REM          *****
1920 REM CALCULATION OF DC TERMS
1930 REM          *****
1940 REM          *****
1950 REM PRINT OUT OF FINAL VALUES
1960 REM          *****
1970 PRINT'E3AR=',E3AR

```

```

1980 PRINT'E4AI=',E4AI
1990 E9RR=E9RR+R*A/2/(A+H)
2000 ERI=ERI+R*A/2/(A+H)+2*(PI)↑2*F*10↑(-7)*((A+H)↑2-A↑2)/(A+H)
2010 H9RR=H9RR+1/2
2020 PRINT'TOTAL E-FIELD';E9RR'+J';ERI
2030 HRI=HRI
2040 PRINT'TOTAL H-FIELD';H9RR'+J';HRI
2050 PRINT'J1=',J1
2060 GOTO 310
2070 REM
2080 REM          *****
2090 REM
3000 REM SUB TO CALCULATE I0(X),I1(X)
3010 REM K0(X) AND K1(X) SEE HANDBOOK
3020 REM OF MATHEMATICAL FUNCTIONS BY
3030 REM M ABRAMOWITZ AND I.A.STEGUN
3040 REM   PAGE 378-379 FOR THE
3050 REM POLYNOMIAL APPROXIMATIONS
3060 REM
3070 REM          *****
3080 REM
3090 T1=P1/3.75
3100 T2=P2/3.75
3110 T3=P3/3.75
3120 REM
3130 REM
3140 IF P1>3.75 GOTO 3940
3150 GOTO 3230
3160 IF P2>3.75 GOTO 4000
3170 GOTO 3260
3180 IF P3>3.75 GOTO 4060
3190 GOTO 3290
3200 REM
3210 REM          I0(X)
3220 REM
3230 IAOP1=1+3.5156229*T1↑(2)+3.0899424*T1↑(4)+1.2067492*T1↑(6)
3240 IAOP1=IAOP1+0.2659732*T1↑(8)+0.0360768*T1↑(10)+0.0045813*T1↑(12)
3250 GOTO 3350
3260 IBOP2=1+3.5156229*T2↑(2)+3.0899424*T2↑(4)+1.2067492*T2↑(6)
3270 IBOP2=IBOP2+0.2659732*T2↑(8)+0.0360768*T2↑(10)+0.0045813*T2↑(12)
3280 GOTO 3380
3290 ICOP3=1+3.5156229*T3↑(2)+3.0899424*T3↑(4)+1.2067492*T3↑(6)
3300 ICOP3=ICOP3+0.2659732*T3↑(8)+0.0360768*T3↑(10)+0.0045813*T3↑(12)
3310 GOTO 3410
3320 REM
3330 REM          I1(X)
3340 REM
3350 ID1P1=P1*(0.5+0.87890594*T1↑(2)+0.51498869*T1↑(4)+0.15084934*T1↑(6))
3360 ID1P1=ID1P1+P1*(.02658733*T1↑(8)+0.00301532*T1↑(10)+0.00032411*T1↑(12))
3370 GOTO 3160

```

```

3380 IE1P2=P2*(0.5+0.87890594*T2↑(2)+0.51498869*T2↑(4)+0.15084934*T2↑(6))
3390 IE1P2=IE1P2+P2*(.02658733*T2↑(8)+0.00301532*T2↑(10)+0.00032411*T2↑(12))
3400 GOTO 3180
3410 IG1P3=P3*(0.5+0.87890594*T3↑(2)+0.51498869*T3↑(4)+0.15084934*T3↑(6))
3420 IG1P3=IG1P3+P3*(.02658733*T3↑(8)+0.00301532*T3↑(10)+0.00032411*T3↑(12))
3430 REM
3440 REM
3450 IF P1>2 GOTO 4400
3460 GOTO 3560
3470 IF P2>2 GOTO 4450
3480 GOTO 3590
3490 IF P3>2 GOTO 4500
3500 GOTO 3620
3510 REM
3520 REM
3530 REM          KO(X)
3540 REM
3550 REM
3560 KAOP1=-LOG(P1/2)*IAOP1-0.57721566+0.4227842*(P1/2)↑2+0.23069756*(P1/2)↑4
3570 KAOP1=KAOP1+0.0348859*(P1/2)↑6+0.00262698*(P1/2)↑8+0.0001075*(P1/2)↑10
3580 GOTO 3680
3590 KBOP2=-LOG(P2/2)*IBOP2-0.57721566+0.4227842*(P2/2)↑2+0.23069756*(P2/2)↑4
3600 KBOP2=KBOP2+0.0348859*(P2/2)↑6+0.00262698*(P2/2)↑8+0.0001075*(P2/2)↑10
3610 GOTO 3720
3620 KCOP3=-LOG(P3/2)*ICOP3-0.57721566+0.4227842*(P3/2)↑2+0.23069756*(P3/2)↑4
3630 KCOP3=KCOP3+0.0348859*(P3/2)↑6+0.00262698*(P3/2)↑8+0.0001075*(P3/2)↑10
3640 GOTO 3760
3650 REM
3660 REM          K1(X)
3670 REM
3680 KD1P1=P1*LOG(P1/2)*ID1P1+1+0.15443144*(P1/2)↑2-0.67278579*(P1/2)↑4
3690 KD1P1=KD1P1-0.18156897*(P1/2)↑6-.01919402*(P1/2)↑8-0.00110404*(P1/2)↑10
3700 KD1P1=KD1P1/P1
3710 GOTO 3470
3720 KE1P2=P2*LOG(P2/2)*IE1P2+1+0.15443144*(P2/2)↑2-0.67278579*(P2/2)↑4
3730 KE1P2=KE1P2-0.18156897*(P2/2)↑6-.01919402*(P2/2)↑8-0.00110404*(P2/2)↑10
3740 KE1P2=KE1P2/P2
3750 GOTO 3490
3760 KF1P3=P3*LOG(P3/2)*IG1P3+1+0.15443144*(P3/2)↑2-0.67278579*(P3/2)↑4
3770 KF1P3=KF1P3-0.18156897*(P3/2)↑6-.01919402*(P3/2)↑8-0.00110404*(P3/2)↑10
3780 KF1P3=KF1P3/P3
3790 GOTO 8000
3800 REM
3810 REM          *****
3820 REM
3830 REM THIS SECTION IS FOR X>3.75
3840 REM FOR IO(X) AND I1(X) AND FOR
3850 REM X>2 FOR KO(X) AND K1(X),SEE
3860 REM ABRAMOWITZ AND STEGUN PAGE
3870 REM    378 TO 379

```

```

3880 REM
3890 REM          *****
3900 REM
3910 REM          I0(X)
3920 REM
3930 REM
3940 A1=((P1)+(-1/2))*(EXP(P1))
3950 IAOP1=.39894228+.01328592*T1+(-1)+.00225319*T1+(-2)-.00157565*T1+(-3)
3960 IAOP1=IAOP1+0.00916281*T1+(-4)-0.02057706*T1+(-5)+0.02635537*T1+(-6)
3970 IAOP1=IAOP1-0.01647633*T1+(-7)+0.00392377*T1+(-8)
3980 IAOP1=A1*IAOP1
3990 GOTO 4170
4000 A2=((P2)+(-1/2))*(EXP(+P2))
4010 IBOP2=.39894228+.01328592*T2+(-1)+.00225319*T2+(-2)-.00157565*T2+(-3)
4020 IBOP2=IBOP2+0.00916281*T2+(-4)-0.02057706*T2+(-5)+0.02635537*T2+(-6)
4030 IBOP2=IBOP2-0.01647633*T2+(-7)+0.00392377*T2+(-8)
4040 IBOP2=IBOP2*A2
4050 GOTO 4230
4060 A3=((P3)+(-1/2))*(EXP(+P3))
4070 ICOP3=.39894228+.01328592*T3+(-1)+.00225319*T3+(-2)-.00157565*T3+(-3)
4080 ICOP3=ICOP3+0.00916281*T3+(-4)-0.02057706*T3+(-5)+0.02635537*T3+(-6)
4090 ICOP3=ICOP3-0.01647633*T3+(-7)+0.00392377*T3+(-8)
4100 ICOP3=ICOP3*A3
4110 GOTO 4290
4120 REM
4130 REM
4140 REM          I1(X)
4150 REM
4160 REM
4170 A1=((P1)+(-1/2))*(EXP(+P1))
4180 ID1P1=.39894228-.03988024*T1+(-1)-.00362018*T1+(-2)+.00163801*T1+(-3)
4190 ID1P1=ID1P1-0.01031555*T1+(-4)+0.02282967*T1+(-5)-0.02895312*T1+(-6)
4200 ID1P1=ID1P1+0.01787654*T1+(-7)-0.00420059*T1+(-8)
4210 ID1P1=ID1P1*A1
4220 GOTO 3160
4230 A2=((P2)+(-1/2))*(EXP(+P2))
4240 IE1P2=.39894228-.03988024*T2+(-1)-.00362018*T2+(-2)+.00163801*T2+(-3)
4250 IE1P2=IE1P2-0.01031555*T2+(-4)+0.02282967*T2+(-5)-0.02895312*T2+(-6)
4260 IE1P2=IE1P2+0.01787654*T2+(-7)-0.00420059*T2+(-8)
4270 IE1P2=IE1P2*A2
4280 GOTO 3180
4290 A3=((P3)+(-1/2))*(EXP(+P3))
4300 IG1P3=.39894228-.03988024*T3+(-1)-.00362018*T3+(-2)+.00163801*T3+(-3)
4310 IG1P3=IG1P3-0.01031555*T3+(-4)+0.02282967*T3+(-5)-0.02895312*T3+(-6)
4320 IG1P3=IG1P3+0.01787654*T3+(-7)-0.00420059*T3+(-8)
4330 IG1P3=IG1P3*A3
4340 GOTO 3450
4350 REM
4360 REM
4370 REM          K0(X)

```

```
4380 REM
4390 REM
4400 A4=((P1)†(-1/2))*(EXP(-P1))
4410 KAOP1=1.25331414-.07832358*(2/P1)+.02189568*(2/P1)†2-.01062446*(2/P1)†3
4420 KAOP1=KAOP1+0.00587872*(2/P1)†4-0.0025154*(2/P1)†5+0.00053208*(2/P1)†6
4430 KAOP1=KAOP1*A4
4440 GOTO 4600
4450 A5=((P2)†(-1/2))*(EXP(-P2))
4460 KBOP2=1.25331414-.07832358*(2/P2)+.02189568*(2/P2)†2-.01062446*(2/P2)†3
4470 KBOP2=KBOP2+0.00587872*(2/P2)†4-0.0025154*(2/P2)†5+0.00053208*(2/P2)†6
4480 KBOP2=KBOP2*A5
4490 GOTO 4650
4500 A6=((P3)†(-1/2))*(EXP(-P3))
4510 KCOP3=1.25331414-.07832358*(2/P3)+.02189568*(2/P3)†2-.01062446*(2/P3)†3
4520 KCOP3=KCOP3+0.00587872*(2/P3)†4-0.0025154*(2/P3)†5+0.00053208*(2/P3)†6
4530 KCOP3=KCOP3*A6
4540 GOTO 4700
4550 REM
4560 REM
4570 REM          K1(X)
4580 REM
4590 REM
4600 A7=((P1)†(-1/2))*(EXP(-P1))
4610 KD1P1=1.25331414+.23498619*(2/P1)-.0365562*(2/P1)†2+.01504268*(2/P1)†3
4620 KD1P1=KD1P1-0.00780353*(2/P1)†4+0.00325614*(2/P1)†5-0.00068245*(2/P1)†6
4630 KD1P1=KD1P1*A7
4640 GOTO 3470
4650 A8=((P2)†(-1/2))*(EXP(-P2))
4660 KE1P2=1.25331414+.23498619*(2/P2)-.0365562*(2/P1)†2+.01504268*(2/P2)†3
4670 KE1P2=KE1P2-0.00780353*(2/P2)†4+0.00325614*(2/P2)†5-0.00068245*(2/P2)†6
4680 KE1P2=KE1P2*A8
4690 GOTO 3490
4700 A9=((P3)†(-1/2))*(EXP(-P3))
4710 KF1P3=1.25331414+.23498619*(2/P3)-.0365562*(2/P3)†2+.01504268*(2/P3)†3
4720 KF1P3=KF1P3-0.00780353*(2/P3)†4+0.00325614*(2/P3)†5-0.00068245*(2/P3)†6
4730 KF1P3=KF1P3*A9
4740 REM
4750 REM END OF THIS SECTION
4760 REM
8000 RETURN
9000 STOP
9100 END
```

APPENDIX 4B

```

10 REM
20 REM
30 REM      *****
40 REM EDDY CURRENT GAUGING
50 REM SIMPLE TREATMENT
60 REM      *****
70 REM
80 REM
90 PRINT'ENTER LO IN MM,CO IN MM,FO IN KHZ'
100 INPUT LO,CO,F
110 PRINT'ENTER MU THE REL. PERMEABILITY AND'
120 PRINT' THE CONDUCTIVITY IN UNIITS OF 10-7'
130 INPUT MU,SIG
140 L=LO/PI/1000
150 C=CO/1000
160 GOTO 250
170 PRINT'DO YOU WISH TO CONTINUE '
180 PRINT'TYPE Y/N'
190 INPUT AS
200 IF AS='N' THEN GOTO 810
210 IF AS='Y' THEN GOTO 250
220 PRINT'I SAID TYPE Y/N PLEASE READ'
230 PRINT' THE INSTRUCTIONS'
240 GOTO 170
250 PRINT'ENTER THE HT IN MM'
260 INPUT HO
270 REM
280 REM END OF INPUTS
290 REM
300 H=HO/1000
310 HR=0.5
320 HJ=0
330 ER=0
340 EJ=0
350 IF HO=333 THEN GOTO 810
360 REM
370 REM START OF LOOP
380 REM
390 FOR N=1 TO 59 STEP 2
400 R=6.28*10†(-5)*(F*MU/(10*SIG))†(1/2)
410 X=8.0*PI*PI*F*L/N/10000
420 S=2*R/X
430 T=S*S/2
440 D=1+S+T
450 KR=(1-T)/D

```

```
460 KJ=S/D
470 B=(N-1)/4
480 B1=INT(B)
490 B2=B-B1
500 IF B2=0 THEN A=1:GOTO 520
510 IF B2> 0 THEN A=-1:GOTO 520
520 FA=(A/PI/N)*EXP(C*N/L)
530 FB=EXP(H*N/L)
540 HR=FA*(FB+KR/FB)+HR
550 HJ=FA*KJ/FB+HJ
560 ER=X*FA*KJ/FB+ER
570 EJ=X*FA*(FB-KR/FB)+EJ
580 NEXT N
590 REM
600 REM          *****
610 REM
620 REM END OF LOOP
630 REM
640 REM PRINT OUT OF FIELD VALUES
650 PRINT'E-FIELDS ARE:'
660 G1=ER+R/2
670 G2=EJ+R/2+F*H*PI*PI*4/10000
680 PRINT'ER=JO*';G1
690 PRINT'EJ=JO*';G2
700 PRINT'H-FIELDS ARE:'
710 PRINT'REAL H= ,JO*';HR
720 PRINT'IMG. H= ,JO*';HJ
730 REM
740 REM          *****
750 REM
760 REM END OF PROGRAM
770 REM
780 REM          *****
790 REM
800 GOTO 170
810 STOP
820 END
```

APPENDIX 5Composition of Brass and Aluminium BarsBrass

Brass bar 25.4 mm (1.00 in) diameter

Manufactured to BS 249

and BS 2874/CZ121M

Weight 4.278 kg/m

or 2.880 lbs/ft

Composition (%)

Cu	Pb	Zn
56.0/59.0	2.0/3.5	Rem

Aluminium

Aluminium bar 25.4 mm (1.00 in) diameter

Manufactured to BS 1474 HE 30 TF

Weight 1.368 kg/m

or 0.920 lbs/ft

Composition (%)

Al	Mg	Si	Mn
97.5	0.8	1.0	0.7

APPENDIX 6

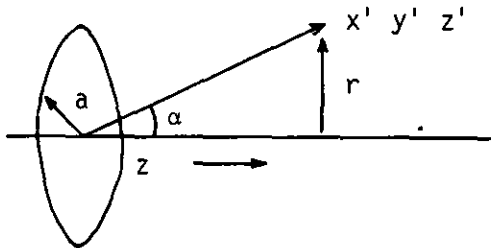
Determination of Magnetic Field Strength for a Single Wire of Loop

Figure A6.1

The expression for the vector potential at $x' y' z'$ is given by:

$$\underline{A} (x' y' z') = \frac{\mu_0}{4\pi} \int \underline{J} (x_1 y_1 z) \frac{1}{g} dv = \frac{\mu_0 I}{4\pi} \int_C \frac{1}{g} ds$$

$$\text{where } g = (a^2 + r^2 + z^2 - 2ar \cos \alpha)^{\frac{1}{2}}$$

$$\text{and } ds = a \cos \alpha d\alpha$$

$$\therefore \underline{A} (x' y' z') = \frac{\mu_0 I}{\pi^2} \int_0^{2\pi} \frac{a \cos \alpha d\alpha}{(a^2 + r^2 + z^2 - 2ar \cos \alpha)^{\frac{1}{2}}}$$

Integration yields

$$\underline{A}_\theta = \frac{\mu_0 I}{\pi k} \left(\frac{a}{r}\right)^{\frac{1}{2}} \left[\left(1 - \frac{1}{2}k^2\right)K(k) - E(k) \right]$$

$$\text{where } k^2 = \frac{4ar}{(a+r)^2 + z^2}$$

and $K(k)$ and $E(k)$ are complete elliptic integrals of the 1st and 2nd kind.

$$\text{Also } \underline{u}_0 \underline{H} = \text{curl } \underline{A} = \begin{vmatrix} \underline{u}_r/r & \underline{u}_\theta & \underline{u}_z/r \\ \partial/\partial r & \partial/\partial \theta & \partial/\partial z \\ A_r & rA_\theta & A_z \end{vmatrix}$$

$$\text{Hence } \underline{H}_r = \frac{I}{2\pi} \frac{z}{r[(u+r)^2 + z^2]} \frac{1}{2} \left[-K(k) + \frac{(a^2 + r^2 + z^2) E(k)}{(a-r)^2 + z^2} \right]$$

$$\text{and } \underline{H}_z = \frac{I}{2\pi} \frac{1}{[(a+r)^2 + z^2]} \frac{1}{2} \left[K(k) + \frac{(a^2 - r^2 - z^2) E(k)}{(a-r)^2 + z^2} \right]$$

note For $z = 0$ $\underline{H}_r = 0$ ie no radial component

and for $z = 0$, and $r = 0$

$$\underline{H}_z = \frac{I}{2\pi a} [K(0) + E(0)]$$

but $\underline{H}_r \propto \frac{z}{r}$ which is indeterminate for z and $r = 0$

APPENDIX 7

ISIS- II 8080/8085 MACRO ASSEMBLER,V4.0 MODULE PAGE 1
PROGRAM TO MEASURE AND DISPLAY SURFACE IMPEDANCE VALUES

LOC	OBJ	LINE	SOURCE STATEMENT		
		1	\$TITLE(_PROG TO MEAS. & DSP. SURFACE IMD. VALUES_)		
		2	\$MOD85		
		3			
		4			
		5	***** EQUATE LABLES *****		
		6			
		7			
0000		8	PORTA	EQU	00H #8355 PORT A
0001		9	PORTB	EQU	01H #8355 PORT B
2003		10	BUFFER	EQU	2003H #MEMORY RESERVATION
		11			#A/D VALUES
20HE		12	ADPNT	EQU	20AEH #TEMPORARY LOCATION FOR
		13			#BUFFER MEN. LOC. POINTER
2002		14	STCK	EQU	2002H #STACK LOCATION
07FA		15	CO	EQU	07FAH #CONSOLE O>P (ASCII CODE)
05EB		16	CROUT	EQU	05EBH #SENDS CARRIAGE RETURN LINE
		17			#FEED TO LINE PRINTER
0607		18	NMOUT	EQU	0607H #HEX NO. PRNT. (ASCII CODE)
		19			
		20			
		21			
0800		22		ORG	0800H #DEFINE 1ST BYTE LOCATION
		23			#OF EPROM
		24			
0800	31C220	25		LXI	SP,STCK #SET STACK
0803	F3	26		DI	#DISABLE ALL INTR#ERUPTS
		27			
		28			
		29			
		30			
		31	#*****INITIALISE 8355 PORTS A AND B *****		
		32			
0804	3E00	33		MVI	A,00H #PORT B DDR
0806	D303	34		OUT	PORTB+2
		35			
0808	3E0F	36		MVI	A,0FH #PORT A DDR
080A	D302	37		OUT	PORTA+2
		38			
		39			
		40			
		41			

```

42          #*****SET UP INT. ADD. FROM RAM*****
43
080C 210820 44      LXI    H,2008H  #LOAD INTO RAM MONITOR
080F 3603   45      MVI    M,0C3H   #LOCATIONS 20C8 TO 20CA
0811 2A6108 46      LHLD   INTR10  #WITH JUMP INTR10
0814 220920 47      SHLD   2009H   #FOR 0.5 RST
0817 21CE20 48      LXI    H,20CEH  #LOAD INTO RAM MONITOR
081A 36C3   49      MVI    M,0C3H   #LOCATIONS 20CE TO 20D0
081C 2A5708 50      LHLD   INTR50  #WITH JUMP,INTR50
081F 22CF20 51      SHLD   200FH   #FOR 7.5 RST
52
53
54
55          #*****ROUTINE TO PREVENT OP. TIMES BEING*****
56          #*****LESS THEN A VALUE OF ONE*****
57
0822 21FF1F 58      LXI    H,1FFFH
0825 0603   59      MVI    B,03H    #LOOP UNTIL ALL 3 OPERATOR
0827 05     60 THOPTR DCR    B      #TIMES HAVE BEEN CHECKED
0828 0A3609 61      JZ     START   #FOR ZERO TIMES
082B 23     62      INX   H
082C AF     63      XRA   A
082D B6     64      ORA   M
082E C22708 65      JNZ   THOPT
0831 3601   66      MVI    M,01H
0833 C32708 67      JMP    THOPTR
68
69
70
71          #*****PROG TO OBTAIN SAMPLED DATA VALUES*****
72          #*****SELECTED BY OPERATOR *****
73
0836 210320 74 START LXI    H,BUFFER #TOP OF A/D BUFFER
75
0839 22AE20 76 HZ50  SHLD   ADPNT  #RETAIN LATEST MEMORY LOC.
083C 210020 77      LXI    H,2000H
083F 4E     78      MOV    C,M     #MOVE 50HZ COUNT INTO C REG
0840 23     79      INX   H
0841 56     80      MOV    D,M     #MOVE TIME BEFORE SAMPLING
0842 23     81      INX   H     #INTO D REG
0843 5E     82      MOV    E,M     #MOVE NO OF A/D SAMPLES TO
0844 2AAE20 83      LHLD   ADPNT  #BE TAKEN OVER 50HZ CYCLE
84
0847 3E0B   85      MVI    A,0BH
0849 30     86      SIM
084A 3E02   87 WAIT  MVI    A,02H   #SET 7.5 INTR
084C D300   88      OUT   PORTA  #CLEAR F/F AND SET S/H
084E 31C220 89      LXI    SP,STCK #TO SAMPLE MODE
0851 3E03   90      MVI    A,03H   #ENABLE FLIPFLOPS
0853 D300   91      OUT   PORTA

```

```

0855 FB          92          EI          #ENABLE INTERRUPT
0856 76          93          HLT         #WAIT FOR INTERUPT
          94
0857 0D          95 INTR50 DCR          C          #DECREMENT 50HZ COUNT
0858 C24A08     96          JNZ          WAIT
085B 3E0D       97          MVI          A,0DH    #WHEN 50HZ COUNT IS ZERO
085D 30         98          SIM          #SET 6.5 INT & MASK 7.5 INT
085E C34A08     99          JMP          WAIT
          100
0861 15         101 INTR10 DCR          D          #DECREMENT 10 KHZ COUNT
0862 C24A08     102          JNZ          WAIT
0865 1601       103          MVI          D,01
0867 1D         104          DCR          E          #DECREMENT SAMPLE NO.
0868 CA3908     105          JZ           HZ50    #IF ZERO RELOAD OP. TIMES
          106
086B 3E00       107          MVI          A,00H
086D D300       108          OUT         PORTA   #SET S/H TO HOLD MODE
          109
086F DE00       110 EOC      IN          PORTA   #END OF CONVERSION
0871 E610       111          ANI          10H    #IF YES
0873 CA6F08     112          JZ           EOC      #INPUT CONVERTED VALUE
0876 DB01       113          IN          PORTB   #A/D VALUE
0878 77         114          MOV          M,A      #STORE CONVERTED VALUE
0879 23         115          INX          H
087A 3EAD       116          MVI          A,0ADH  #CHECK FOR LAST EOC
087C E610       117          ANI          10H    #IF YES
087E CA6F08     118          JZ           EOC      #INPUT CONVERTED VALUE
0881 DB01       119          IN          PORTB   #A/D VALUE
0883 77         120          MOV          M,A      #STORE CONVERTED VALUE
0884 23         121          INX          H
0885 3EAD       122          A,0ADH  #CHECK FOR LAST A/D MEM.
0887 BD         123          CMP          L          #LOCATION
0888 C24A08     124          JNZ          WAIT
088B 3E0E       125          MVI          A,0EH  #MASK 7.5,6.5 INTERRUPTS
088D 30         126          SIM          #AND SET 5.5 INT.
088E FB         127          EI
          128
          129
          130
          131          #*****ROUTINE FOR CONV. ANALOGUE VALUES*****
          132          #*****INTO BCD & OUTPUTING TO LINE*****
          133          #*****PRINTER IN UNITS OF MILLI VOLTS*****
          134
          135
088F CD0509     136          CALL         PRHDNG  #CALL THE SUBROUTINE
          137          #TO OUTPUT A HEADING
0892 210320     138          LXI          H,BUFFER
0895 3A0220     139 SMPLNO LDA          2002H  #LOAD E REG. WITH SAMPLE
0898 5F         140          MOV          E,A      #NUMBER
0899 160A       141          MVI          D,0AH  #10 VALUES PER LINE

```



```

178
179
180 *****
181 *****SUBROUTINES*****
182 *****
183
184
185
186 ****A HEADING TO OUTPUT TO LINE PRINTER****
187
188
08D7 OD      189 HDING   DB      ODH,0AH #CR,LF
08D8 OA
08D9 31304B48 190      DB  _10KHZ PEAK SAMPLED VALUE (MILLI VOLTS)
08DD 5A205045
08E1 414B2053
08E5 414D504C
08E9 45442056
08ED 414C5545
08F1 5320284D
085F 494C4049
08F9 20564F4C
08FD 545329
0900 OD      191      DB      ODH,0AH,0AH,0AH      #CR,_S
0901 OA
0902 OA
0903 OA
0904 00      192      DB      00H      #END OF HEADING
193
194
0905 C5      195 PRHDNG  PUSH   B
0906 E5      196          PUSH   H
0907 21D708  197          LXI   H,HDING
090A 4E      198 NEXT    MOV   C,M      #INTO C REG
090B AF      199          XRH   A
090C B1      200          ORA   C      #IF BYTE IS ZERO
090D CA1709  201          JZ   ENDING #RETURN FROM SUB.
0910 CDFA07  202          CALL CO      #TRANS. ASCII CODE TO LP
0913 23      203          INX   H      #INCREMENT MEMORY FOR
0914 C30A09  204          JMP  NEXT    #NEXT BYTE OF HDING
0917 E1      205 ENDING  POP   H
0918 C1      206          POP   B
0919          207          RET
208
209
210
211
212 *****SUB. TO CONV. A/D HEX VALUES INTO*****
213 *****DEC. VALUES REP. MILLI VOLTS*****
214

```

```

215 ADVRT
091A E5      216 PUSH      H
091B D5      217 PUSH      D
091C 21C208  218 LXI      H, TABLE-1#LOAD MEM. WITH TABLE LOG
091F 1600    219 MVI      D, 00H
0921 1E00    220 MVI      E, 00H
0923 3AAE20  221 BYTCNT LDA      ADPNT
0926 A7      222 ANA      A
0927 CA4409  223 JZ       RESULT
092A 23      224 INMEM   INX      H
092B 1F      225 RAR     #SHIFT A REG RIGHT 1 BIT
092C DA3309  226 JC     #IF CARRY CONVERT BIT
092F 23      227 INX    H
0930 C32A09  228 JMP    INMEM
          229
0933 32AE20  230 CVTBYT STA    ADPNT #CVTBYT CONVS. HEX VALUES
0936 4E      231 MOV    C, M #INTO BCD VALUES
0937 34      232 INR    M
0938 46      233 MOV    B, M #REGS B AND C CONTAIN
0939 79      234 MOV    A, C #MOST SIGNIFICANT NUMBER
093A 83      235 ADD    E
093B 27      236 DAA   #DECIMAL ADJ. FOR BCD
093C 5F      237 MOV    E, A
093D 78      238 MOV    A, B #REGS D & E CONTAIN
093E 8A      239 ADC    D #LEAST SIGN. NUMBER
093F 27      240 DAA
0940 57      241 MOV    D, A
0941 C32309  242 JMP    BYTCNT
          243
0944 7A      244 RESULT MOV    A, D #PRINTS OUT BCD VALUE
0945 CDC706  245 CALL   NMOUT #ON LP
0948 0E2E    246 MVI    C, 2EH #PINTS DECIMAL POINT
094A CDFA07  247 CALL   CO #ON LP
094D 7B      248 MOV    A, E #PRINTS OUT BCD VALUE
094E CDC706  249 CALL   NMOUT #ON LP
0951 0E20    250 MVI    C, 20H #PRINTS TWO SPACES
0953 CDFA07  251 CALL   CO #BEFORE NEXT BCD
0956 0E20    252 MVI    C, 20H #VALUE
0958 CDFA07  253 CALL   CO
095B D1      254 POP    D
095C E1      255 POP    H
095D C9      256 RET
          257
          258 END

```